火山灰質粗粒土の内部浸食に関する安定性評価

STABILITY EVALUATION ON INTERNAL EROSION OF VOLCANIC COARSE GRAINED SOILS

By

DAO MINH HIEU

MURORAN INSTITUTE OF TECHNOLOGY

March 2018

Table of contents

CHAPTER 1:

INTRODUCTION

1.1 General

Japan has a variety of volcanic ash soils that cause complicated geotechnical engineering problems in all the regions of the islands, i.e., in Hokkaido, Tohoku, Kanto, Chubu, Chugoku and Kyushu. The distribution of volcanic ground was widespread and each volcanoes has acted numerously over geological time. In Hokkaido, Japan, there are over forty Quaternary volcanoes, and pyroclastic materials cover over 40 % of its area. Sedimentary structure, components, distributional area and degrees of the weathering greatly differ with the depositional environment. Therefore, it is anticipated that the mechanical property of volcanic soil grounds will be diverged (Miura, 2012). Such volcanic soils have been also used as useful construction materials, especially man-made earth structures (embankments and cut slopes, etc.). However, a large number of earthquake- and rainfall-induced failures of artificial slopes such as cut slopes or embankments has been reported in Japan. One of the areas, where a significant number of slope failures occur, is Hokkaido. Earthquakes and heavy rainfall in Hokkaido have been a leading cause of serious ground, natural slope, cut slope, and embankment damage; specifically where these are composed of volcanic soils (e.g., Japanese Geotechnical Society [JGS], 2004). Examples include embankment slope failures due to the 1968 and the 2003 Tokachi-oki earthquakes, failure of cut slope (including volcanic soil layers) on the Hokkaido Expressway (1999) due to rainfall and snow-thaw water in the spring (Yamazaki, Tomojiri and Sasaki, 2000), and slope collapse around Aso Volcano due to 2016 Kumamoto earthquake.

In recent decades, volcanic soils have been classified as “problematic soils” in Japan engineering research (IS-Tohoku, 1998). However, the research on volcanic soils from the engineering standpoint is extremely superficial in comparison with cohesion and cohesionless soils (e.g., Miura, 2012; Miura et al., 2003). In addition, the most classifiable feature of the volcanic coarse-grained soils in Hokkaido is that effect of particle breakage on static and cyclic deformation-strength characteristics is strong (e.q, Miura et al., 1993; Nakata and Miura, 2007; Matsumura et al., 2015). Especially, crushing of the particles of

Hokkaido's volcanic coarse-grained soils leads to increase of amount of finer soil particles. This might cause internal instability and influence to seepage performance of embankment constructed by volcanic coarse grained soil.

In this study, internal erosion of volcanic coarse grained soil and a stability evaluation for seepage flow-induced internal erosion were investigated. Internal erosion occurs when soil particles within an embankment structure are out flowed downstream by infiltration. Through to efforts of many researchers, it has been well known that internal erosion leads to an increased hydraulic conductivity and induces a reduction of soil strength (Ke and Takahashi, 2012). In addition, it has been clarified that the transport of fine particles in soil matrix results in piping phenomenon or in collapse of soil structures (Zhang and Chen, 2006; Richards and Reddy, 2007; Fujisawa et al., 2010).

The final goal of this study are to grasp internal erosion of compacted volcanic coarse grained soils (like embankment) such as embankments and to clarify the effects of geotechnical conditions (grain size distribution and fines content etc.) and compaction conditions (degree of compaction) on piping mechanisms of volcanic coarse grained soils. The first purpose in this study is to investigate features of internal erosion of a full-scale embankment constructed by volcanic coarse grained soils. Secondly, a stability evaluation of volcanic soils was investigated based on empirical geotechnical criteria. Thereafter, a series of model tests was performed compacted volcanic soils using a conventional piping test apparatus. In the experiments, the movement of soil particles in seepage flow tests was observed using an X-ray CT scanner in detail. Finally, a simple method to evaluate critical hydraulic gradient was proposed on volcanic coarse grained soils.

1.2 Outline of present study

The primary purpose of this thesis is composed of five research contents as follows;

① Stability evaluation of volcanic coarse grained soils based on empirical criteria
② Observation of piping phenomenon in original volcanic soil
③ Seepage performance of compacted volcanic soils.
④ Influence of fines on piping phenomenon
⑤ Evaluation of internal stability of volcanic soils using critical void ratio

Regarding (1), as mentioned in 1.1, Features of internal erosion of soils are important to assess the mechanisms of slope failure. Seepage flow-induced internal erosion, referring to loss and migration of fine particles through constrictions of coarse particles, is usually observed in internally unstable soils. Based on those standpoints and field observation of a full-scale embankment, evaluating the internal stability of volcanic soils under empirical geometric criteria was examined.

Secondly, since visual observation on movement of particles in seepage process has been difficult, therefore, piping tests were performed using a small apparatus and X-ray CT

machine in this study. It was originally designed for assessment of piping phenomenon on volcanic coarse grained soil. Images from X-ray CT scanner which are analyzed by 2-dimensional Digital Image Correlation analysis. The detailed results are indicated in this thesis.

Thirdly, in order to accomplish the purpose above, a test apparatus capable of simulating the seepage flow process was conducted, and the effect of internal erosion on the compacted soil was examined. Hokkaido island in Japan is located in a cold region where varieties of volcanic soils have widely deposited. Volcanic soils were useful for man-made earth structures. In which compaction condition of volcanic soil plays an important role in quality of these constructions. In particular, the degree of compaction influences on effective porosity of the soils, as a result, this is leading to a change of permeability. In addition, the separation between compaction layers is a significant sign influencing internal instability of man-made earth structures in the field.

Subsequently, in Hokkaido, the compaction and the freeze-thaw sequence could be the causes of particle crushing after construction. Thus, although the embankment is generally stabilized with the consolidation progressing, the fact does not always agree with the coarse-grained volcanic soil embankment. Particle crushing of volcanic coarse grained soils is significant for an evaluation of the mechanical behavior of man-made soil structures and affects internal erosion. Therefore, it is pointed out that the influence of particle crushing on the mechanical properties of compacted soil is required for estimation of internal erosion of soil. The effect of particle crushing on hydro-mechanical characteristics was elucidated by using six kinds of coarse-grained volcanic soils gradation-controlled by changing of finer fractions.

Finally, the effect of void structure on internal erosion of coarse-grained volcanic soil was examined in this study, so volcanic soil contains a relatively-high amount of finer fractions and they cover coarse-grained particles (including pumices). The porosity and particle crushability are considered to characterize the mechanical properties of volcanic coarse-grained soil (Nakata and Miura, 2007). According to their test results, volcanic coarse-grained soils in Hokkaido are composed of “opening intra-particle void” at a high rate, which leads to significant particle breakage and internal erosion. This is important to evaluate the effect on the hydraulic mechanical properties of volcanic soils.

1.3 Organization of thesis

This thesis includes seven chapters, which are briefly outlined as follows:

• Chapter 1, general assessment of volcanic soil and its phenomenon of internal instability are indicated as introduction, a background, highlight of the objectives, scope, and organization of the thesis.

• Chapter 2, brief reviews on the internal instability of soils are described. Then, the

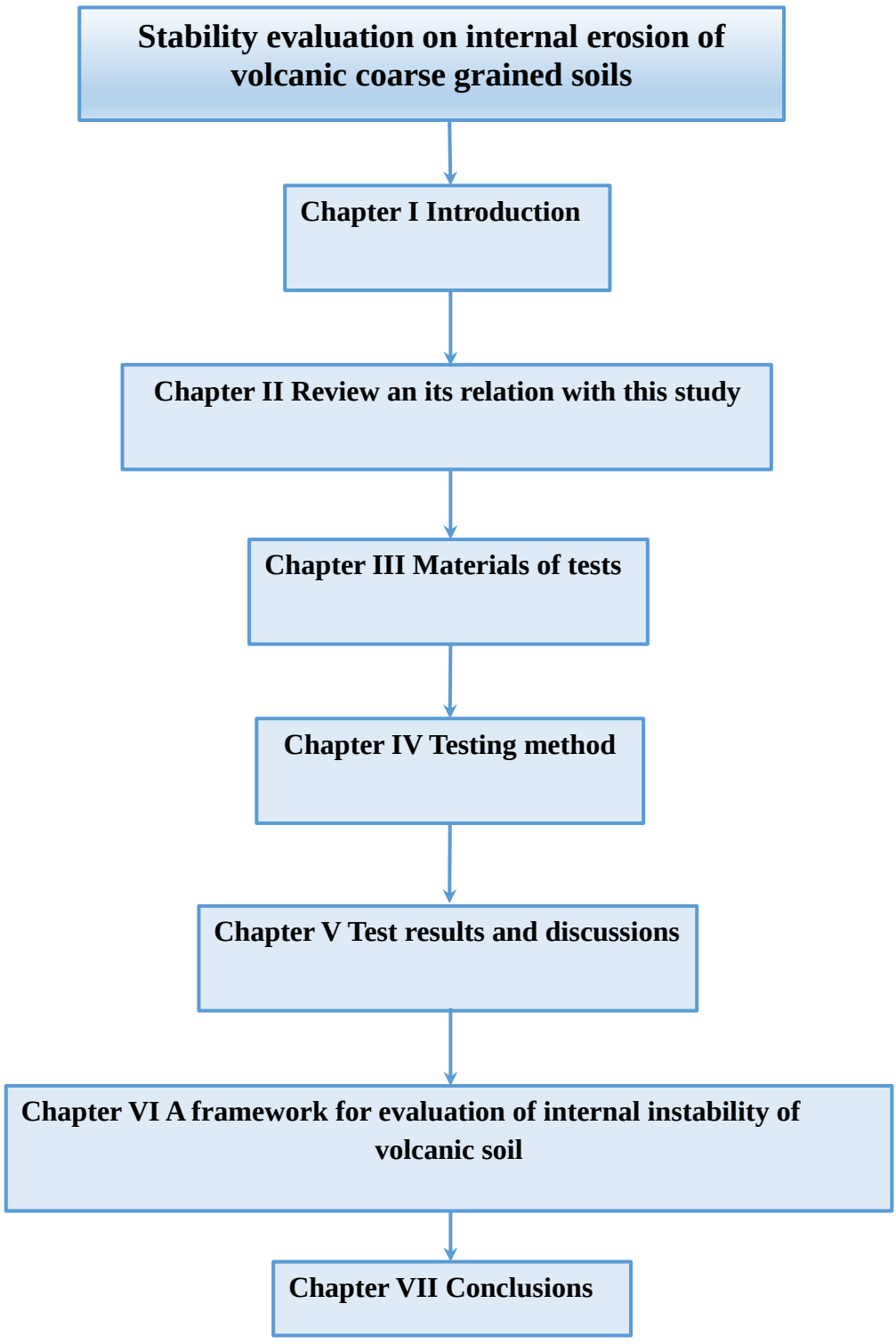

commonly-used criteria to assess the potential of internal instability are summarized. In addition, an investigation on the internal instability of volcanic soil is conducted.

• Chapter 3, the test materials used in this experimental study are presented. Additionally, properties of the materials are reported.

• Chapter 4, the testing methods is introduced including testing apparatuses, specimen preparation, and piping test procedures.

• Chapter 5, test results and discussions, in particular, assessment and classification of piping

mechanisms on volcanic coarse grained soils affected by geotechnical conditions and compaction conditions are presented.

• Chapter 6, a framework for the evaluation of internal instability on the volcanic coarse grained soils is proposed.

• Chapter 7, theoretical and experimental works presented in this thesis are summarized, and the recommendations is provided for future research.

CHAPTER 2:

LITERATURE REVIEW

2.1 Internal erosion in embankment

2.1.1. Overview of stability evaluation of embankments

Geotechnical engineers relating to construction of soil structures such as embankments have been always plagued by the complexity of soil behavior. Therefore, evaluation of the stability of slopes is the most important and challenging attempts for civil engineering.

The author focus on internal stability of embankments. Internal erosion is the main cause of slope failures and accidents to embankments. For example, piping phenomenon is one of failure modes on internal erosion resulting from soil particle migration within its pore spaces network along seepage flow. This phenomenon is widely observed in both natural soil deposits and artificial slopes such as cut slopes or embankments. In order to discuss internal erosion, the estimation of the following physical characteristics of soils is very important as shown by many researchers; distribution of pore sizes, grain size distribution, density, permeability and internal resistance.

In a large number of investigation on embankment, it has been shown that internal erosion failures occur on weaknesses of first construction in the embankment or its foundation under the rising water for many cases. After that, internal erosion failures will be a threat to embankment because settlement cracking can occur as a result of extreme load as the rise of extreme water level due to rainfall and earthquakes. In addition, owing to aging causes, deterioration of quality of embankment leading to internal erosion may be initiated.

In Volume 1 of ICOLD Bulletin 164 (2015), the authors were summarized the records of embankment dam incidents and the dam register in ICOLD (1974, 1983, 1995), Foster et al, (1998, 2000a) based on analyzing the statistics of dam failures for large dams constructed between 1800 and 1986, excluding dams constructed in Japan pre 1930 and in China (adapted from Foster et al, 1998, 2000a), as shown in Tables 2.1, 2.2 and 2.3. In Table

2.1 shows the statistic of failures and accidents in embankment dams and around conduits or walls. In addition, proportion of failures and accidents on first and after first construction of embankments were shown in the table. Furthermore, an overview failures of embankment due to erosion and slides is shown in Table 2.2. It can be seen from the data in Table 2.2 that internal erosion has been responsible for about half of embankment dam failures. Contrarily, there are only 4% and 2% of embankment failures due to slides and earthquakes, respectively. In addition, Table 2.3 shows ratio of failures to the number of dams between two stages of 1970 to 1979 and 1980 to 1989. By comparing these ratios, a better trend of improved design and construction methods was recognized.

Table 2.1: Statistics of failure and accidents in embankment constructed from 1800 to 1986 (revision of Foster et al, 1998, 2000a)

Case	Total	In dam	Around conduits or walls
Internal erosion failures	36	19	17
Internal erosion accidents	75	52	23
Seepage accidents with no detected erosion	36	30	6
Total no. of failures and accidents	146	101	46
Population of dams	11192	11192	5,596
Historical frequency for failures and accidents	0.013	0.009	0.0082
Proportion of failures and accidents on first fill	36%		
Proportion of failures and accidents after first fill	64%		

Table 2.2: Failure statistic of embankment dams (revision of Volume 1 of ICOLD Bulletin 164 (2015))

Failure Mechanism	Embankment Sliding		Erosion	
Mode of failure	Static Instability	Seismic instability	Internal erosion	External erosion (overtopping)
% over the world	4%	2%	46%	48%
% over the world	6%		94%	

In addition, Richards and Reddy 2007 summarized 267 dam piping failures based on piping data taken from Jones (1981), Lane (1934) and National performance of Dams program. These failures were divided into four categories; (I) Foundation related piping failures; (II) Conduit and internal erosion piping failures; (III) Possible backwards erosion and suffusion piping failures; (IV) Piping failures induced by biological activity, with

failure ratios are 15%, 49.8%, 31.1% and 4.1%, respectively. In addition, Fry (2016) investigated embankment failure reported by the Erinoh R&D project, merged with Foster& Fell Erdata and NPDP program in the USA. He indicated that internal erosion occurs easily on residual soils and volcanic soil associated with high permeability and void.

Table 2.3: Statistics of embankment failures excluding China from 1970 to 1989 (revision of Foster et al, 1998, 2000a)

Modes of failure	Ratio of failures to the number of dams 1970-1979	Ratio of failures to the number of dams 1980-1989
Internal erosion	0.0020	0.0016
Overtopping and appurtenant structure failure resulting in overtopping	0.0026	0.0019
Sliding	0.0004	0.0001

2.1.2. Internal erosion mechanisms

Internal erosion is a mechanical process which occurs when soil particles within an embankment or its foundation are detached and transported to downstream by seepage flow. According to Foster and Fell 1999b, the overall process of internal erosion was expressed into four phases: Initiation, continuation, progression and breach of erosion. Figure 2.1 shows models for development of failure by internal erosion through embankment initiated by losing particles at leak.

The mechanism of internal erosion is particle detachment phenomenon under seepage flow. This phenomenon may depend on consistency of natural soil. In particular, soils having high plasticity such as clays, clayey sands, and clayey sandy gravels seem to be more resistant to internal erosion than cohesionless. These soils should be related by contact erosion and concentrated leak erosion because they will hold a crack even when saturated. On the other hand, cohesionless (non plastic) soils such as silts, sands and gravels are subjected to suffusion, backward erosion or contact erosion depending on grain size distribution of soils. These soils will be collapsed a crack when saturated. Therefore, cohesionless soils are easily eroded. In addition, the degree of saturation also influences the evaluation of erosion of soil. Wan and Fell (2002, 2004 a,b) indicated that clays have significantly slower erosion and have higher critical shear stresses than those soils at the saturated compaction condition. However, cohesionless soils few depend on the degree of saturation for these phenomena. In this study, volcanic coarse grained soils were classified into non plastic soils. Evaluation of internal erosion on volcanic coarse grained soil is adopted in this study including the influence of particle size distribution and compaction condition of test materials.

According to assessment of internal erosion on embankment, Fell and Fry (2007)

classified internal erosion in four mechanisms; concentrated leak, backward erosion, contact erosion, and suffusion are as follows (see Figure.2.2).

(1) For concentrated leak erosion, the erosion occurs in the crack or concentrated leak leads to the opening of a pipe. The causes of this phenomenon may be due to differential settlement during construction or in operation of embankments such as collapse settlement of poorly compacted fill or seismic loading. Wan (2006), Wan and Fell (2002, 2004 a, b) and Fell et al (2008) proposed a method to estimate the hydraulic shear stresses in vertical transverse cracks and cylindrical pipe based on head loss in pipe or crack due to friction in meters and shape factors. In addition, Kawamura et al. (2010a) and Kawamura and Miura (2013, 2014) investigated the effect of frost-heaving in cut slope constructed by volcanic soils on slope stability. Frost actions generate cracks in cut slope surface.

(2) For backward erosion, the erosion process detaches soil particles when the seepage flow exits on the ground surface or at downstream face of the embankment, then a pipe forms. Backward erosion occurs where critically hydraulic gradients at the toe of an embankment erode particles upwards and backwards below the dam through small erosion channels and flow velocity can transport the eroded particles to downstream. Terzaghi and Peck (1948) show that backward erosion piping will initiate when zero effective stress condition occurs in cohesionless soils at the toe of an embankment. In addition, Van Beek et al (2010) and Sellmeijer et al (2012) proposed three factors: resistance factor (F_R), scale factor (F_S) and geometrical shape factor (F_G) using to determine the critical gradient at the onset of piping.

(3) For suffusion, some of the fine particles of internal unstable soils are eroded and left from the coarse matrix of the soil. The pipe is not formed but the permeability of the soil may be increased significantly. Suffusion occurs when water flows through internally unstable widely graded or gap graded non plastic soils. These soils assure three specificities. Firstly, the size of finer particles must be smaller than size of constrictions between coarse particles. Secondly, the amount of finer particles must be less than enough to fill void of coarse particles. Finally, the hydraulic gradient must impose a high enough velocity flow to move the finer particles through the constriction between coarse particles.

(4) For contact erosion, the fine particles is eroded into the coarser layer by the seepage flow passing to the coarser particles. Contact erosion initiates when the velocity of flow in the coarse soil is sufficient to initiate erosion of the fine particles. Figure.2.2 shows these mechanisms.

Initiation	Continuation	Progression	Breach
Concentrated leak forms, erosion initiates along walls of crack	Continuation of erosion	Enlargement of concentrated leak	Breach mechanism forms

(A) Piping in the embankment initiated by erosion in a concentrated leak

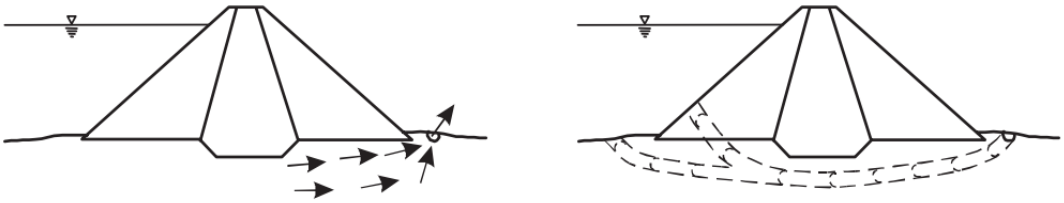

Initiation	Continuation	Progression	Breach
Leakage exits from the foundation and backward erosion initiates	Continuation of erosion	Backward erosion in progresses to form a pipe	Breach mechanism forms

(B) Piping in the foundation initiated by backward erosion

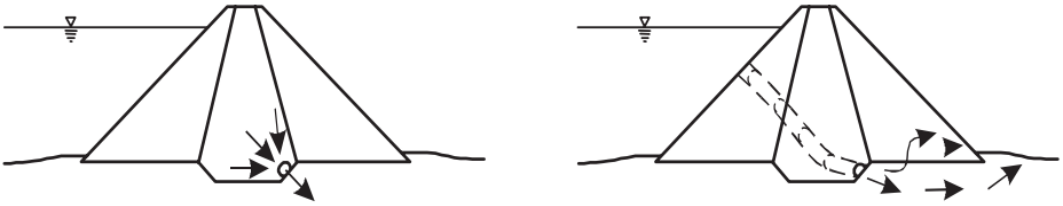

Initiation	Continuation	Progression	Breach
Leakage exits the core into the foundation and backward erosion initiates as core erodes into the foundation	Continuation of erosion	Backward erosion progresses to form a pipe. Eroded soil is transported in the foundation	Breach mechanism forms

(C) Piping from the embankment to foundation initiated by backward erosion

Figure.2.1 Typical types of the failure development due to internal erosion (Foster and Fell 1999b)

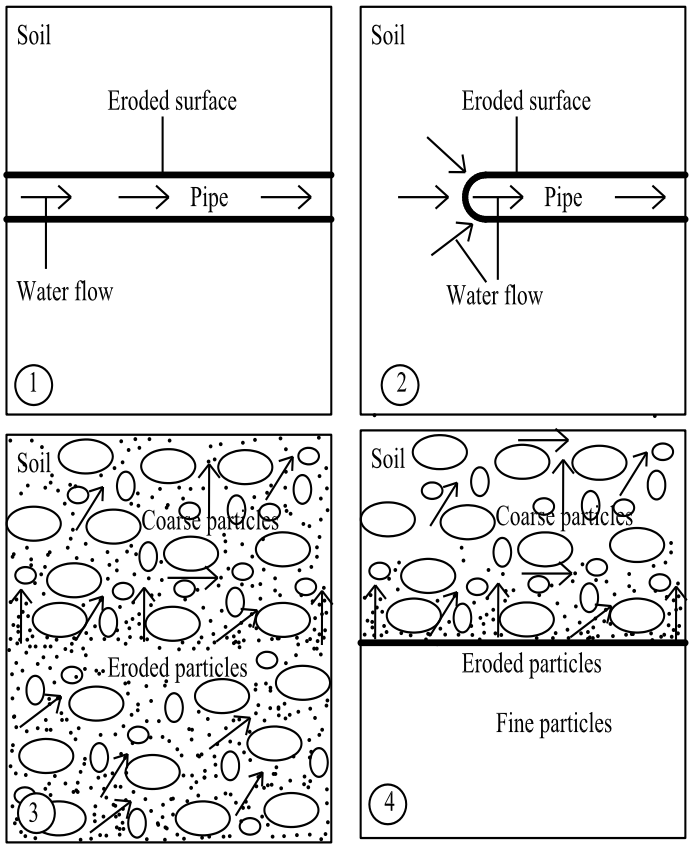

Figure.2.2 The mechanisms of internal erosion (Revision of Fell and Fry 2007):
(1). Concentrated leaks, (2). Backward erosion, (3). Suffusion, (4). Contact erosion**.**

Based on observation of seepage tests, internal erosion can be divided into two categories: Piping studies and boiling studies. Piping is the first sign of fine particles detachment from the soil fabric and transport of these particles out of the soil mass, which increases porosity of soil (e.g., Khilar et al., 1985; Reddi et al., 2000; Wan and Fell, 2004). Boiling is the failure of a soil skeleton induced by an intergranular seepage force greater than the resistible force of the soil mass due to its weight that means the effective stress of soil becomes zero. As a result, a critical hydraulic gradient i_c with the value was given by a theoretical equation (Terzaghi, 1925)

$$\mathrm{i_c} = \frac{\mathrm{G_s} - 1}{1 + \mathrm{e}} \tag{2.1}$$

where e is void ratio of material and G_s is specific gravity of the soil grains. In addition, the studies on boiling have focus on the determination of the critical hydraulic head or the gradient depending on internal stability of soil (Skempton and Brogan., 1994; Ke and Takahashi., 2012). Accordingly, internal instability of an unstable soil occurs at a hydraulic gradient i_c'= about one fifth to one third of the theoretical value (i_c).

Furthermore, in a significant amount of research on the internal erosion, it has been clarified that they are influenced by geometric conditions, hydrological mechanism, and compaction conditions. For instance, the geometric criterion for evaluating internal instability was presented by Kezdi (1979) based on the conception of Terzaghi's filter rule (Terzaghi, 1939). Kenney and Lau (1985, 1986) criterion was proposed to assess the internal stability of granular soils. Li and Fannin (2008) had synthesized Kenzi's criterion and Kenney and Lau's criterion. Burenkova (1993) proposed a method to evaluate the internal stability of granular soils, therein their soils were deemed stable if the fine particles fully filled the voids of the coarse particles that constitutes the primary fabric. In addition, Skempton and Brogan (1994) presented internal erosion induces the instability of the soils leading to decrease of critical hydraulic gradient compared to the theory of Terzaghi.

2.2 Geometric criteria to evaluate internal erosion of soil under seepage flow

Evaluating internal erosion of a soil is classified into two categories: stable and unstable soil. In which, stable soil refers to the ability of coarser particles to prevent the loss of fine particles of soil. On the other hand, a soil will be described as unstable soil if it lose particles due to seepage flow. This part provides a brief review of those previous investigations, including geometric criteria proposed to evaluate internal instability, and grasps the hydraulic conditions of soils. Based on reviewing literature, appropriate methods to evaluate internal instability of volcanic coarse grained soils under seepage flow are discussed.

2.2.1. Kezdi method (1979)

Terzaghi (1939) indicated that the filter rule for internal stability of soil has to assure the two conditions. Firstly, the size of the fine particles must be bigger than the size of the constrictions between the coarser particles, which is assessed by the following equation:

$$D_s \leq 4\, D_f \tag{2.2}$$

where D_f is diameters of fine particles; D_s is diameter of coarse particles; D_p is pore size constrictions of coarser particles, as shown Figure.2.3. Secondly, to prevent the foundation material from passing through the pores of the filter, the 15 percent size of the filter material (D_{15}) must not exceed 4 to 5 times the 85 percent size of foundation (D_{85}). This means the amount of fine soil particles must be more than enough to fill the voids of the basic skeleton formed by the coarser particles. A criterion which was proposed by Terzaghi, and which, after investigations of its validity, has been recommended by the U.S. Waterways Experimental Station (1941) may be written

$$\frac{D_{15}\ (\text{of filter})}{D_{85}\ (\text{of foundation})} < (4 \text{ to } 5) \tag{2.3}$$

Based on the concept of Terzaghi's filter rule, Kezdi proposed a geometric criterion for assessing the internal stability of soils. In this method, the gradation curve is split into a coarser fraction and a finer fraction at any arbitrary point along its grain size distribution curve. Consequently, if both fractions satisfy the value of internal stability $D'_{15}/D'_{85} < 4$ the soil is considered internally stable. In the criterion, D'_{15} is the diameter for 15% mass passing in the coarser fraction and D'_{85} is the diameter for 85% mass passing in the finer fraction. The filter layers can be made of several individual layers or they can be mixed filters that the pores of one fraction will just be filled by the grains of the next fraction. Accordingly, both methods are essentially the same, and the final being less severe. If the two components assure the filter rule then the grains of the filter component will not wash out of the soil's frame. The division of soil into two components is shown in Figure.2.4. On the grain size distribution curve of the soil, the arbitrary diameter d_0 as a divisor and determine S_0, S_1, S_2, as shown in Figure.2.4.

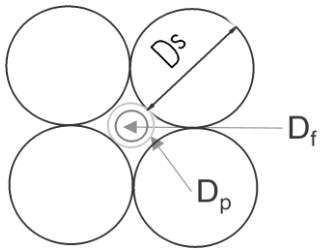

Figure.2.3 Illustration of a filter requirement

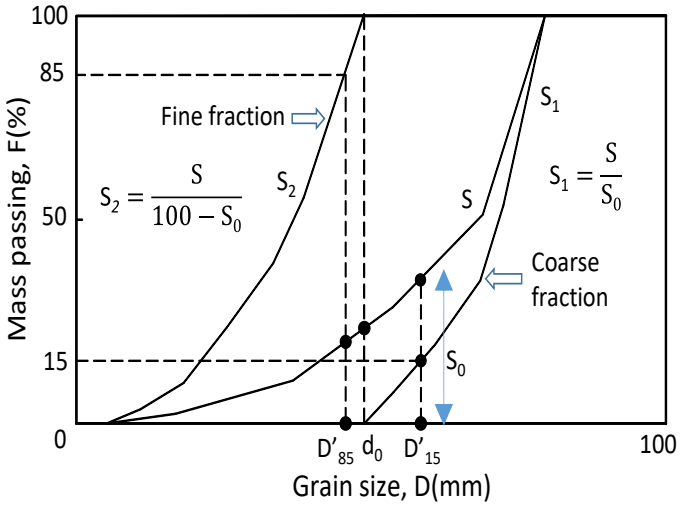

Figure.2.4 Kezdi stability criterion

2.2.2. Kenney and Lau method (1985, 1986)

The Kenney and Lau (1985) proposed a method to assess the internal stability of soils, which is a criterion applied for the evaluation of granular filter materials based on

laboratory test results from seepage tests on cohesionless sands and gravels with particles up to 100 mm. They found that loose particles can be existed within pores of primary fabric of cohesionless and granular materials. These particles can be transported by seepage flow depending on grain size distribution, density of compacted soil and the disturbing forces. Therefore, Kenney and Lau (1985) studied the effect of disturbing forces such as seepage and vibration on internal stability of a granular material. In addition, the analysis on characteristic of the shape of the grain size distribution curve was performed to assess the internal stability of granular soils. In order to accomplish the purposes, seepage tests were performed on samples with 245mm and 580mm of cylinder diameter (see Figure.2.5). For test procedure, a coarse drainage layer or sequence of layer with the coarsest at the bottom was first placed on the bottom of the cylinder. Holes were made through the side of the cylinder to prevent clogging of the drainage layer. Relative density was determined for five layers of the sample, and values close to 100% were obtained for the apparatus with 240mm in diameter and slightly above 80% for the apparatus with 550mm in diameter. Then, water from the upper reservoir flowed through the specimen. Each test lasted at least 30h and until particles no longer flushed out. The longest testing periods being about 100hours.

The test results showed that granular materials contain loose particles and when the potential travel distances of certain sizes of loose particle are larger than the filter thickness, these particles can be lost from throughout the filter (unstable grading). As a result, the characteristic of grain size distribution can be changed. On the other hand, grading of materials, which do not contain fine particles washed out from the specimen by seepage flow, is stable grading. Kenney and Lau criterion presented a boundary dividing stable and unstable grading in seepage tests based on the grain size characteristic of soils. In particular,

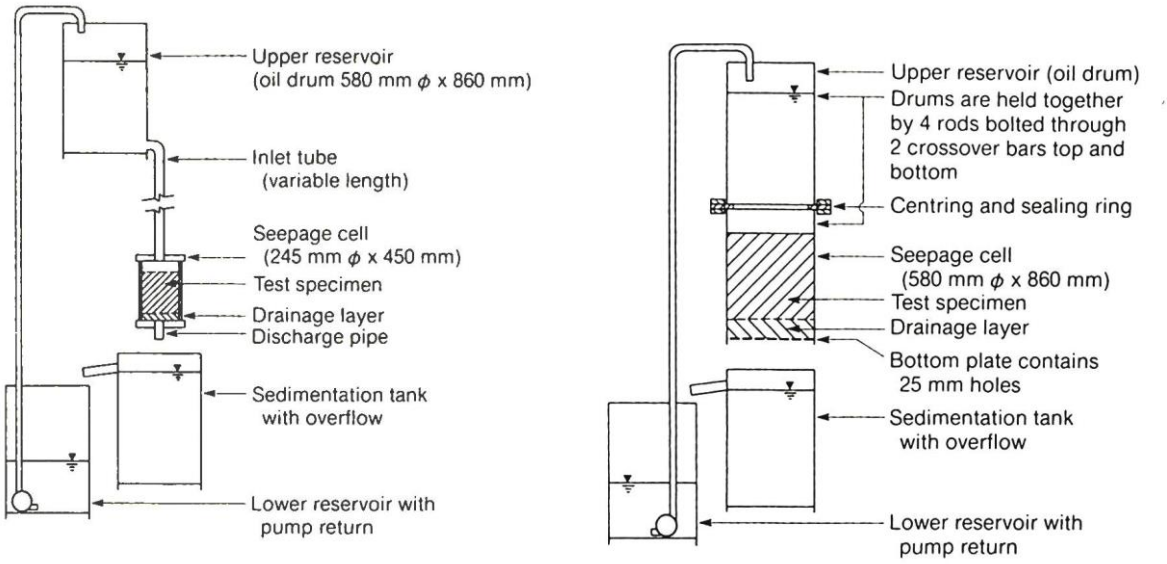

Figure.2.5 Test arrangement using 245mm and 580mm diameter seepage cell (Kenney and Lau, 1985)

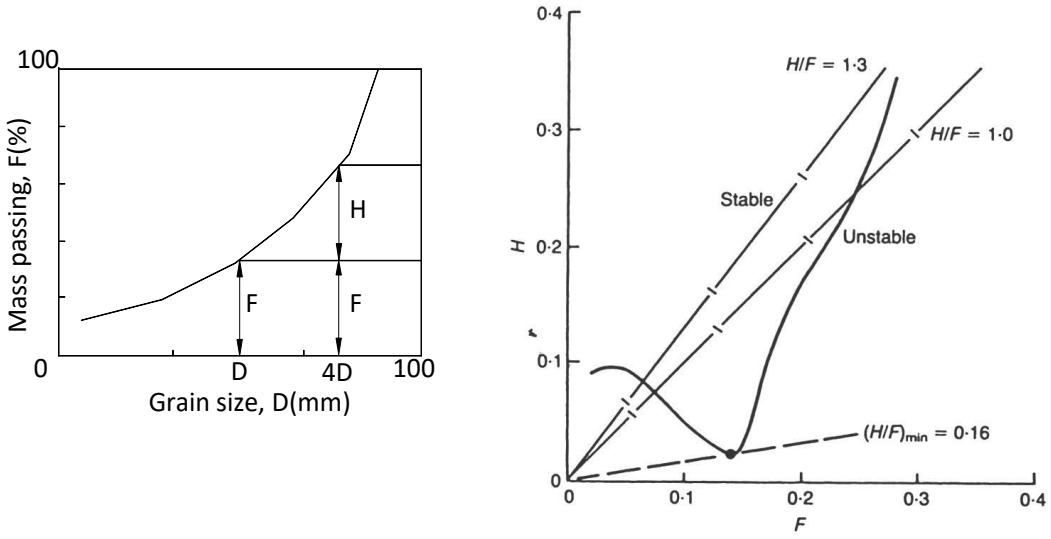

Figure.2.6 Kenney and Lau criterion
(Synthesized by Skempton and Brogan 1994)

its shape is described using the mass fraction (H) that occurs over a designated grain size interval of D to 4D compared to the mass passing (F) at grain size D. If the grading curve (Relationship between H and F) lies below a boundary defined by H = 1.0F (Kenney and Lau, 1986), over a portion of its finer fraction given by F ≤ 20% for soils with a primary fabric that is widely-graded (U_c > 3), and by F ≤ 30% for soils with a primary fabric that is narrowly-graded (U_c ≤ 3), and then it is deemed potentially unstable (see Figure.2.6).

2.2.3. Comparison of the Kezdi and the Kenney and Lau methods

Chapuis (1992) demonstrated the methods of the Kezdi (1979) and the Kenney and Lau (1985, 1986) in similar mathematical expressions. The secant line was established by the gradation curve at any point of slope. The secant slope of the grain-size distribution curve

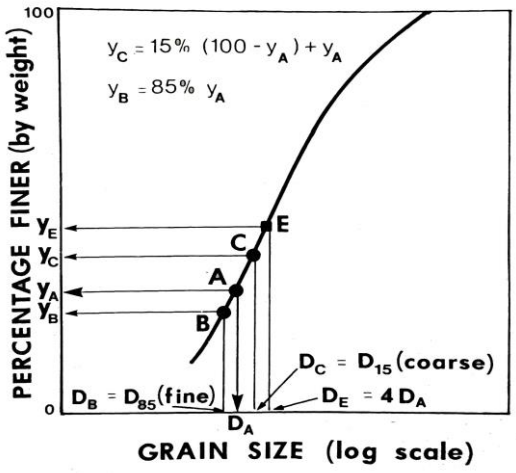

Figure.2.7 Illustration of relationship between the criteria about suffusion by Chapuis (1992)

indicates the risk of internal instability. Consequently, the Kezdi criterion is equivalent to the following: if a soil has in its gradation curve a slope lower than 24.9%, it will be unable to stabilize its own particles finer than the grain size at which such a slope occurs. Similarly, the Kenney and Lau method is equivalent to the following; at a particle size Dy ($y \leq D_{20}$), the slope per cycle of the gradation curve must be higher than 1.66 y_A to be internal stability (see Figure.2.7). Chapuis also suggested that these criteria must be applied with caution by experienced people. In particular, there is little information on the influence of such factors as (i) the severity of disturbance forces, due to either vibration or seepage; (ii) the stabilizing or destabilizing effects of disturbing forces; (iii) the void ratio; (iv) the initial segregation of the soil.

Li and Fannin (2008) have assessed both of the methods of Kezdi (1979) and the Kenney and Lau (1985, 1986). The criteria are similar, in which assessment on internal instability of soil requires an evaluation of the slope of grain size distribution curve. However, both of these methods are a little conservative. In particular, the Kezdi method is relatively more conservative at F < 15% and Lau method is more conservative at F > 15 %. Li and Fannin found a plot of the respective Kezdi and Kenny and Lau boundaries, in index relationship between F and H. In particular, at values of F> 15%, the criterion of Kenny and Lau defines a boundary to internal stability locates above that of the Kezdi criterion. Conversely, the boundary in the criteria of Kezdi locates above that of Kenny and Lau criteria at F<15%. Li & Fannin (2008) suggested that "limit values to the stability of D'15/D'85 = 4 and H/F = 1 yield a unique point on the gradation curve where both criteria

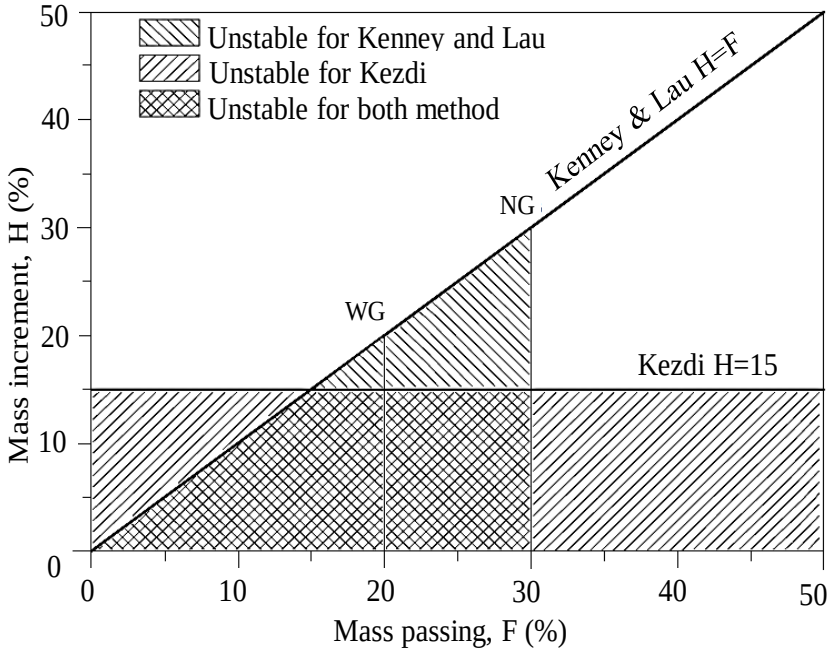

Figure.2.8 Synthesis of Kezdi A's and Kenney TC and Lau's criteria (Li and Fannin (2008))

converge at F=15%". In addition, the Kenney and Lau criterion at H/F<1 yields a more accurate distinction between stable and unstable gradations at F<15%. On the other hand, the Kezdi criterion yields a more accurate distinction at F>15%. The comparison between two criteria is summarized in Figure.2.8.

2.2.4. Burenkova method (1993)

Burenkova (1993) proposed boundaries separating the "suffosive soils" from "non-suffosive soils" based on results of laboratory tests on cohesionless and graded soils of maximum particle size up to 100mm, and coefficient of uniformity, C_u, up to 200. In test process, the soils were divided into various size fractions, and then dry-mixed in a container. Based on the three representative fractions d_{15}, d_{60}, and d_{90}, the internal stability of granular soils was deemed stable if the finer particles fully filled the voids of the coarse fraction that forms the primary fabric. Burenkova (1993) suggested that the internal stability of the soil was described by two ratios called conditional factors of uniformity d_{90}/d_{60} and d_{90}/d_{15}. Based on these two ratios, boundaries separating the "suffosive soils" and the "non-suffosive soils" as shown in Figure.2.9. Zones I and III represent suffosive granular soils; Zone II represents non-suffosive granular soils; Zone IV represents artificial soils. The zone for non-suffusive granular soils can approximately be expressed in function of the defined conditional factors of uniformity as follows:

$$0.76 \log(d_{90}/d_{15}) + 1 < d_{90}/d_{60} < 1.86\log(d_{90}/d_{15}) + 1 \qquad (2.4)$$

where d_{90}, d_{60} and d_{15} are the particle size when the cumulative percentage pass are 90%, 60% and 15%, respectively.

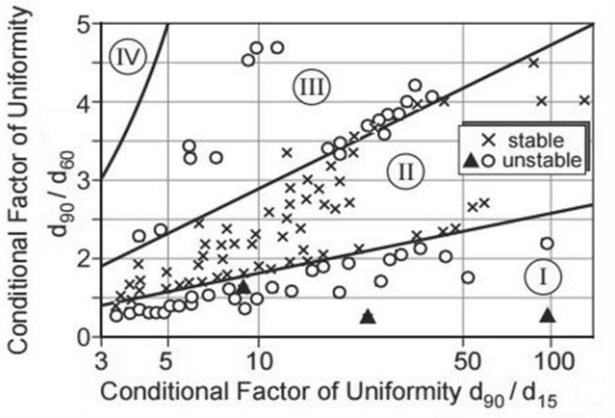

Figure.2.9 Burenkova criterion

2.2.5. Skempton and Brogan (1994)

Skempton and Brogan (1994) reported new findings from piping tests on well-graded and gap-graded of sandy gravels. The purpose of this criterion is proposing a relationship between the full theoretical gradient and the internal erosion process of soils. In order to accomplish the purpose, test specimens were performed by the apparatus with a transparent 13.9 cm in diameter and a length of approximately 15.5 cm as shown in Figure.2.10. About test procedure, test material is mixed well with target water content to avoid segregation. Then, it is placed in the cylinder, and four layers each about 40 mm thick were packed by hand. Under a small water head, the sample becomes saturated and water comes out from the top surface of the sample. After saturation of the specimen is completed in a cylinder, upward water flow was imposed and increased until piping occurred. Internal instability yields a big increase in the velocity of seepage flow. An abrupt transition was used for confirming the Kenney and Lau (1985, 1986) criterion for internal stability, and also the Kezdi (1979) criterion. The test results show that migration and the strong piping of fine particles take place in unstable materials can occur at hydraulic gradients of about one-third to one-fifth of the theoretical critical hydraulic gradient, based on Terzaghi's equation. Therefore, a relation was proposed between critical gradient ($i_c < 1$) and Kenney and Lau's stability index $(H/F)_{min}$, as shown in Figure.2.11. In addition, according to Skempton and

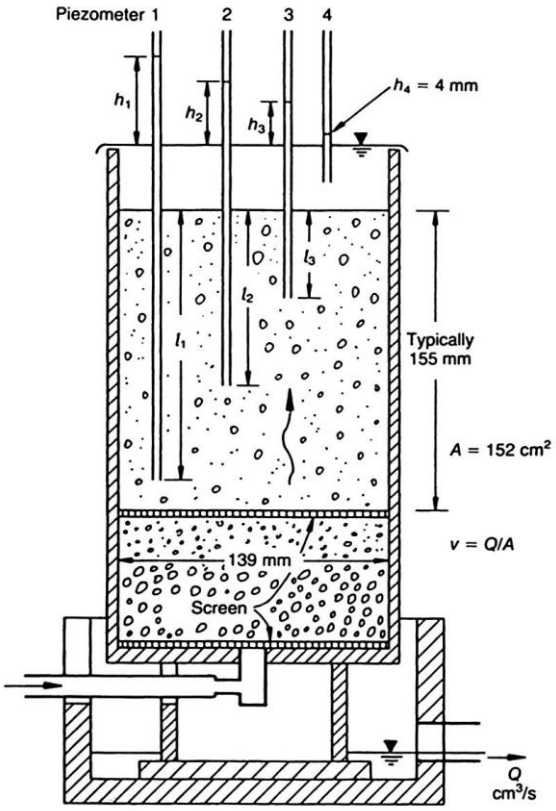

Figure.2.10 Schematic diagram of piping testing apparatus (Skempton and Brogan, 1994)

Brogan (1994), coarse particles float in a matrix of fines if the fines content exceeds approximately 35%. The coarse particles are no longer in contact with each other and they would become less effective filter medium.

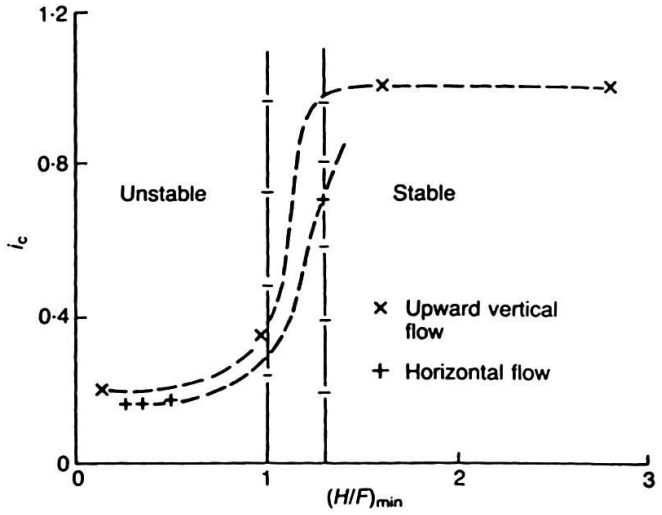

Figure.2.11 Relationship between critical gradient (i_c) and $(H/F)_{min}$ (Skempton and Brogan, 1994)

2.2.6. Chang and Zhang (2013)

Chang and Zhang (2013) used three geometric criteria of Istonima, Kezdi, and Kenney and Lau to assess the internal stability of 131 soils in a laboratory test from literature. These soils divided into three categories: Category I (with fines contents less than 5% for well-graded soils and 10% for gap-graded soils), Category II (with fines contents more than 20% for well-graded soils and 35% for gap-graded soils), and category III (with fines contents between 5% and 20% for well-graded soils and between 10% and 35% for gap-

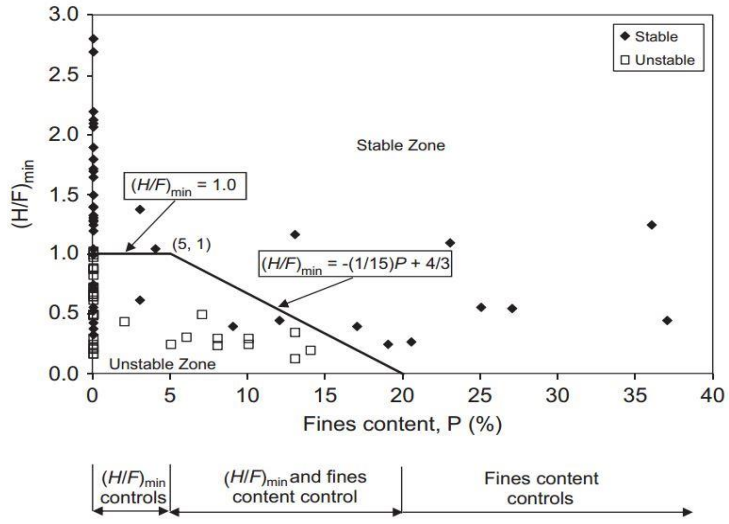

Figure.2.12 Hydraulic criterion for well-graded soils (Chang and Zhang 2013)

graded soils). Chang and Zhang (2013) proposed extending internal stability criteria for well-graded and gap-graded soils using control variables fines contents based on their microstructures. As a result, the composite internal stability criteria for both well-graded and gap-graded soils are proposed based on components such as fine fraction, $(H/F)_{min}$ and gap ratio of materials. The internal stability of a well-graded soil with a fines content of less than 5% and between 5% and 20% can be assessed according to a relation between $(H/F)_{min}$ and fines content (see Figure.2.12). A well-graded soil with a fines content of more than 20% is deemed to be internally stable. The internal stability of a gap-graded soil with a fines content of less than 10% can be assessed using the gap ratio equal to 3.0 (see Figure.2.13), and the internal stability of a gap-graded with a fines content of between 10% and 35% can be assessed based on gap ratio and fines content of soils (see Figure.2.14). A gap-graded soil with a fines content of more than 35% is deemed to be internally stable.

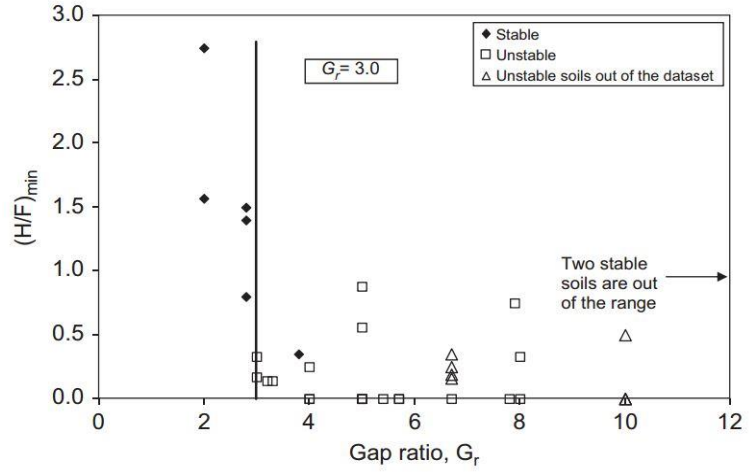

Figure.2.13 Hydraulic criterion for gap-graded soil with a fines content of less than 10% (Chang and Zhang 2013)

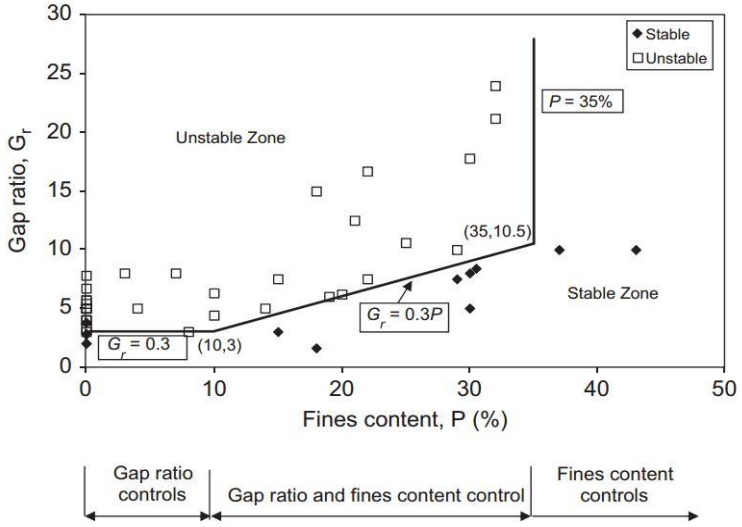

Figure.2.14 Hydraulic criterion for gap-graded soil with a fines content of of between 10% and 35% (Chang and Zhang 2013)

2.3 Engineering problem of volcanic soils deposited in Hokkaido

Volcanic soils were created by eruptions of volcanoes. Volcanic ash soils cover approximately 124 million hectares or 0.84% of the world's land surface (Leamy, 1984). Approximately 60% of volcanic ash soils occur in tropical countries. They were used for building of continents, oceanic islands, and the ocean floor; creation of magnificent scenery and recreation areas, and the development and rejuvenation of soils which provide an environment favorable to the eventual establishment of lush vegetation and the ecology of organisms, including human beings.

Japanese islands exist within the Pacific orogenic zone. Consequently, there are numerous volcanic activity in Japan. Volcanic soils, which are a product of explosive eruption of volcanoes, have many kinds. Their deposition characteristics and physical properties have been introduced by Shimizu (1999). Volcanic activities create the clastic materials ejected from volcanoes and transported through the air, namely Tephra. Classification for the deposits of Tephra could be divided the following two groups by the generating process: Tephra fall deposit (*fa*); pyroclastic flow deposit (*fl*). The tephra fall deposit formed through the aerial transportation of volcanic ejecta are deemed to comparatively-uniform grain size distribution, and the distance from the volcano affects the texture and shape of the tephra fall deposit. The distribution of volcanic ground was widespread and relates most of failures and damages induced by earthquakes in Japan. Figure.2.15 shown distribution of volcanic deposits in the Japanese islands and recent great earthquakes induced the serious damages to each region. Especially, in 2011 off the Pacific

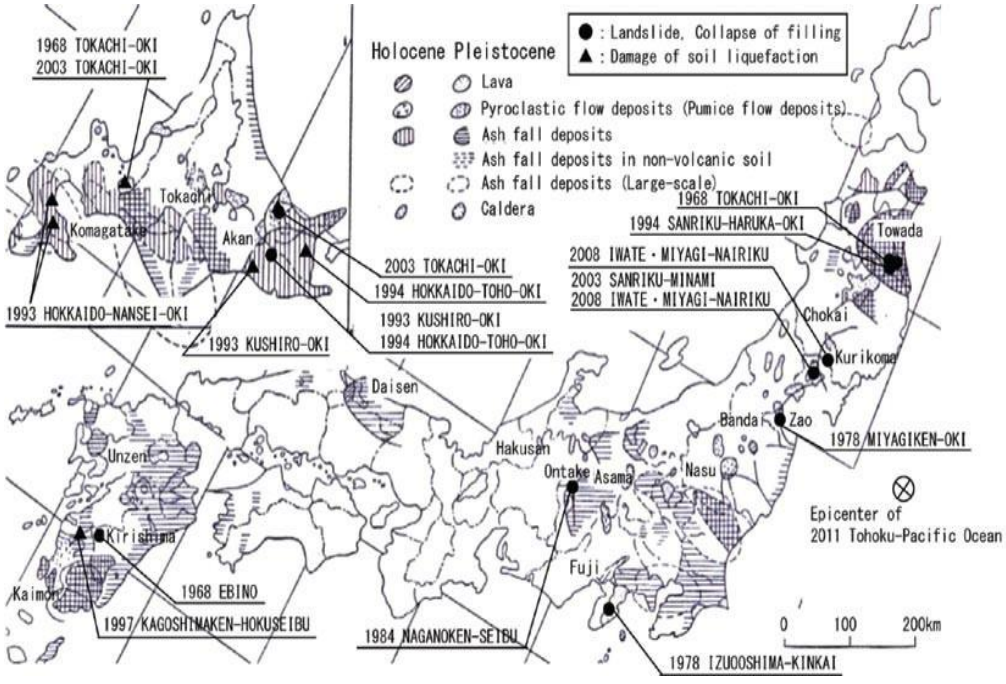

Figure.2.15 Recent great earthquakes induced serious effect on volcanic deposits areas at Japan islands.

coast of Tohoku Earthquake, serious damage by subsequent tsunami was widely generated in Japan, and road embankments in Tohoku expressway. After that terrible disaster, construction of embankment having a high performance and quality will be required in Japan.

2.3.1. Volcanic soils in Hokkaido and its classification

In Hokkaido, there are over forty Quaternary volcanoes, and pyroclastic materials cover over 40 % of its area. The mechanical property of volcanic soil grounds vitally depends on the sedimentary structure, components, distributional area and degrees of the weathering. In this study, typical volcanic coarse grained soils were mainly used, which spouted out from three volcanoes in Hokkaido, as shown in Figure.2.16 (Miura, 2012). Particularly, sampling sites include Pyroclastic fall deposit (*Ko-d*), Shikotsu primary tephra (*Spfa-1*, *Spfl*) and pyroclastic fall deposit (*Ma-l*). In which, *Ko-d* samples were taken from Mori Town in Hokkaido, which originated from the eruption of Mt. Komagatake (1640). secondly, *Spfa-1*, *Spfl* samples were taken from five sites in Hokkaido such as Tomikawa district in Monbetsu Town (Tomikawa volcanic soil), Kashiwabara and Utonai districts in Tomakomai City (Kashiwabara volcanic soil and Utonai volcanic soil), Bibi district in Chitose City (Bibi volcanic soil) and Hayakita Town (Hayakita volcanic soil), which was result of the eruption of volcanoes from 31,000~34,000 years ago. Finally, pyroclastic fall deposit (*Ma-l*) were sampled from Musa district (Nakashibetsu Musa volcanic soil), Touhoro district (Touhoro volcanic soil) and the airport area in Nakashibetsu town (Nakashibetsu A volcanic soil). These volcanic soils were formed 11,000~13,000 years ago. Consequently, it will be diverged (e.g., Miura, 2012; Miura et al., 2003). Pyroclastic materials could be classified as pyroclastic fall deposit (*fa*) and pyroclastic flow deposit (*fl*) by the generating process, as represented above. Figure.2.17 shows the distribution area of pyroclastic deposits in Hokkaido, those symbols separating the pyroclastic fall deposit and the pyroclastic flow deposit.

Such volcanic soils have been also used as useful construction materials, especially man-made earth structures (embankments and cut slopes, etc.) in Hokkaido. In recent decades, although volcanic soils have been classified as “problematic soils” in Japan engineering research (IS-Tohoku, 1998). However, the research on volcanic soils from the engineering standpoint is extremely superficial in comparison with cohesionless soils (e.g., Miura et al., 2003). A large number of earthquake- and rainfall-induced failures of artificial slopes such as cut slopes or embankments has been reported in Hokkaido, Japan which are composed of volcanic soils (e.g., JSSMFE, 1995; JSCE, 2004). Examples, the liquefaction include embankment slope failures in Sapporo due to 2003 Tokachi-oki earthquake, Slope failure at Aratozawa due to 2008 Iwate-Miyagi earthquake and Slope collapse around Aso Volcano due to 2016 Kumamoto earthquake. Figure.2.18 shown some disasters due to earthquakes in Hokkaido. In addition, many cases of rainfall-induced failure occur mainly

from spring to summer in Hokkaido, Japan; for example, cut slope failure on the Hokkaido Expressway (1999) due to rainfall and snow-thaw water in the spring of 2012 and 2013 (Yamazaki, et al, 2000). A significant amount of research has been accumulated on the mechanisms of slope failure induced by rainfall and earthquake. However, researches on failure of volcanic slopes have been limited in cold regions. Kawamura et al., (2015) elucidated failure mechanisms of volcanic slopes in cold regions, and proposed a prediction method on the failure based on observation of a full-scale embankment slope which has 5 m in height and 2.7 m in width and 4 m in length which was constructed by volcanic soils in Sapporo city Japan, and laboratory tests. The volcanic soil in the field was adopted as a test material. After the completing construction of the embankment, the changes in soil moisture, temperature, and pore water pressure in the embankment were investigated until slope failure by using several monitoring devices such as soil moisture meters and thermocouple sensor, etc. Simultaneously, a series of model tests in the laboratory was performed on small size slopes constructed by the same soil material as that in the field. According to Kawamura et al., (2015), the failure mechanisms of volcanic slopes in cold regions significantly depend on freeze-thaw action. Moreover, if the changes in water content in slope subjected to rainfall are simply estimated, slope failure can be predicted. Mechanisms of volcanic slope failure in cold regions are depicted in Figure.2.19.

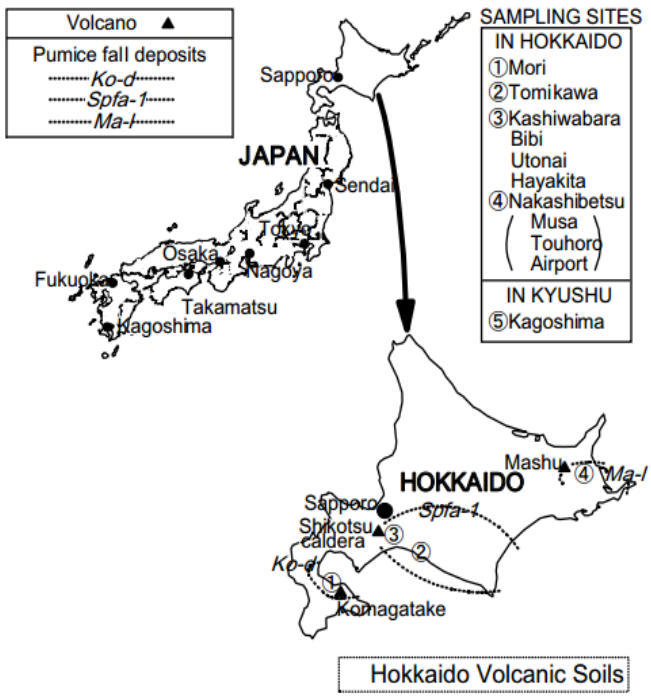

Figure.2.16 Typical volcanoes and sampling sites in Hokkaido (Revision of Miura, 2012)

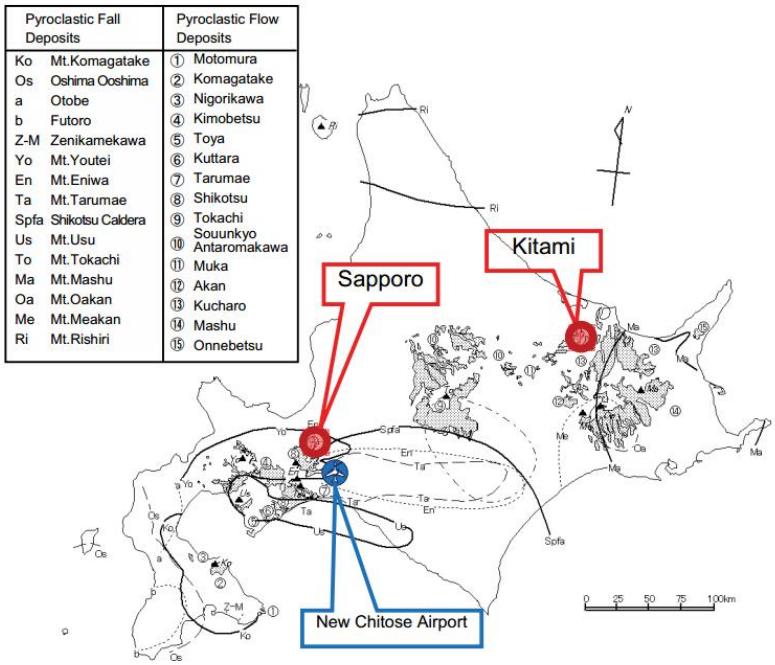

Figure.2.17 Distribution of pyroclastic deposits in Hokkaido (Revision of Miura, 2012)

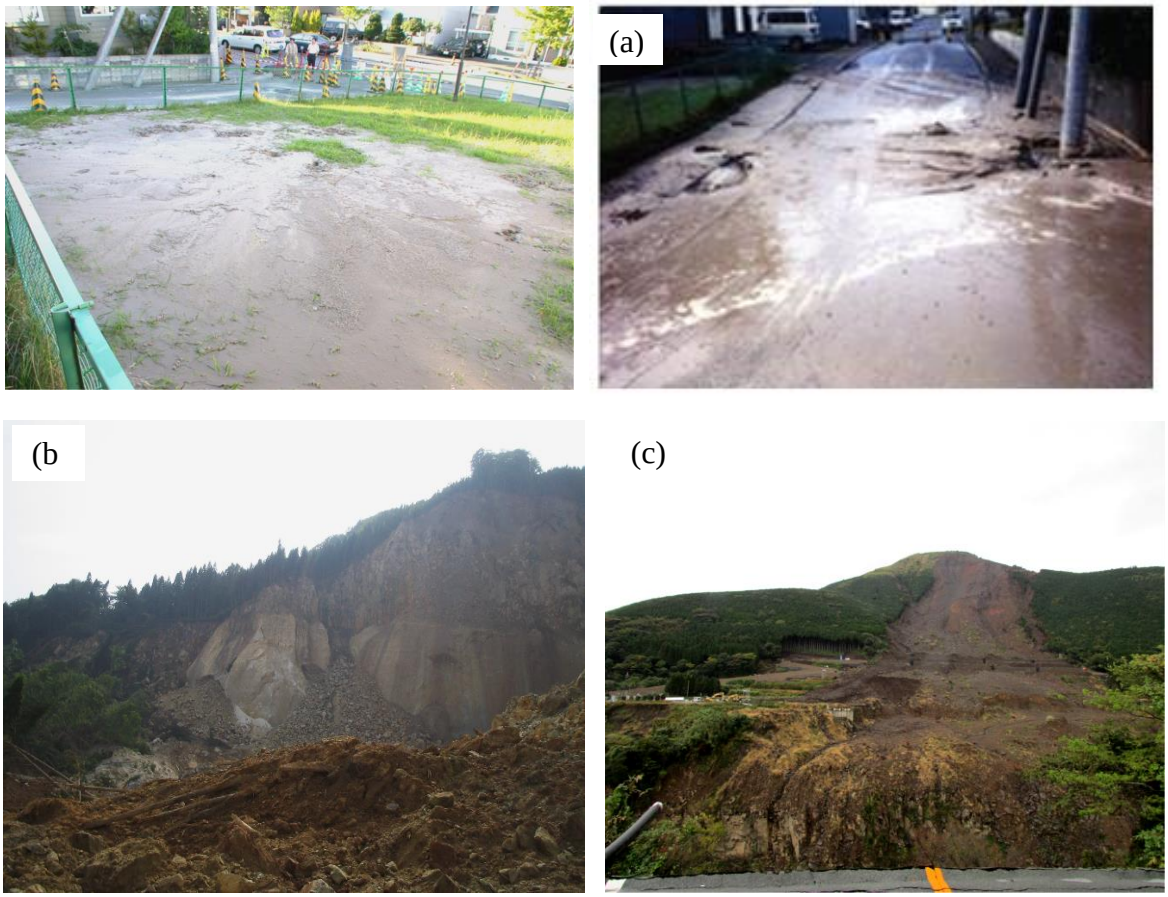

Figure.2.18 Some typical disasters due to earthquake in Hokkaido: (a) Liquefaction in Sapporo due to 2003 Tokachi-oki earthquake (Miura 2012); (b) Slope failure at Aratozawa due to 2008 Iwate-Miyagi earthquake; (c) Slope collapse around Aso Volcano due to 2016 Kumamoto earthquake

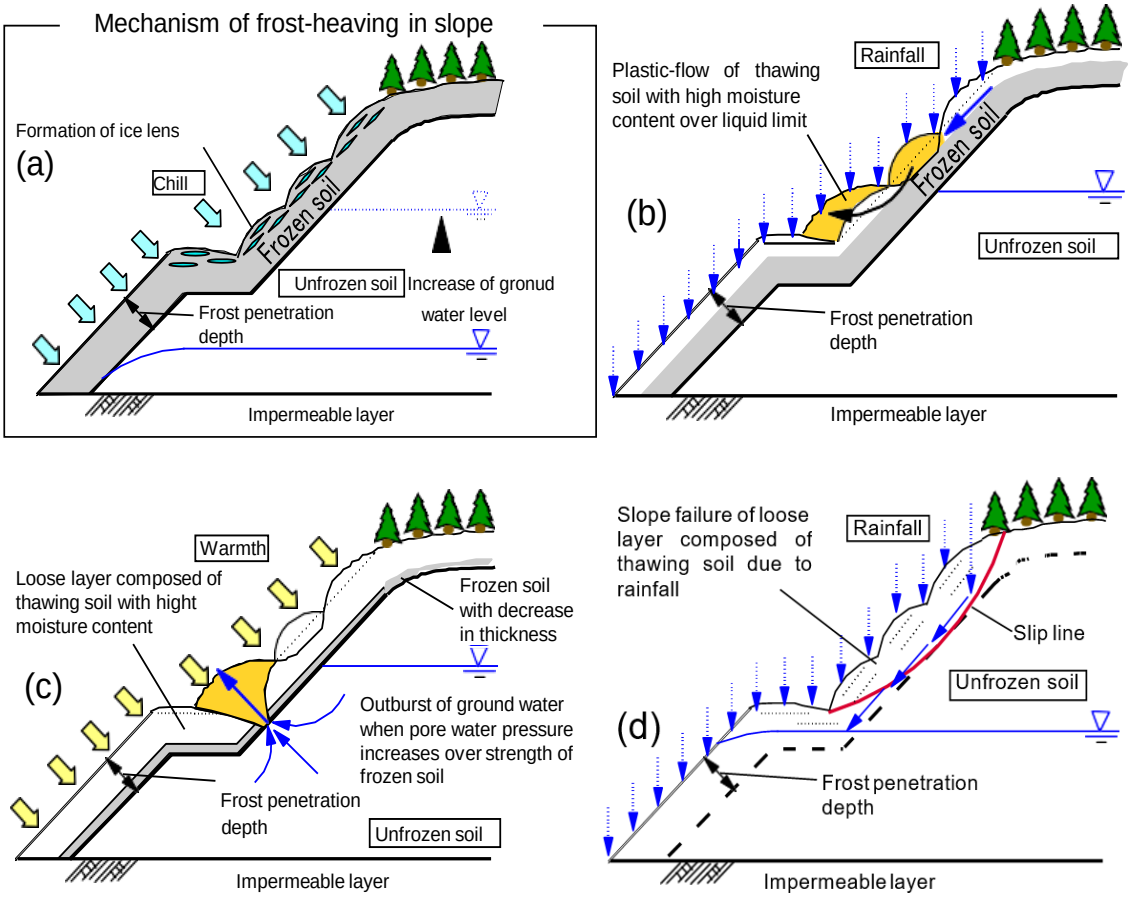

Figure.2.19 Failure mechanism of cut slope observed for cold regions: (a) mechanism of frost-heaving in slope, (b) surface failure due to flowing soil, (c) slope failure due to internal erosion, (d) slope failure due to rainfall

2.3.2. Mechanical properties of volcanic soil in Hokkaido

The mechanical properties of volcanic soils depend on the generating process such as pyroclastic fall deposit (*fa*) and pyroclastic flow deposit (*fl*). In addition, sedimentary structure, components, distributional area and degrees of the weathering greatly differ with the depositional environment also affect these properties of volcanic soils. For example, the pyroclastic flow deposit which is products of gravity action of pumice, volcanic ash soil and scoria ejected and flowed above the ground from the volcano was evaluated to well-grained soils. Meanwhile, the pyroclastic fall deposit has comparatively-uniform grain size distribution, which depends on the distance of falling down of volcanic ash and pumice from the volcano.

The mechanical property of volcanic coarse-grained soils is considered based on knowledge about features such as porosity and crushability, etc. Miura and Yagi (1997) presented that the mechanical behavior of volcanic soils, which was varied in a different stress or consolidation history, connecting with the particle crushability. The crushability evaluation depends on finer content increment ΔFc (%) for volcanic soils. The validity of

the Δ*F*c evaluation was discussed as shown in Figure.2.20. In addition, Nakata and Miura (2007) focused on analyzing the porosity and crushability of constitutive particles of the volcanic coarse-grained soils. They proposed an estimation method of void structure and its change for the volcanic coarse-grained soil. In research process on those particles, the void inside of particles such as "opening intra-particle void" and "closing intra-particle void" was modeled as shown in Figure.2.21 and 2.22. From a series of test results on the volcanic coarse-grained soils in Hokkaido, void ratio was calculated, based on relating to the dry density of these volcanic soils. They indicated that the particle breakage characteristic strongly depended on opening intra-particle void ratio.

In addition, based on finer content *F*c (%) (< 0.075 mm) and the liquid limit w_L, etc. the Japanese Geotechnical Society, JGS has proposed the geotechnical classification of the volcanic soils. Based on amount of fine particles of volcanic soils, Hokkaido soil classification committee classified volcanic soil into main two groups. In particular, volcanic soils with *F*c < 50 % and *F*c ≥ 50 % are qualified for as "volcanic coarse-grained soil" and "volcanic fine-grained soil", respectively. The volcanic coarse-grained soil is primary sediment or secondary one generated by the volcanic ash, the pumice, and the scoria, while the volcanic fine-grained soil relates to the weathered volcanic coarse-grained soil. Table 2.4 shows classification of volcanic soils by the Japanese Geotechnical Society. In this study, the sampling site from the Shikotsu caldera in Hokkaido was used. This sample is hereafter referred to as Komaoka volcanic coarse-grained soil, which will be discussed in detail.

Table 2.4: Volcanic soils classification by the Japanese Geotechnical Society

<table>
<tr><td></td><td>Fine-grained soil</td><td colspan="2">Coarse-grained soil</td></tr>
<tr><td rowspan="2">Finer fraction F_c(%)</td><td rowspan="2">$F_c \geq 50\%$</td><td rowspan="2">$F_c \leq 50\%$</td><td>Volcanic soil (G-V, S-V): $5\% \leq W_L < 15\%$</td></tr>
<tr><td>Volcanic soil (GV, SV): $15\% \leq W_L < 50\%$</td></tr>
<tr><td rowspan="3">Volcanic cohesive soil (V)</td><td>Low liquid: $W_L < 50\%$</td><td colspan="2" rowspan="3"></td></tr>
<tr><td>Type I (VH1): $50 \leq W_L < 80\%$</td></tr>
<tr><td>Type II (VH2): $80\% \leq W_L$</td></tr>
</table>

Shirasu (SV), Kanto loam (VH1, VH2), Hachinohe loam (VL).

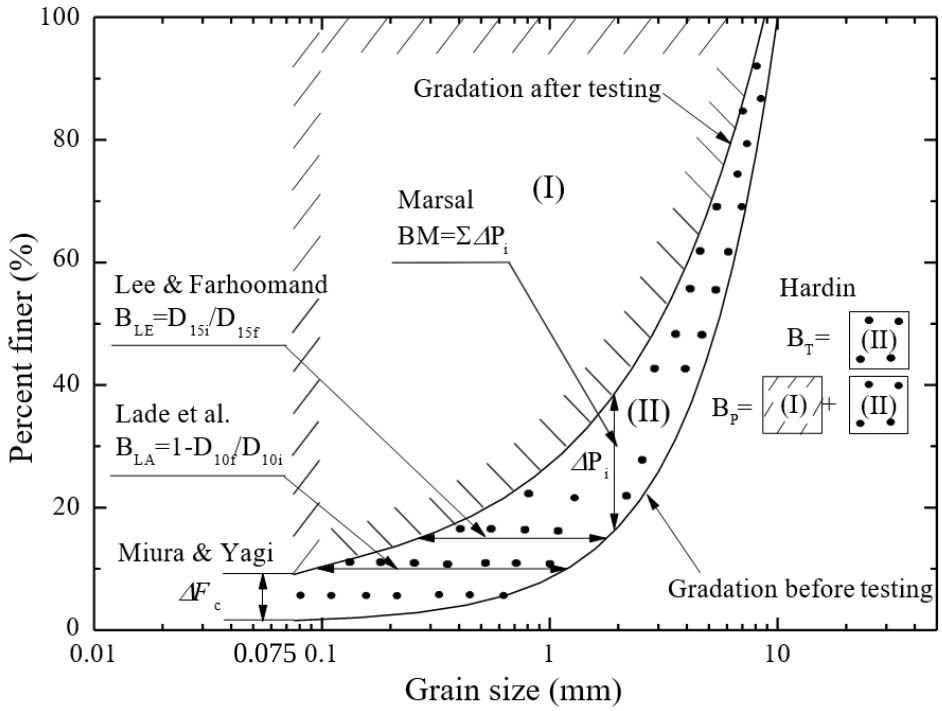

Figure.2.20 Schematic diagram of index for particle breakage (Miura and Yagi 1997)

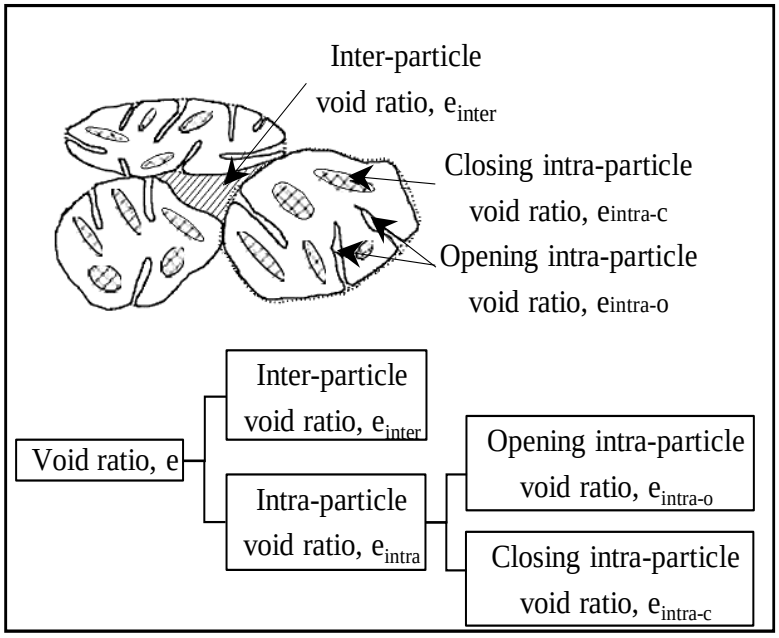

Figure.2.21 Schematic diagram of void ratio in volcanic soil
(revision of Nakata and Miura 2007)

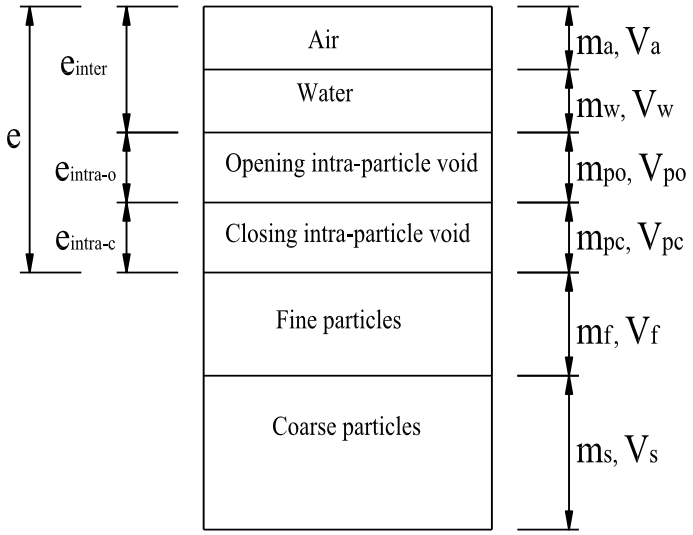

Figure.2.22 Diagrammatic representation of volcanic soil model
(revision of Nakata and Miura 2007)

2.3.3. Internal instability for volcanic coarse grained soils under seepage

Seepage flow in a soil mass induces seepage forces. Natural soils under the influence of seepage forces can induce a behavior in which grains of finer fraction pass through the pores of the coarse soil matrix. The phenomenon is termed internal instability that can occur in natural soil deposits and also in geotechnical structures such as embankment. Internal instability can be examined on geometric criteria such as the distribution of constriction sizes in the soil matrix. In particular, the grain size distribution is used for the assessment, as represented above.

In this study, investigation on internal instability under seepage of a full-scale embankment constructed by volcanic coarse grained soils was performed. Particularly, On November in 2012, a full-scale embankment of which the boundary conditions on each side (the right, left sides and back, bottom) were controlled, was constructed to generate slope failure with large deformation in Sapporo, Japan. The purposes of this construction are to grasp the mechanical behavior of the volcanic embankment in cold regions during all seasons and to confirm the validity of a proposed method for the rainfall-induced failure of slopes (Kawamura et al., 2015). The embankment was constructed using a road roller (weight of 5.88kN) by compacting a typical volcanic soil described later so as to be more than the degree of compaction Dc of 85% (the desired dry density is more than ρ_d =0.9 g/cm^3) for each layer of 0.25 m, as shown in Figure.2.23.

For the embankment, both sides were confined to wooden boards, back and bottom are covered by plastic sheets. The number of roller compactions was 3 times for each layer. According to the in-situ tests, the degree of compaction and water content was 95.9% (average) and 42.5% (average), respectively. The slope size was 5 m in height, 4 m in length,

2.7 m in width and the angle of 45 deg. (see Figure.2.24). The water supply pipes depicted in Figure.2.25 have holes at certain locations and intervals. The water was reserved in three tanks and provided through each pipe into the embankment. Water supply through the surface of the embankment was started from May 7, 2013. The amount of water supply was 1000~3000 l/day. Field monitoring was continued to November 15, 2013, from November 01, 2012. The details of construction procedures and test results were reported by Matsumura (2014) and Kawamura et al. (2015).

During field monitoring, exudation routes of water in the full-scale embankment were observed (Miura, 2014). For example, Figure.2.26 shows traces of exudation routes of water during field monitoring. The phenomenon occurred along embankment boundaries. According to the in-situ observation, fine particles were flowing out. This means that piping and exudation routes might be easily generated in volcanic man-made soil structures, although the embankment was actually compacted by more than the degree of compaction Dc= 95%. Figure.2.27 shows the aspects of cross-section after dismantling of the embankment. It can be seen from the photos that piping routes from holes of water supply pipe extend laterally. Through the field observation, it was pointed out that the evaluation of internal instability under seepage flow is significant for volcanic man-made structures containing a significant amount of fine particles.

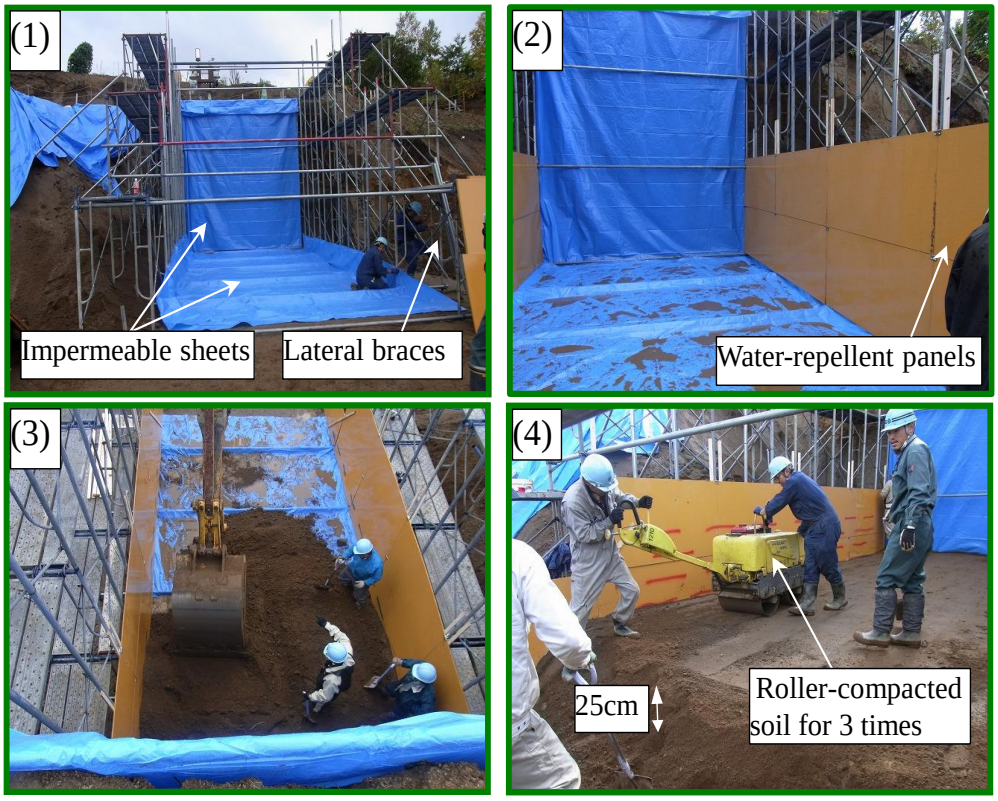

Figure.2.23 Construction procedures of FE-2012: (1) setting impermeable sheets and lateral braces; (2) setting water-repellent panels; (3) Filling soil; (4) Compacted soil

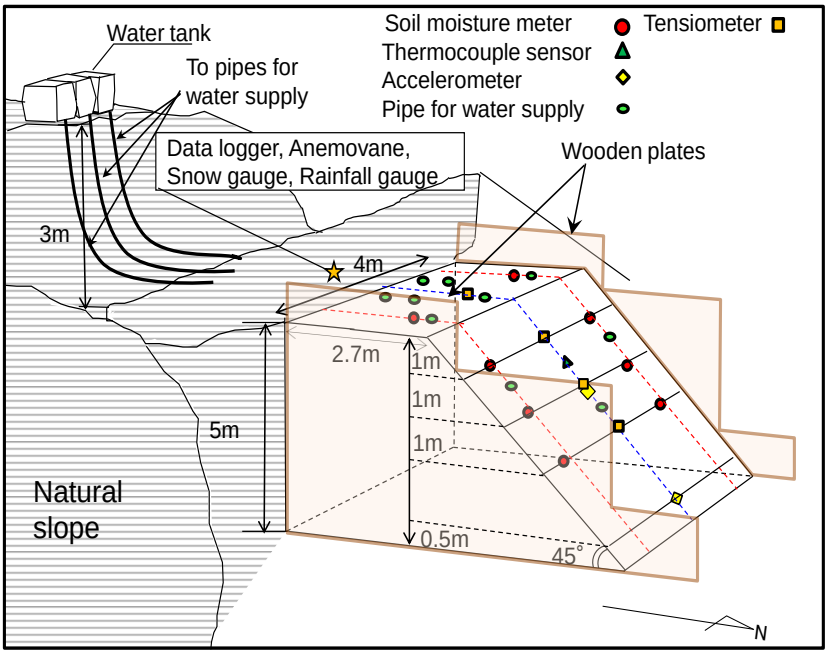

Figure.2.24 The whole view of full-scale embankment

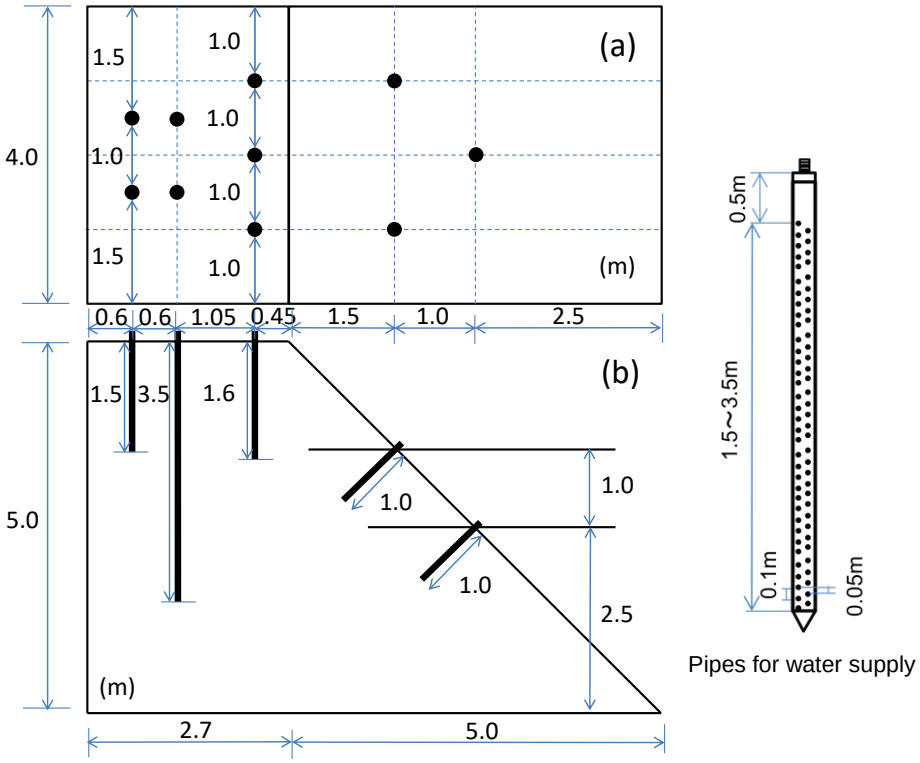

Figure.2.25 Locations and specification of pipes for water supply:
(a) plane view, (b) side view.

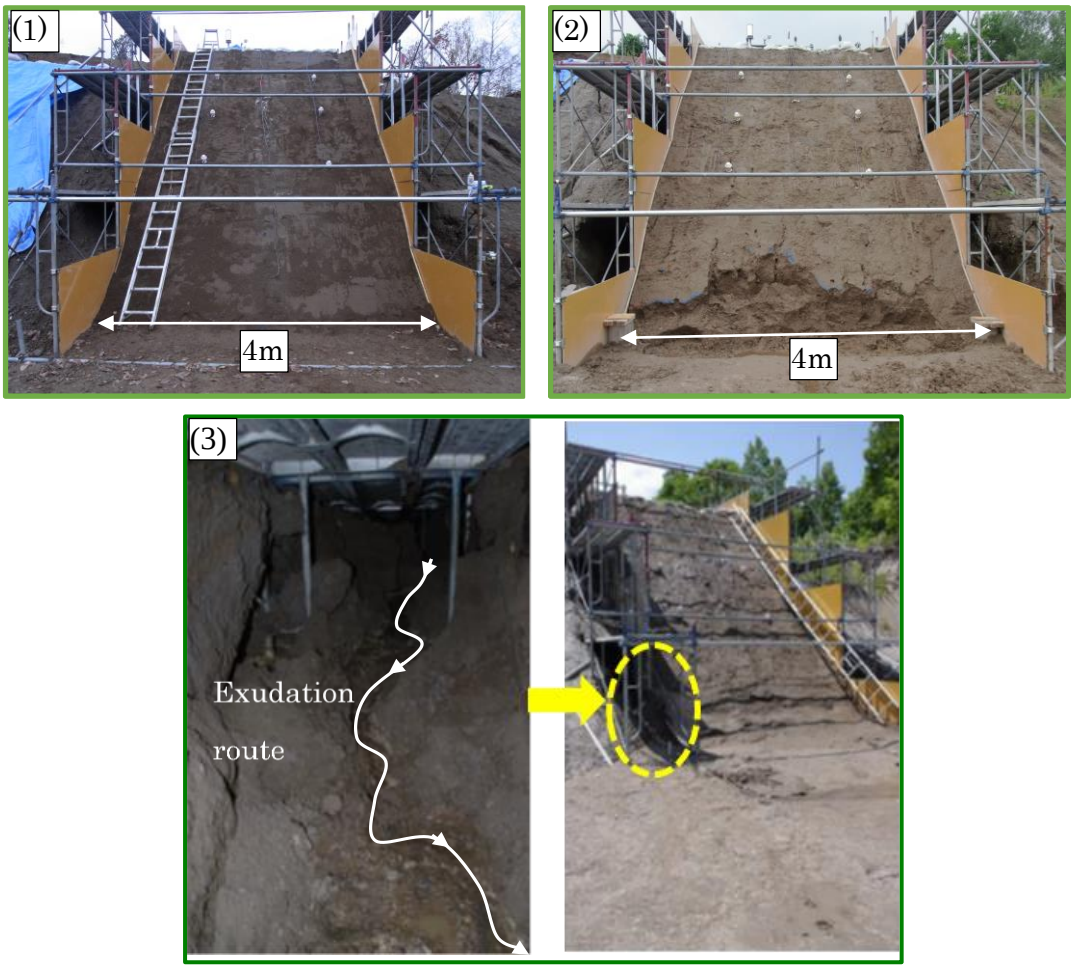

Figure.2.26 Observation of erosion process of embankment: (1) FE-2012 completely constructed; (2) slope shape after surface failure; (3) Trace of exudation routes during field monitoring (July 2013).

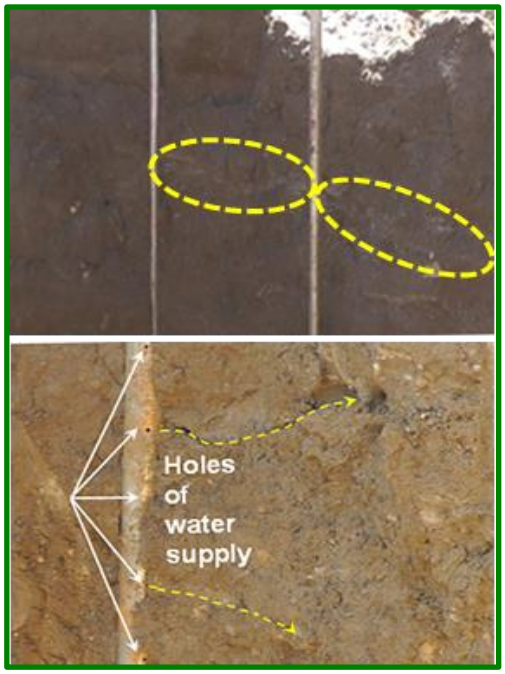

Figure.2.27 Aspects of cross-section after dismantling of full scale embankment.

2.3.4. Rainfall-induced failure of volcanic embankments subjected to cyclic loadings in cold regions

A heavy rainfall can induce gully and rill- erosion on surface of the embankment especially volcanic soil (JGS, 2011). For a reason, evaluation of rainfall infiltration is important for embankment subjected to cyclic loadings such as earthquake and freeze-thaw action. In previous study, the effect of freeze-thaw action and pre-deformation due to cyclic loading on seepage slope failure was elucidated by Kawamura et al. (2016). In this section, failure mechanism of volcanic embankments subjected to cyclic loadings in cold regions due to rainfall infiltration (seepage) is discussed based on experimental results.

In the mode test, volcanic coarse-grained soil which was sampled from the Shikotsu caldera in Hokkaido was used in the study. This sample is hereafter referred to as Komaoka volcanic soil. The model testing under a conventional approach to element testing is taken in terms of the 1g model testing. Figure.2.28 depicts a complete view of the apparatus used in the rainfall test and in the shaking table test. The soil container was 2,000 mm long, 700 mm deep, and 600 mm wide, and its front wall was made of reinforced glass to enable observation of deformation when failure occurred. In order to reveal the mechanical behavior of volcanic embankments subjected to pre-deformation due to cyclic loadings, a shaking table was also equipped in the soil container. The shaking table was 400 mm long, 450 mm deep, and 580 mm wide. The details of specifications were reported by Kawamura and Miura, (2014). Model slopes were constructed by compacting to attain the desired value where constituent particles were not broken by compaction under the initial water contents. The desired initial water content of the model slope w_0 is also shown in Table 2.5. In particular, two kinds of water content w_0=37 % and 43 % were adopted to evaluate the difference in water content between the drier and wetter sides as the boundary of the optimum water content on slope failure. For the cases of volcanic model slopes using a shaking table, after the desired shearing deformations (shear strain, γ=1.0%, 2.0%, 3.0%, 4.0% and 6.0%) for model embankments of w_0=37 % generated by cyclic loading of 200 gal, 280 gal or 550 gal, a series of rainfall model tests was conducted. The same input-accelerations as those for w_0=37 % were adopted as cyclic loads for model embankments of w_0= 43 %. The number of cycles was 20 times for all tests. For the cases of volcanic model embankments having pre-deformation subjected to freezing-thawing sequence, the surface of the slopes was frozen with dry ice over eight hours and was then thawed at 20^{o}C, frozen layers of around 50 mm in thickness were formed for the model embankments. Finally, rainfall intensity of 100 mm/hr. was typically adopted and was accurately simulated using spray-nozzles. Figure.2.29 shows the slope shape (45 deg. slope) and the setting positions of measurement devices. During the rainfall test, changes in deformation behavior, saturation degree and temperature were monitored using digital video cameras, soil moisture meters and thermocouple sensors,

respectively. Pore water pressure was monitored simultaneously. In the study, mechanical behavior at a shear strain of 6 %, as estimated by the deformations of seven strings of a kite, was defined as failure. According to the test procedure, the rainfall model testing was performed until slope failure was induced.

Figure.2.30 illustrates typical variation of accelerations at basement and crown for w_0 =43 %, compared with that of the shaking table. As shown in Figure.2.30, the maximum acceleration at the crown of embankment (A point) for both cases is larger than those at other points (B and C points).

The data of rainfall model tests after cyclic loadings on both the behavior of pore water pressure and changes in the degree of saturation for w_0= 43 % are exhibited in Figure 2.31 (a) and (b). A shear strain of γ=1.6 % was caused by cyclic loading of 280 gal for the model slope of w_0=43 % in advance. Rainfall-induced failure did not occur for this case although pore water pressure exhibited a high value, as shown in Figure.2.31 (a). This is due to the increases of both slope density and saturation degree derived by cyclic loadings. Actually, in comparison with the initial state, the degree of compaction D_c increased up to 23 %, and the degree of saturation increased to 1 % after cyclic loadings (see Figure.2.31 (b)). A similar tendency was confirmed for model slopes having γ=1.6 %~ 4.0 % for w_0=43 %. In contrast, slope failure occurred for model embankments having less than γ=1.6 %. On the other hand, slope failure was generated for the embankment for w_0=37 % with a prior cyclic loading of 280 gal. It is interesting that failure mode is changed depending on the difference in initial water content. The details of mechanical behavior of embankments during cyclic loading was reported by Kawamura and Miura (2014).

On the basis of the test results, a series of rainfall model tests after cyclic loadings and freeze-thaw sequence was also carried out for both water contents. Changes in development of water pressure and degree of saturation for w_0=43% are shown in Figure.2.32 (a) and (b). In comparison with cases not subjected to freeze-thaw action (see Figure.2.31), it is found that there are the differences in development of pore water pressure and degree of saturation between both cases for w_0= 43 %. For instance, pore water pressure increases gradually over $\Delta u/\sigma_{v0}'$=1, and then slope failure occurs although slope failure is not induced for the case not subjected to freeze-thaw action. Furthermore, the difference in elapsed time until failure was apparently confirmed, as described later (see Figure.2.33). On the other hand, the elapsed time subjected to freeze-thaw action for w_0 =37 % was almost the same as that of non freeze-thaw action.

In order to clarify the influence of freeze-thaw action on deformation behavior of model embankments, the amount of frost heaving was conventionally investigated for both water contents by using acrylic tubes (diameter is 50mm, height is 100 mm).The

displacement on frozen surface was 5.4 mm (strain, ε_v =5.4 %) for w_0=43 % and 1 mm for w_0 =37 % (strain, ε_v =1.0%). As a results, this fact implies that hollows caused by thawing generate loose structures in the frozen layer compared with before the freeze thaw process. Therefore, the effect of freezing-thaw action is significant for stability evaluation in cold regions; especially high water content (wetter side in this study).

Figure.2.33 summarizes the relationship between the elapsed time at failure for each case normalized by that of rainfall-induced failure of slopes for w_0=37 % (1,400 sec) and shear strain induced by cyclic loadings. It is apparent that the elapsed time at failure decreases with an increase of shear strain for the case of w_0 =37 %, and that the time slightly increases until γ=1.0 % and decreases for more than γ=4.0 % for the case of w_0 =43 %. Specifically, there is no failure zone in the range of 1.6 % to 4.0 % for the case of w_0 =43 % in rainfall test after cyclic loadings. Slope failure seems to differ depending on the stress-strain history due to cyclic loadings. On the other hand, for the cases subjected by freeze-thaw action, the elapsed time until failure becomes faster with the increase of shear strain for w_0 =37 and 43 %. Especially, the tendency is remarkable for w_0 =43 %. It is interesting that rainfall-induced failure is derived by freeze-thaw sequence for the case of which the degree of compaction of embankment increased due to cyclic loadings and did not fail. Therefore, the effect of stress-strain history due to both cyclic loadings and freeze-thaw action on failure mechanisms of embankments is significant for discussion on slope stability.

Figure.2.34 also shows the relationship between water content at failure and initial water content for all data. It is conspicuous that there are unique relationships between both water contents as well as those reported in previous study (Kawamura and Miura, 2013). For instance, the relationships can be expressed as follows;

$$w_f = \beta w_0^{\gamma} \tag{2.5}$$

where β and γ are coefficients of a give curve whose values are shown in Table 2.6. However, the trends are changed depending on the difference in stress history or initial water content. For example, water content at failure decreases for w_0 =37 % (water content in drier side on the optimum water content) with cyclic loadings only or both cyclic loading and freeze-thaw action, and also decreases for w_0 =43% (water content in wetter side) with freeze-thaw action. This indicates that void structures of constituent particles are loose structures due to cyclic loadings (for water content in drier side) or freezing and thawing (for water content in wetter side). As a result, it can also be said that slope failure can be predicted if the water retention capacity is estimated for embankments subjected to rainfall and cyclic loadings and freeze-thaw action in cold regions, as shown in Equation (2.5).

From the results, it was found that cyclic loadings and freeze-thaw action may cause the changes in fabric structures of soils. Therefore, evaluation of void structures is significant for internal stability of embankment subjected to freeze-thaw action and cyclic loadings such as earthquake.

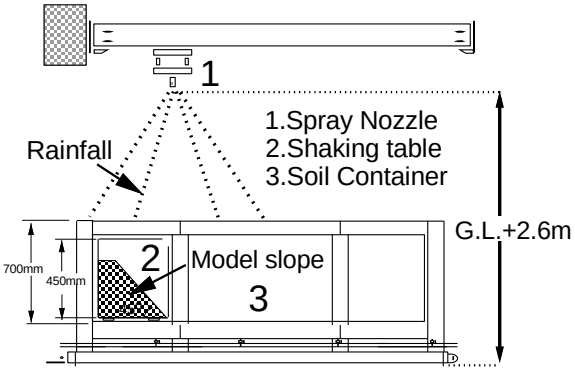

Figure.2.28 Whole view of apparatus

Table 2.5. Test conditions for this study

Slope condition	Non freeze-thaw action	Freeze-thaw action
Slope angle (°)	45	45
Length of base, B (mm)	750	750
Initial water content, w_0(%)	37,43	37,43
Dry density, ρ_d(g/cm^3)	0.90	0.90
Ranfall intensity, R(mm/h)	100	100
Acceleration (gal) [desired shear strain(%)]	200[1.0], 280[3.0], 550[6.0]	200[1.0], 280[3.0], 550[6.0]
Number of cycles	20	20

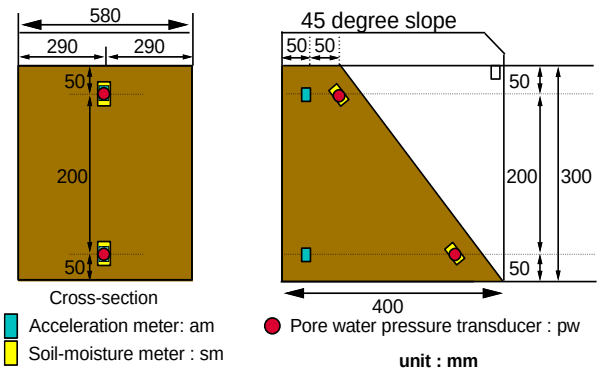

Figure.2.29 Model shapes and locations of measurement devices

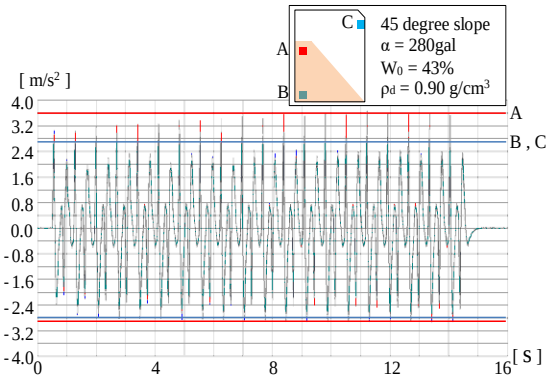

Figure.2.30 Variation of accelerations at basement, crown of embankment and shaking table for w_0=43 %

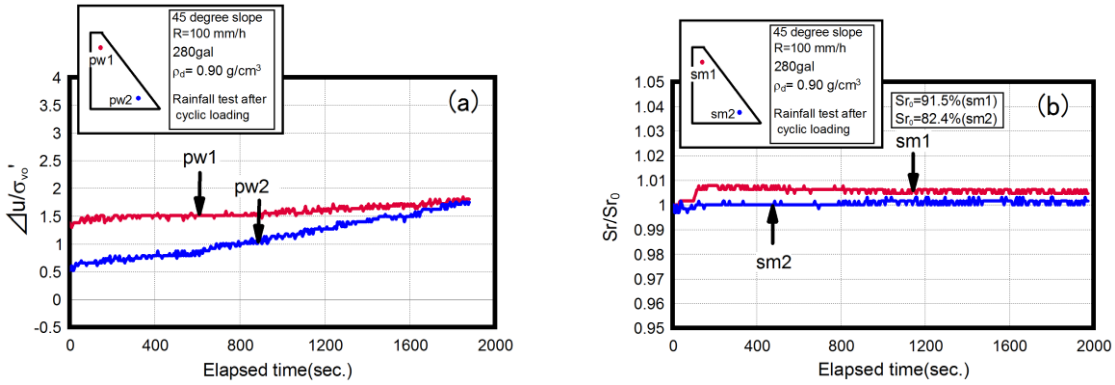

Figure.2.31 Changes in pore water pressure and saturation degree during rainfall test after cyclic loadings for w_0=43 %: (a) pore water pressure, (b) degree of saturation

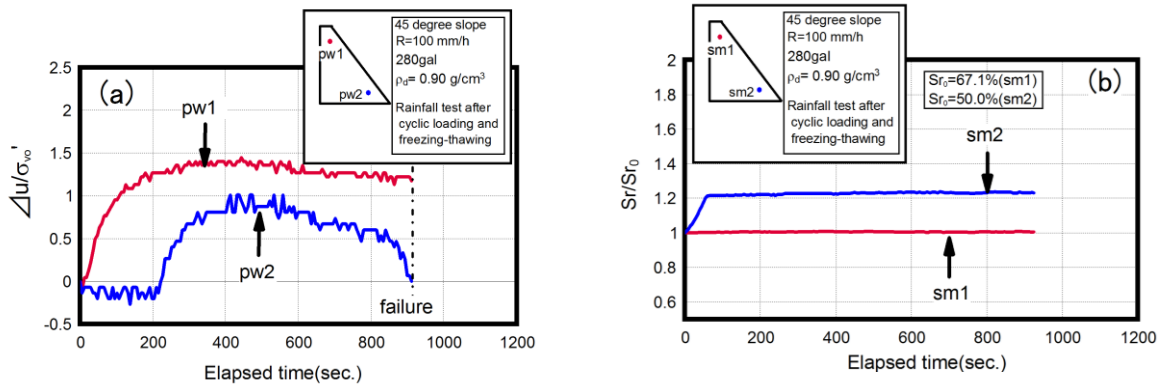

Figure.2.32 Changes in pore water pressure and saturation degree during rainfall test after cyclic loadings and freeze-thaw action for w_0=43 %: (a) pore water pressure, (b) degree of saturation

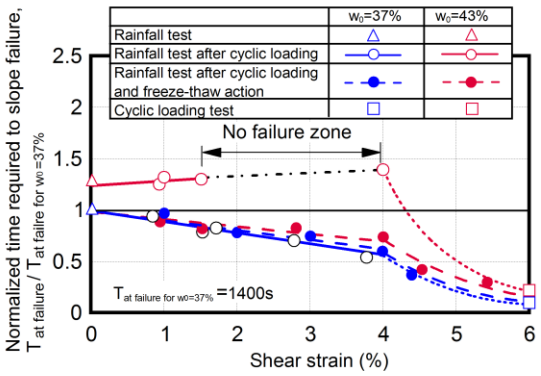

Figure.2.33 Relationship between elapsed time at failure and shear strain

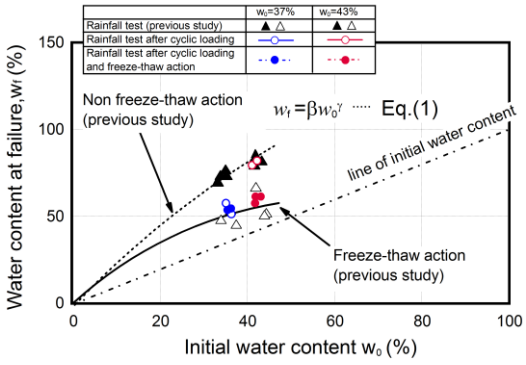

Figure.2.34 Relationship between water content at failure and at initial

Table 2.6. Coefficients of β and γ

		Komaoka	
		β	γ
Rainfall test without freeze-thaw action	37, 43	2.34	0.96
Rainfall test after freeze-thaw action	37, 43	2.78	0.80
Rainfall test after cyclic loadings	37	2.81	0.82
	43	2.34	0.96
Rainfall test after cyclic loading & freeze thaw action	37	2.81	0.84
	43		

2.4 Summary

Internal erosion in embankments and their foundations is the main cause of failures and accidents at embankments. In the world, half of the embankments were failed by internal erosion. Furthermore, many internal erosion problems in embankment appear on first filling but most occur many years after first filling. Therefore, internal erosion is a threat to existing embankments and improving the knowledge about assessing internal erosion is an important issue of the safety of these embankments.

Internal erosion initiates when the seepage force imposed by water flow through embankment exceed the resistance of the initial fabric structure of soil. Subsequently, soil particles within the embankment are transported to downward by seepage flow. These seepage forces are directly related to water level of the reservoir. Based on previous investigators, the four mechanisms of internal erosion are backward erosion, contact erosion, suffusion and concentrated presented in detail. In addition, internal erosion can be divided into two categories, those are piping studies and boiling studies based on observation of seepage tests.

In this chapter, the researches of previous investigators on internal erosion is summarized. These researches were performed based on assessing geometric conditions, hydrological mechanism and compaction conditions of soils. In particular, the geometric criterion for evaluating internal instability of soils under seepage flow was presented by Kezdi (1979) based on the conception of Terzaghi's filter rule (Terzaghi, 1939). Kenney and Lau (1985, 1986) criterion was proposed to assess the internal stability of granular soils. Li and Fannin (2008) had synthesized Kenzi's criterion and Kenney and Lau's criterion. Burenkova (1993) proposed a method to evaluate the internal stability of granular soils, therein a soil was deemed stable if the fine particles fully filled the voids of the coarse particles that constitutes the primary fabric. Based on dataset of previous internal stability tests, Chang and Zhang (2013) proposed extending internal stability criteria for well-graded and gap-graded soils under seepage flow. In addition, Skempton and Brogan (1994) presented internal erosion induces the instability of the soil leading to decrease of critical hydraulic gradient compared to the theory of Terzaghi. However, the soils tested by most of these authors are sand and gravels. The exception is Burenkova (1993) who investigated silt-sand-gravel soils but tests were conducted under very high gradients which will not occur in embankment. In order to further verify and generalize the previous observations, additional testing is needed on various soil gradations. Especially, soils contain a significant amount of fine particles with low plasticity such as volcanic soil.

Volcanic soils have been also used as useful construction materials, especially man-made earth structures in Hokkaido. However, volcanic soils have been classified as "problematic soils" in Japan engineering research. The mechanical property of volcanic

coarse-grained soils is considered based on knowledge about features such as porosity and crushability, etc. These soils are constituted by porous and brittle particles, and those are prone to significant particle crushing by external loading. Furthermore, previous researches indicated that particles of volcanic soil contain inside void such as “opening intra-particle void” and “closing intra-particle void”. This may influence seepage performance of volcanic soils.

Investigation on internal instability under seepage of a full-scale embankment constructed by volcanic coarse grained soils was performed. As a result, exudation routes of water in the full scale embankment were observed. According to the in-situ observation, fine particles were flowing out. This means that piping and exudation routes might be easily generated in volcanic man-made soil structures. In addition, effects of rainfall-induced failure of volcanic embankments subjected to cyclic loadings in cold regions were examined. Results indicated that void structures play an important role in assessing internal stability of embankment subjected to freeze-thaw action and cyclic loadings such as earthquake.

CHAPTER 3:

TEST MATERIAL

3.1 Introduction

Test specimens were prepared by reconstituting using two materials: Toyoura sand and volcanic coarse grained soils. The rationale for performing tests on Toyoura sand is that it was Japanese standard sand, and that it is used for checking the reliability of test apparatus in the laboratory. The majority of the seepage tests was performed on reconstituted specimens of volcanic coarse grained soils. In order to provide fundamentals and to grasp seepage performance of compacted volcanic coarse grained soils and to clarify the effects of geotechnical conditions (grain size distribution and fines content etc.) and compaction conditions (degree of compaction) on internal erosion mechanisms of volcanic coarse grained soils, these materials were adopted in this study.

3.2 Toyoura sand

Toyoura sand was taken from Yamaguchi prefecture, Japan. Toyoura sand is fine uniform sand that has been widely used in geotechnical engineering laboratories all over

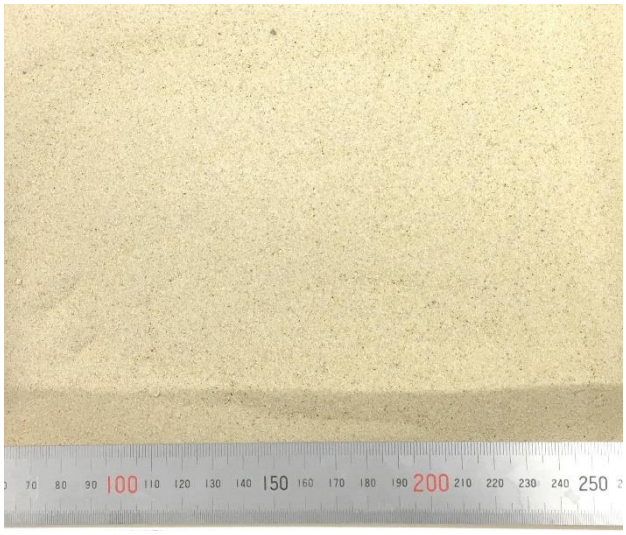

Figure.3.1 Toyoura sand

Japan. Toyoura sand has not been ground or otherwise artificially formed but has been washed, dried and sifted. Figure.3.1 shows an image of Toyoura sand in the laboratory. Grain size distribution and properties of Toyoura sand indicate that the range of grain distribution is stable, as shown later. Therefore, Toyoura sand is useful for calibration and comparison test uses. In this study, a comparison on seepage test result of Toyoura sand between data of Yoshimi et al. (1975) and current laboratory are considered.

3.3 Volcanic coarse grained soils

Volcanic coarse grained soil which was sampled from Komaoka district, Makomanai, Sapporo city in Hokkaido was used in this study. This sample is hereafter referred to as Komaoka volcanic soil (K original soil and K soil). The sample was specified into Shikotsu pumice flow deposit (the notation is *Spfl*) was 31,000~34,000 years ago. The sampling site is depicted in Figure.3.2. The test material profiles and in-situ test results at the sites of Makomanai, Sapporo is showed in Figure.3.3 by Hokkaido branch of JGS 2010. From the figure, the black marks depict the depth of tripe tube sampling, and SPT means the standard penetration. The sampling properties significantly depend on the depth taken sample. Simultaneously, *Spfl* soils contain 10% to 50% finer content and have the permeability coefficient (k) ranging from 4.4×10^{-5} ~ 2.3×10^{-7} (m/s) (Hokkaido branch of JGS 2010). Therefore, *Spfl* indicates relatively-high permeability coefficient including sufficient finer fractions.

Figure.3.4 shows original Komaoka volcanic soil at oven-dried for 24 hours with 110^0c in temperature. After drying, the whitish color of Komaoka soil is realized. Komaoka volcanic soil with *Spfl* was classified into well-grained soils that contain particles of a wide range of grain sizes. Furthermore, Figure.3.5 (a) ~(c) shown the surfaces of coarse particles picked up from the grain size of 4.75 to 9.5 mm (Matsumura 2014). It can be seen that void inside of coarse particles in Komaoka volcanic soil and this void inside is not uniform between coarse particles. The fines content of K original soil ranges from 26.0 % to 42.6 %. The fines were classified into non-plastic material (NP) according to Atterberg limits (liquid limit is 44.5%, plastic limit is NP). Grain size distributions of test materials are shown in Figure.3.6. In addition, characteristics of particle breakage for volcanic coarse-grained soils mainly formed from pumice particles are investigated by previous literature. The void inside of particles of Komaoka volcanic soil such as “opening intra-particle void” and “closing intra-particle void” was modeled by Kimura et al. (2010). They indicated that in in void structure of Komaoka volcanic soils containing a significant amount of the intra-particle voids that can influence the mechanical behavior of soil. Simultaneously, a relationship between opening intra-particle void ($e_{intra\text{-}o}$) and dry density of Komaoka volcanic soil (*Spfl*) was also proposed by Kimura et al. (2010).

Index properties of test materials are shown in Table 3.1. As shown in the table,

specific gravity of test materials is lower than that of Toyoura sand. The aforementioned full-scale embankment was constructed using Komaoka original soil (K original soil). On the other hand, K soil means soil materials composed of soil particles smaller than 9.5 mm in original grain size. In addition, $K_{1.9}$, $K_{8.5A}$, $K_{8.5B}$, K_{40A} and K_{40B} are the gradation-controlled materials using K soil to evaluate the effect of finer fractions on hydromechanical characteristics, where $K_{1.9}$ is prepared sieving particles until the sieve No.200 (0.075mm) to controls amount of fine particles F_c (%) at 1.9%. $K_{8.5A}$, $K_{8.5B}$ are controlled F_c at 8.5% and the subscript of A and B indicates that test materials with A are controlled only by fines content and materials with B are controlled by not only fines content but also mean grain size D_{50}. Similarly, K_{40A} and K_{40B} have F_c=40% and subscript of A and B are described as above. Figure.3.6 shows the experiment on the grain size distribution of test materials.

Besides, three compaction test methods were used for examining relationship between the initial water and dry density of test materials. In particular, Figure.3.7 depicts compaction curves of Komaoka volcanic soils which were obtained from the A-b and A-c methods of Japanese Geotechnical Society (2009) and from a tamping method (see Figure.3.8). The A-b, A-c methods are the same compaction effort (=550 kJ/m^3) and the compaction test results of six samples under tamping method are summarized in Table 3.2. In addition, the relations of fine particles with the optimum water and maximum dry density based on Figure.3.7 are shown in Figure.3.9. It shows that increase of the amount of fine particles of Komaoka volcanic soils leads to the decrease of optimum water and the increase of maximum dry density, respectively.

Furthermore, Figure.3.10 shows synthesis results of variable head permeability test in current laboratory and revision of Matsumura (2014). Curves in the Figure show the relationship between the permeability coefficient k (m/s) of original Komaoka soil (K_{soil}) and the ratio of initial water content and optimum water content (W_i/W_{opt}) under changing

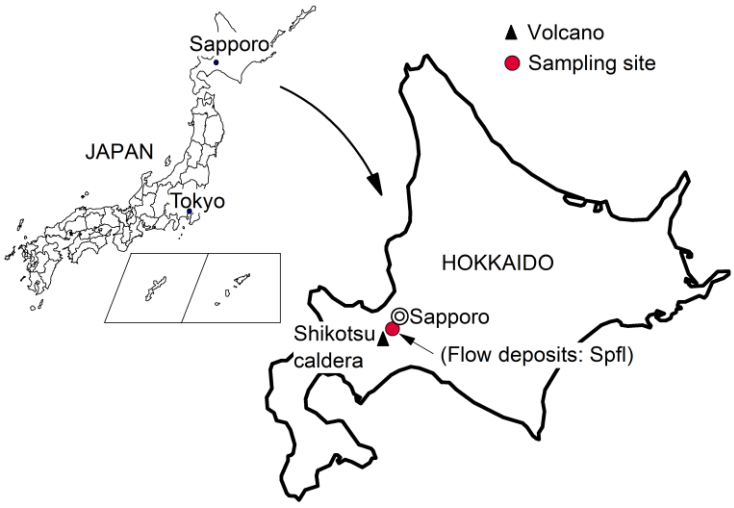

Figure.3.2 Locations of sampling site and field monitoring site of embankment.

the degree of compaction (D_c). Simultaneously, this figure indicates that the k values significantly decrease with the increase of D_c for K_{soil}. In addition, the permeability coefficient value of K_{soil} at drier condition is higher than at wetter condition.

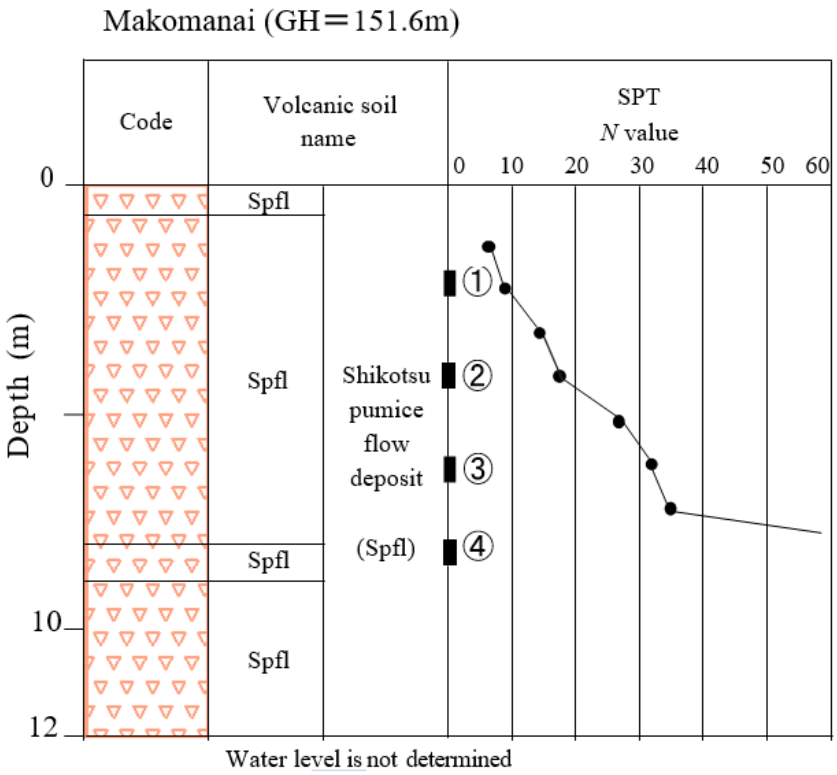

Location	W_n(%)	ρ_s(g/cm^3)	F_c(%)	G_c(%)
①	37	2.48	28	22
②	35	2.40	31	15
③	32	2.36	35	11
④	34	2.28	32	12

Figure.3.3 Soil profiles and in-situ test results

Figure.3.4 Komaoka volcanic coarse grained soil

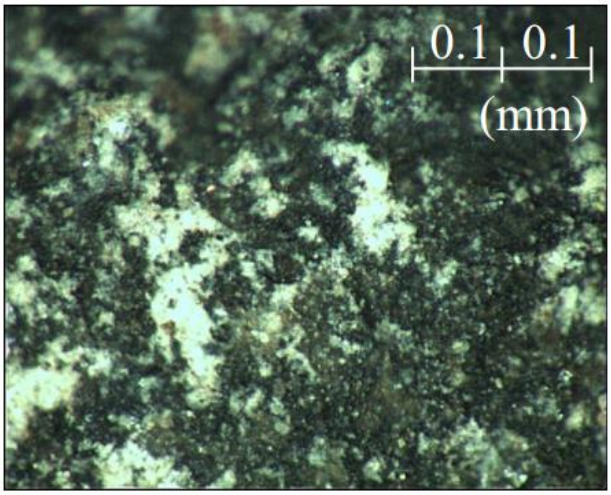

(a) Coarse particle with low porosity

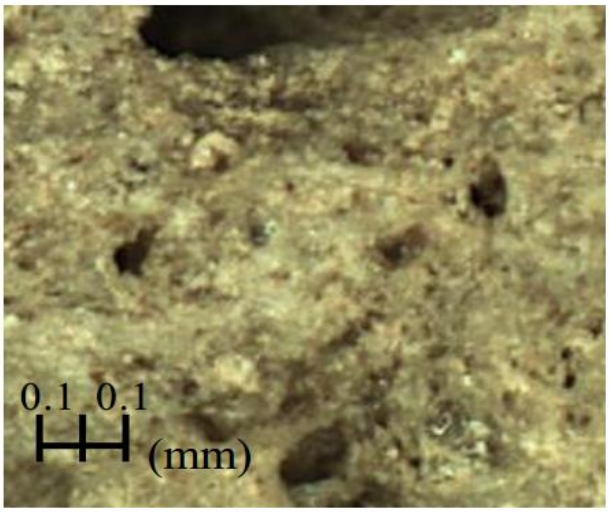

(b) Coarse particle with medium porosity

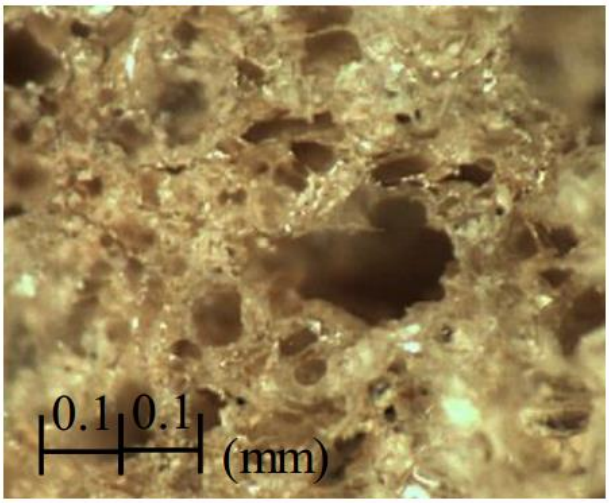

(c) Coarse particle with high porosity

Figure.3.5 Micrographs of coarse particles in Komaoka volcanic soil
(Rivision of Matsumura 2014)

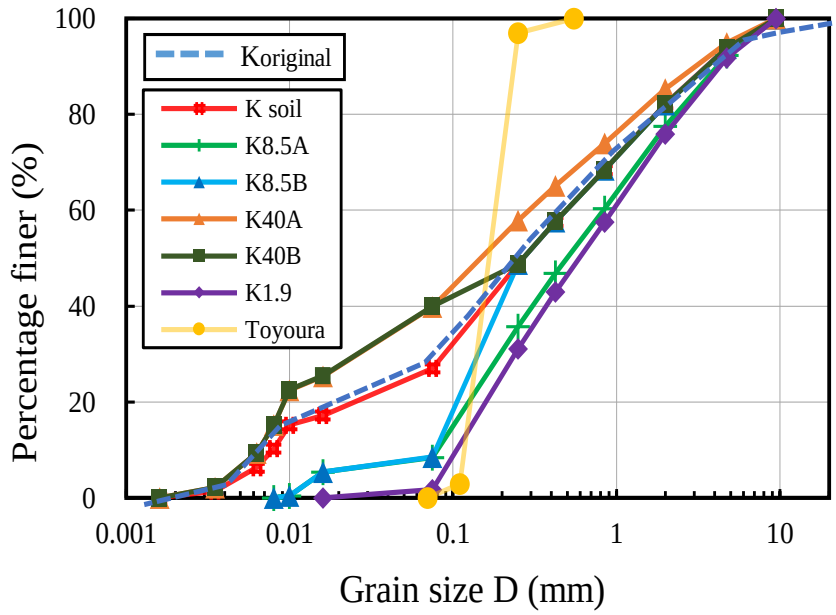

Figure.3.6 Grain size distributions of test materials.

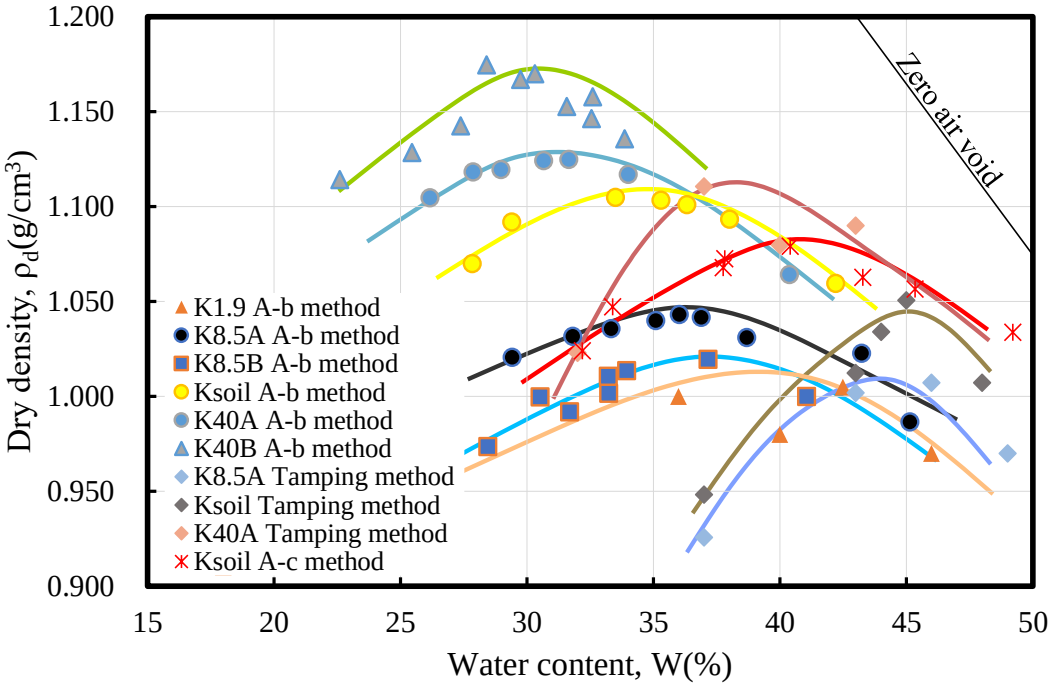

Figure.3.7 Compaction curves of Komaoka volcanic soils

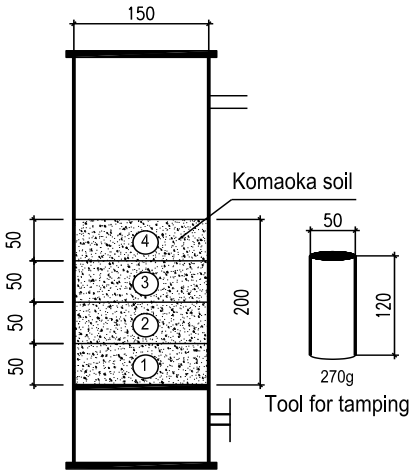

Figure.3.8. Compaction conditions for seepage flow test.

Table 3.1. Index properties of test materials.

Sample name	ρ_s (g/cm^3)	D_{50}(mm)	U_c	F_c(%)
K original	2.48	0.27	43.0	26.0~42.6%
K soil			62.5	27
$K_{8.5A}$		0.50	10.6	8.5
$K_{8.5B}$		0.27	6.30	8.5
K_{40A}		0.16	42.8	40
K_{40B}		0.27	71.4	40
$K_{1.9}$		0.60	7.08	1.9
Toyoura sand	2.68	0.18	1.50	0

D_{50} : Mean grain size, U_c : Coefficient of uniformity, F_c : Fines content.

Table 3.2. Physical properties and compaction test results for reconstituted samples

Sample name	ρ_s (g/cm^3)	w_L (%)	w_P (%)	I_P (%)	Compaction					
					A-c		A-b		Tamping	
					w_{opt} (%)	ρ_{dmax} (g/cm^3)	w_{opt} (%)	ρ_{dmax} (g/cm^3)	w_{opt} (%)	ρ_{dmax} (g/cm^3)
K soil	2.48	46.7	Unavailable	NP	41.0	1.080	34.5	1.120	45.0	1.045
$K_{8.5A}$					-	-	36.0	1.045	44.0	1.015
$K_{8.5B}$					-	-	37.0	1.020	-	-
K_{40A}					-	-	31.0	1.125	38.0	1.120
K_{40B}					-	-	30.5	1.175	-	-
$K_{1.9}$					-	-	38.0	1.020	-	-

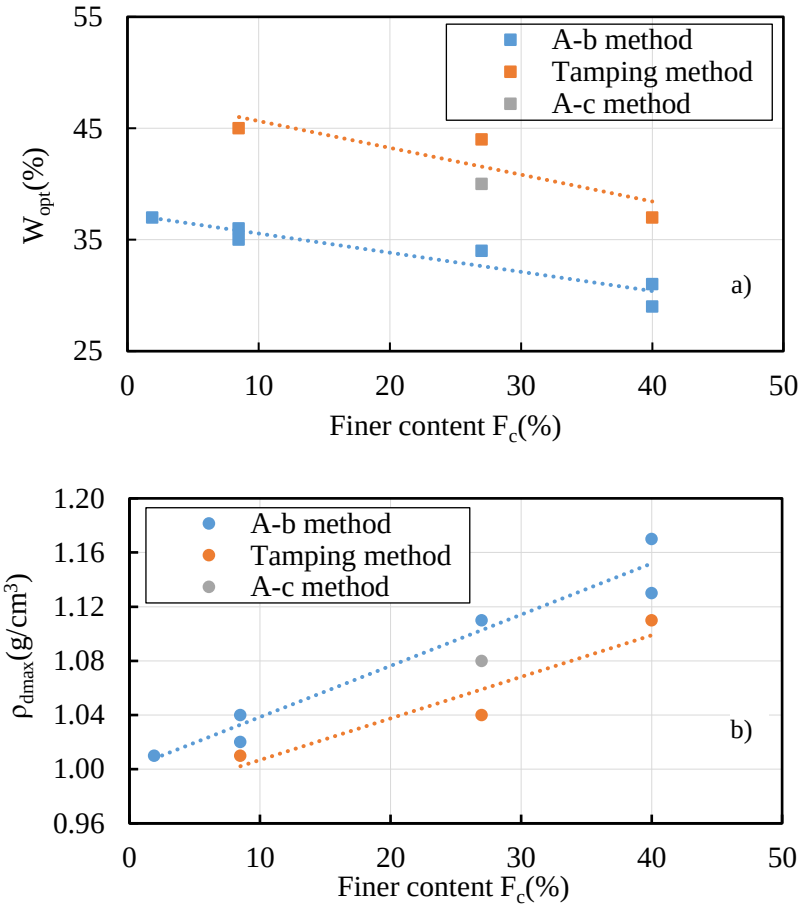

Figures.3.9 Optimum conditions of $K_{1.9}$, $K_{8.5A}$, $K_{8.5B}$, K_{soil}, K_{40A}, and K_{40B}: (a) Water optimum, (b) Maximum dry density

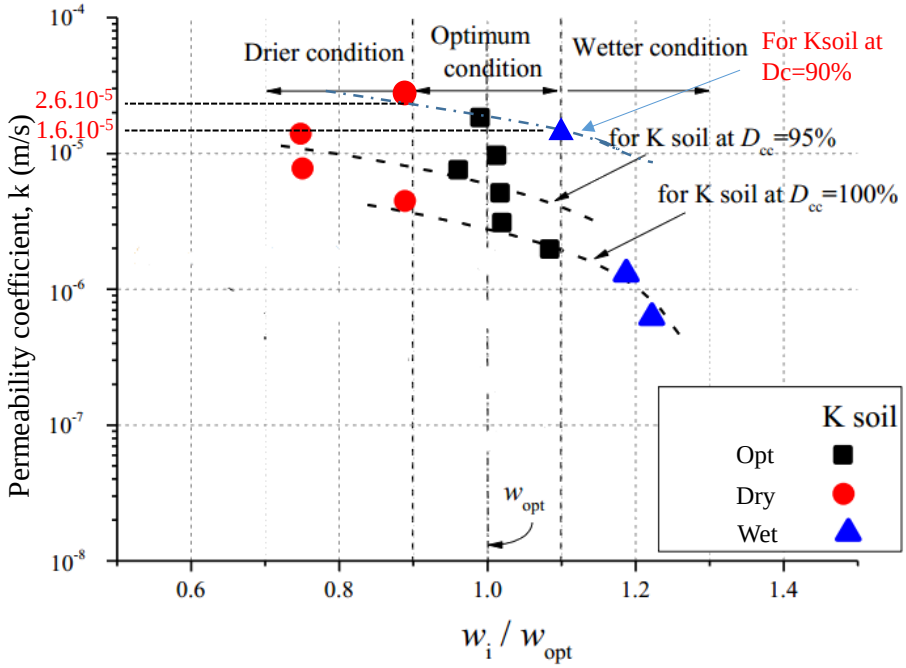

Figure.3.10 Relationship between permeability and initial water content (current laboratory and revision of Matsumura (2014))

3.4 Summary

The program of testing was performed on Toyoura sand and six gradations of Komaoka volcanic soil. Toyoura sand was used in this study for a comparison on seepage test between data of Yoshimi and current laboratory. Komaoka volcanic soil with *Spfl* was classified into well-grained soils that contain particles of a wide range of grain sizes. The fines content of K original soil ranges from 26.0 % to 42.6 %. The fines were classified into non-plastic material (NP). Furthermore, Komaoka volcanic soils containing a significant amount of the intra-particle voids that can influence the mechanical behavior of soil. Test materials for seepage test in the laboratory such as K_{soil}, $K_{1.9}$, $K_{8.5A}$, $K_{8.5B}$, K_{40A} and K_{40B} were created by controlling particles size, finer fraction and mean grain size on original Komaoka volcanic soil. In addition, the relationship between the initial water content and dry density of test materials was examined based on three compaction test methods such as A-c, A-b and tamping methods. Results indicated that increase of the amount of fine particles of Komaoka volcanic soils leads to the decrease of optimum water and the increase of maximum dry density, respectively. Finally, the permeability of the test material strongly depends on the changes of compaction degree and initial water content. In particular, the permeability significantly decrease with the increase of D_c for K_{soil}. In addition, it was shown that the permeability coefficient value of K_{soil} at drier condition is higher than at wetter condition.

CHAPTER 4:

TESTING METHOD

4.1 Introduction

Many researchers have utilized seepage test with upward water flow to measure internal instability of soil, the advantages of this method are that they are simple to assemble and observe internal erosion phenomenon of the sample, as described above. In this study, an experimental approach was conducted to observe the onset of piping and boiling phenomenon on volcanic soils. Two cylindrical apparatuses were used for performing a series of seepage flow tests in the laboratory. In particular, the small apparatus is built with 100mm in internal diameter and 300mm in height and is suited for X-ray CT scanner which was conducted to observe piping phenomenon. Thereafter, a similar seepage flow test was carried out by using a cylindrical seepage cell is 150 mm in internal diameter and 450 mm in height to clarify the effect of fine particles and compaction condition on piping phenomenon. In addition, tests are performed in saturated volcanic soil, seepage flow in unsaturated soils are affected by compressibility of air, generally giving lower estimates of internal erosion than in saturated soils. Simultaneously, test material is non plastic soil. Therefore, this collapse when saturated under liquefaction due to seismic loading or flooding, will not sustain a crack when saturated, and are maybe easily eroded by seepage flow. Following a more detailed description of the small apparatus and large apparatus, and the specimen reconstitution technique, a summary of the test program is provided.

4.2 Test apparatus

4.2.1. Small apparatus

In this study, the small apparatus was originally designed for assessment of piping phenomenon on volcanic coarse grained soils. A schematic diagram of the device is depicted in Figure.4.1. A photograph of the apparatus cell assembly is shown in Figure.4.2. Based on results of comparing images from X-ray CT for cylindrical cell with different inner diameters such as 150mm, 100mm, and 50mm, the apparatus with 100mm

in diameter is chosen for seepage test. The cylindrical cell of small apparatus is made of transparent plastic, with an inner diameter of 100 mm, 300mm in height and a wall thickness of 0.35 mm. The upper cylindrical cell is opened to observe internal erosion of samples under seepage flow from the top surface. An overflow pipe is fitted at the top portion of the seepage cell to manually measure the flow velocity directly measured by a graduated cylinder. The layer of underlying porous stone diffusing filter to ensure a uniform water flow in the area of the specimen. An inlet port with flexible vinyl tube 10mm in diameter allows water flow from upper tank to the cell at the base of the seepage cell. Changing hydraulic gradient across the specimen is performed by changing water level in the upper tank. The valve on the inlet port is used for controlling velocity of water flow from upper tank to seepage cell. A ruler lies along with the height of cell to determine the deformation of specimen and water level in the seepage cell. In addition, an X-ray CT scanner is applied for observation of internal erosion in the specimen under the imposed each hydraulic gradient.

4.2.2. Large apparatus

Most of the main test program was performed in the large apparatus. Figure.4.3 shows a schematic diagram of the device. The cylindrical seepage cell is made of transparent plastic, with 150 mm in internal diameter, 450 mm in height and a wall thickness of 0.5mm. In addition, a porous disk is installed at the bottom of the cylinder to ensure a uniform water flow in the area of the specimen. Figure.4.4 shown a photograph of the seepage apparatus cell assembly. Variation in water head within the specimen was measured by three stand pipes at three different depths, 50mm, 100mm and 150mm in specimen height. An inlet port with flexible vinyl tube 25mm in diameter is used for connecting between the seepage cell and the upper tank. Approximately, the upper tank can be raised or lowered to control the hydraulic gradient across the specimen. The deformation of specimen and water level in the seepage cell is measured by a ruler lay along with the height of the side wall. Water coming out from the top of the container was collected by a graduated cylinder (accuracy is 10 ml), as shown in Figure.4.3. Observation of experiment process is performed by the cameras recording specimen from the top and the side wall of cylindrical seepage cell.

4.2.3. X-ray CT scanner

Radioscopic image data on an inspection object is obtained using an X-ray CT scanner, as shown in Figure.4.5. The sectional images are assured high-resolution by enlarging images geometrically. These images are very powerful tool for the visualization that can help us to more intuitively understand the phenomenon that occurs in ground. Especially, X-ray CT scanner scanning has been applied for observation and evaluation

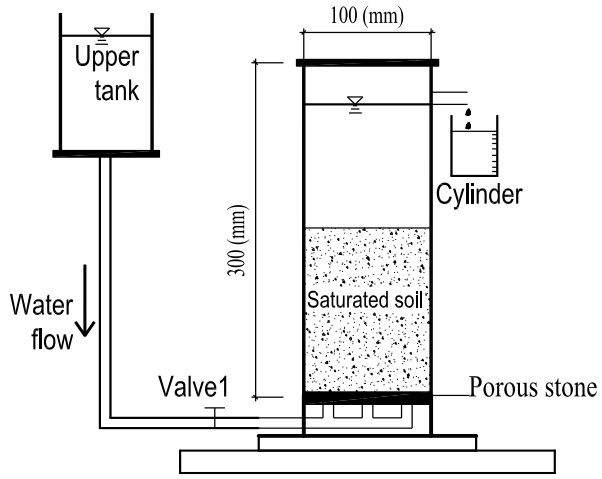

Figure.4.1 Schematic diagram of small apparatus

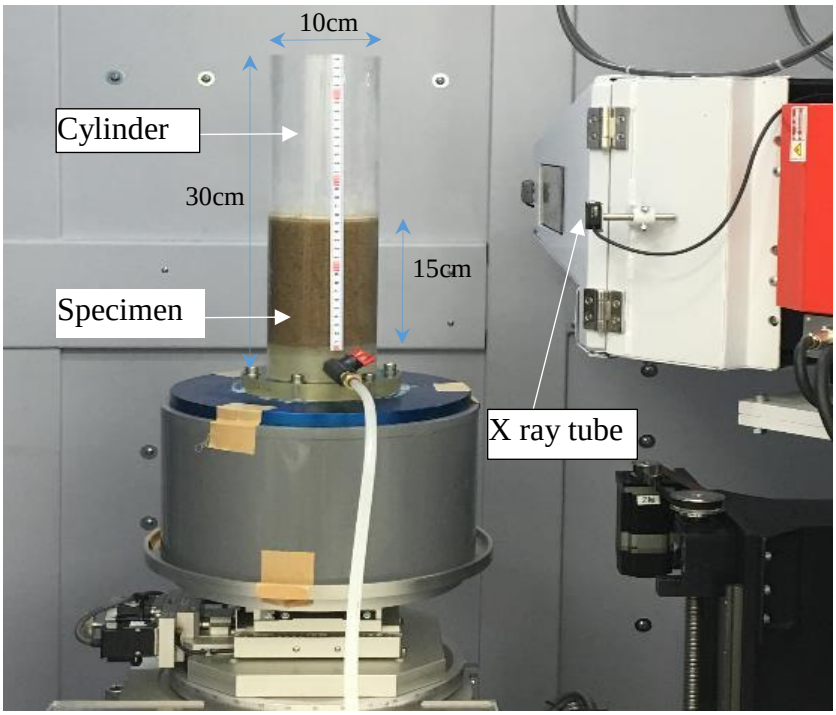

Figure 4.2. View of small apparatus

of microscopic soil based on analyzing sectional images of the interior of inspection specimen. In this study, an X-ray CT scan machine is used for detecting motion of particles in the test sample under seepage flow. It is equipped with the maximum of X-ray tube voltage and current are 225KV and 600μA, respectively. The seepage test sample is put on the lift table then it is moved to the position between the X-ray generator and the X-ray detector. X-ray fluoroscopy data is collected from every angle by rotating the sample 360 degrees, and computed tomography images (CT images) are calculated. Figure.4.6 and Figure.4.7 show schematic diagram of X-ray CT scanner in this study. In addition, principle of X-ray CT image acquisition and reconstruction is represented at Figure.4.8.

The image processing conducted during the seepage test to measure the displacement between a pair of digital images. Firstly, the image is divided into a grid of test patches. Each test patch consists of a sample of the image matrix of size L x L pixels. To find the displacement of the test patch between images, the cross-correlation of patches in a pair of images are evaluated and normalized by the square root of the sum of the squared values. The highest peak in the normalized correlation plane indicates the displacement vector of the test patch. The displacement vector is established to sub-pixel resolution with yielding a system resolution of 0.005 pixels. In particular, the deformation

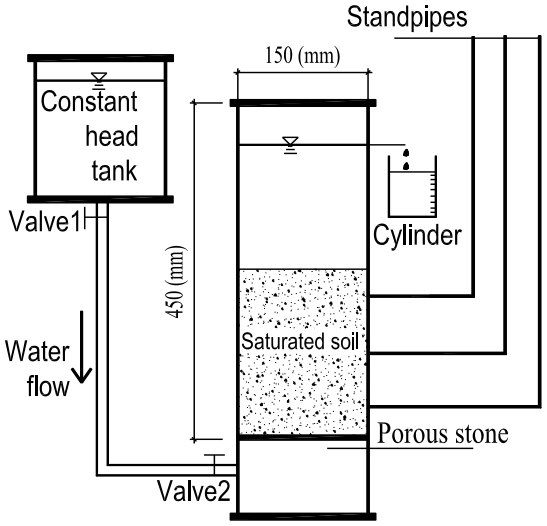

Figure.4.3 Schematic diagram of large apparatus

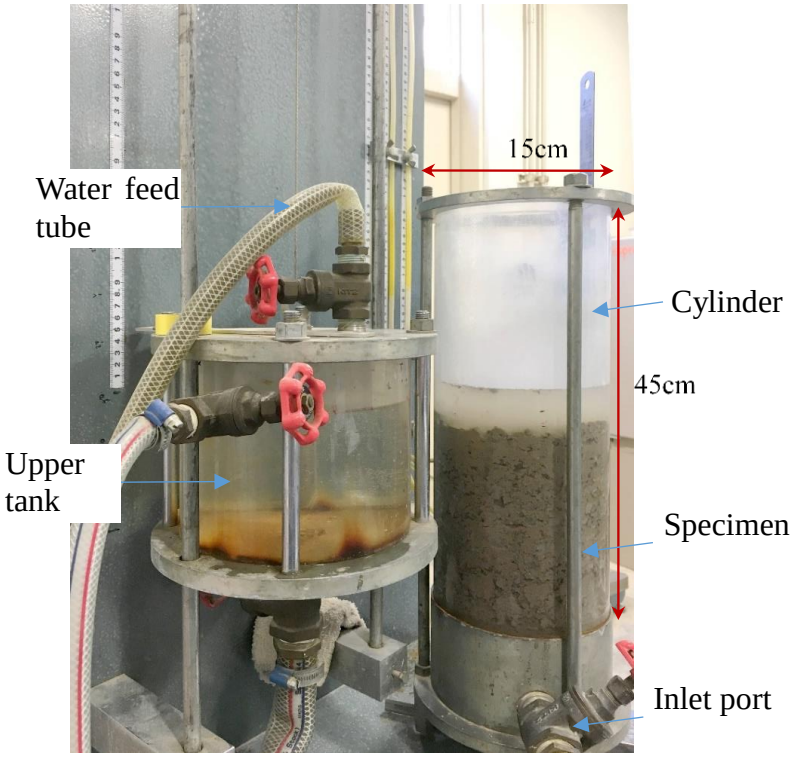

Figure.4.4 View of large apparatus

of soil particles was calculated by 2-dimensional Digital Image Correlation analysis, DIC (White et al. 2003). This method is more accurate and precise than previous image-based methods of displacement measurement.

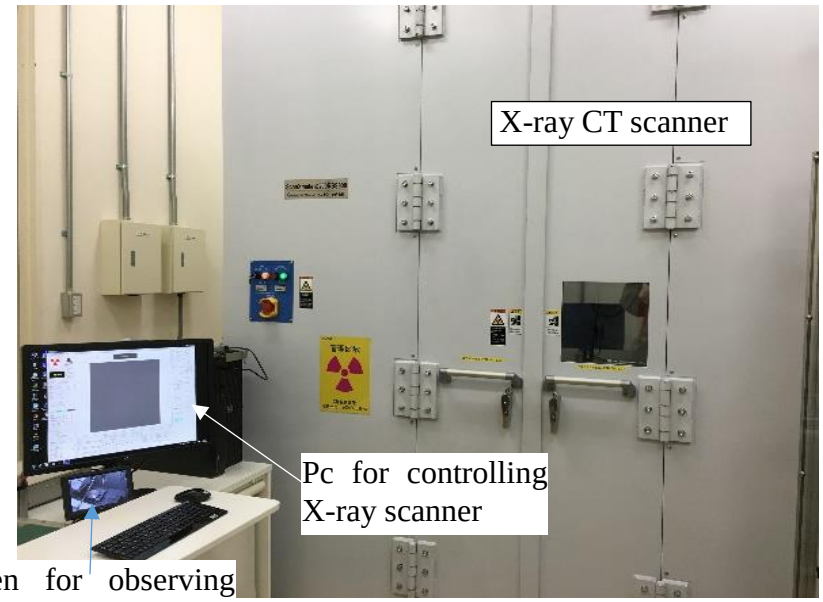

a)

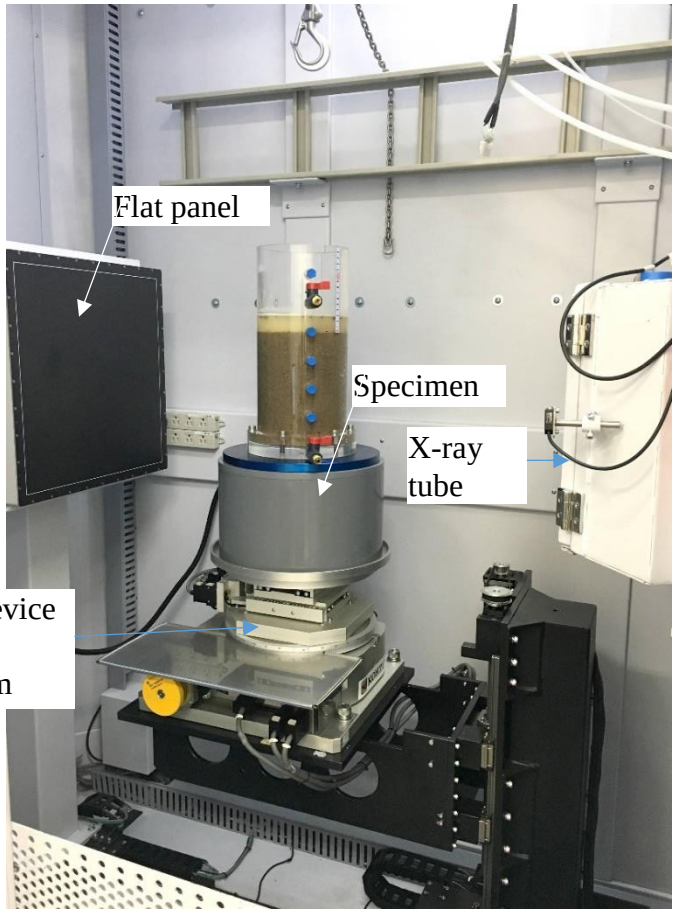

b)

Figure.4.5 View of X-ray CT scanner: a) Outside of machine; b) Inside of machine

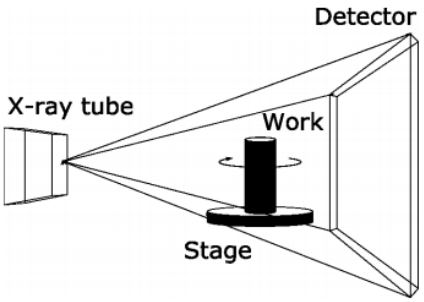

Figure.4.6 Basic schematic of X-ray CT Scanner.

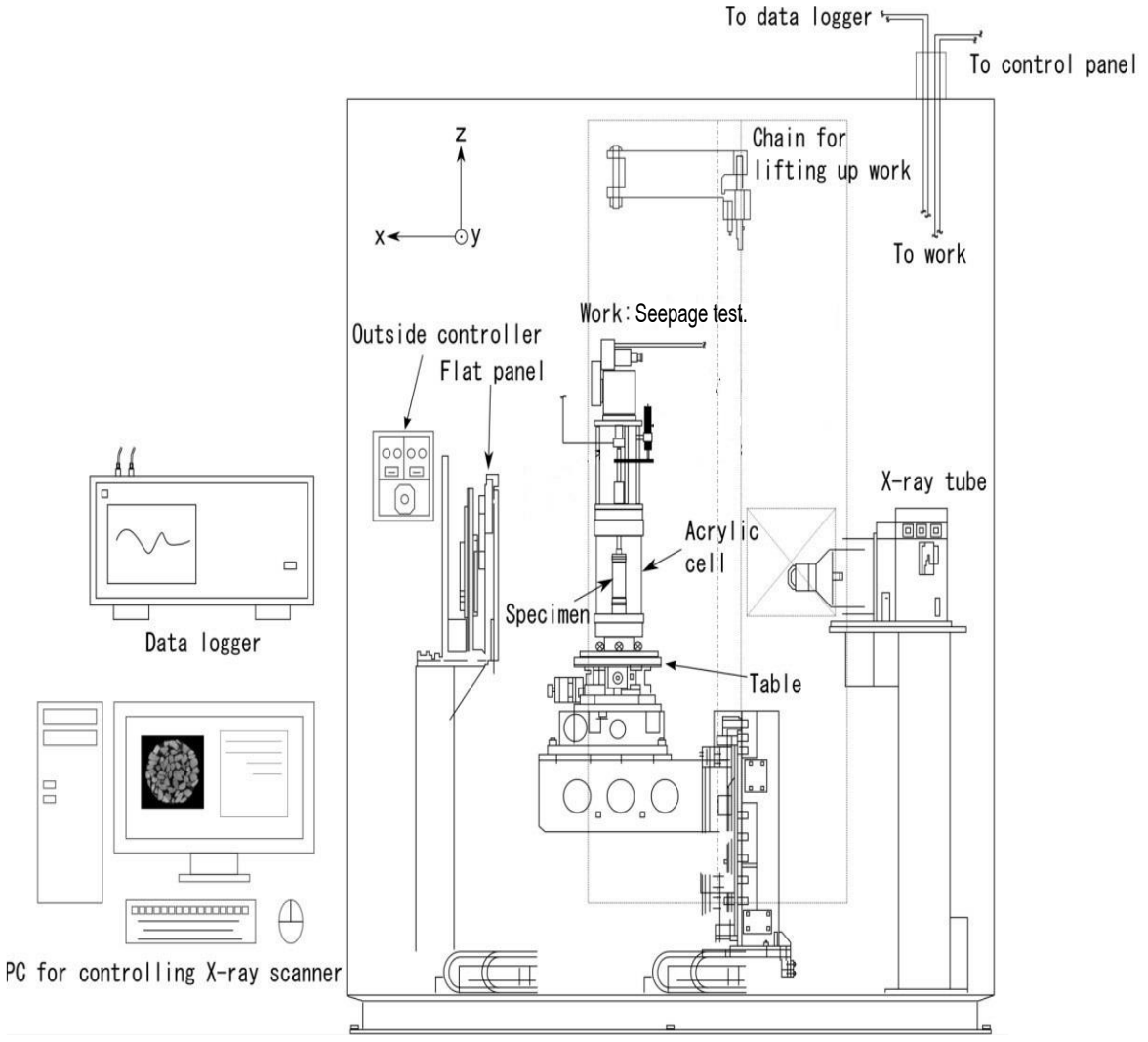

Figure.4.7 Overall schematic of X-ray CT

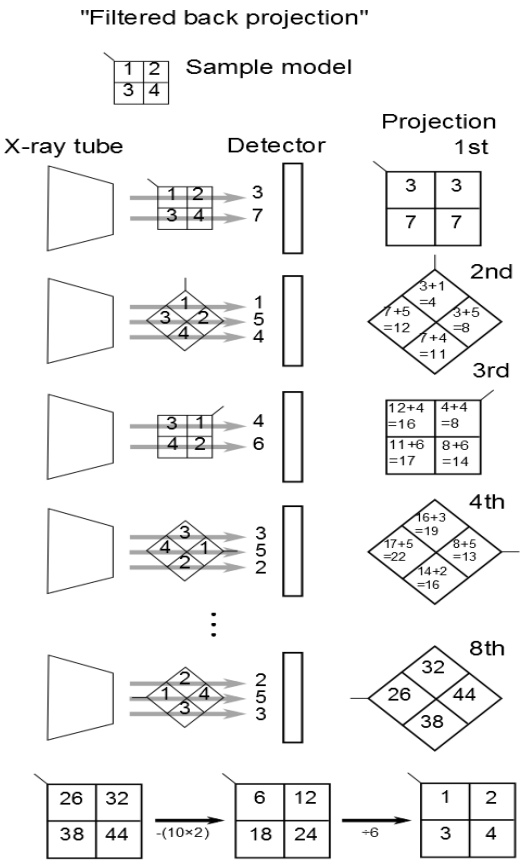

Figure.4.8 Principle of image acquisition and reconstruction

4.3 Specimen preparation

The specimen was prepared in the laboratory after it was taken from Komaoka district, Makomanai, Sapporo city in Hokkaido. Firstly, the Komaoka volcanic soil was dried at 110^0c in temperature and 24 hours. Secondly, compaction test was performed to check optimum water content and maximum dry density of soil. Then, the controlling amount of fine particles (F_c) and mean grain size (D_{50}) were conducted to obtain test samples such as K_{soil}, $K_{1.9}$, $K_{8.5A}$, $K_{8.5B}$, K_{40A}, and K_{40B}. In order to create the homogeneous specimen in comparison to the full scale embankment constructed by Komaoka volcanic soil in Sapporo, the test specimen was divided into a series of layers along the height of seepage cell in the laboratory. Each layer was prepared by mixing water and dry soil with the target value of water content (W_0). The degree of compaction (D_c) was controlled at each layer by calculating dry density (ρ_d) of the soil sample and based on maximum value of the dry density of soil (ρ_{dmax}) which is taken from Figure.3.7. The compaction process of each layer was constructed by a hammer having weight is 270g. Particularly, the moist soil was poured in equal layers. Each layer uniformly was compacted by the hammer. During sample construction, number of tamping was counted for each layer. Before constructing the second layer, the top of the first compacted layer

is scratched for proper bonding of both the layers. The next layers are seminally constructed.

In small apparatus tests, the specimen was reconstituted in three layers, each about 50 mm thick. For example, The K_{soil} specimen with D_c=90% and W_0=37% corresponds 523 g of Komaoka volcanic soil (K_{soil}) per layer. In large apparatus test, the specimens were reconstituted in 4 layers, each about 50 mm thick (K_{soil}, $K_{1.9}$, $K_{8.5A}$, $K_{8.5B}$, K_{40A}, and K_{40B} samples with 0.972 (g/cm^3) in dry density (ρ_d) and W_0=37% approximately correspond 1177 g by weight per layer). Figure.4.9 shows specimen reconstitution of seepage test in the laboratory. The number of compactions and degree of compaction of six samples of large apparatus and four samples of small apparatus under tamping method are summarized in Table 4.1.

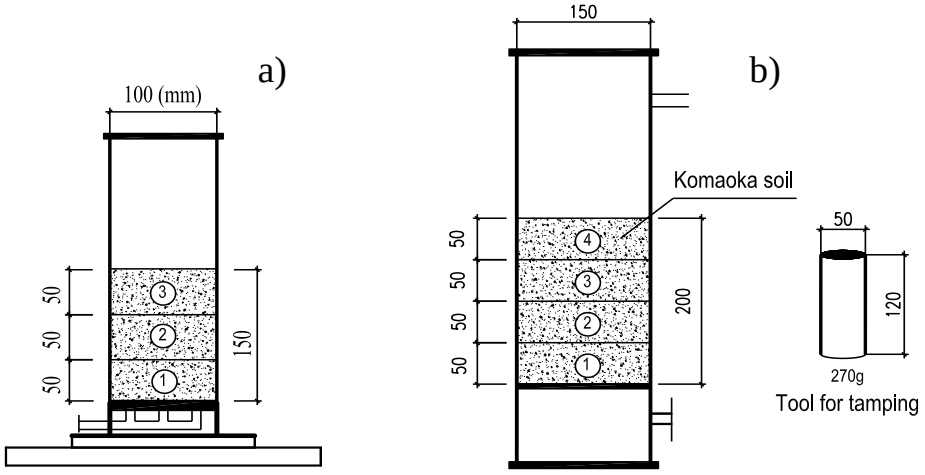

Figure.4.9 Schematic diagram of specimen reconstitution:
a) The small apparatus; b) The large apparatus

Table 4.1. Number of compactions and degree of compaction for each soil.

Sample notation	Desired dry density (g/cm^3)	Weight of roller (N)	Thickness of compacted layer (mm)	Number of compactions (per 1 layer) Small apparatus	Number of compactions (per 1 layer) Large apparatus	Degree of compaction (%)
K soil	1.048	2.65	50	-	120	95
	0.972			20	75	88
	0.918			-	42	83
$K_{1.9}$	0.972			50	170	98
$K_{8.5A}$				-	130	93
$K_{8.5B}$				35	160	96
K_{40A}				-	32	86
K_{40B}				10	24	83

4.4 Test procedure

The main objective of this study was to examine the effects of geotechnical conditions (grain size distribution and fines content etc.) and compaction conditions on the onset of internal instability in volcanic coarse grain soil. The first step in this process is to control the amount of fine particles Fc (%) including F_c=1.9%; 8.5%; 27%; 40%. In addition, $K_{8.5B}$ and K_{40B} with mean grain size (D_{50}) are controlled in this step, as shown in Figure.3.6. Thereafter, the initial water content (W_0) and degree of compaction (D_c) of the specimen are controlled based on values of maximum dry density (ρ_{dmax}) and optimum water content (W_{opt}), as described above. Next step, setting mixture into the apparatus and tamping the soil up to target compaction degree, and the specimen is prepared layer by layer. The saturation process of the specimen is performed into the cylindrical seepage cell. Water is prepared to supply into the specimen from the upper tank at a slow velocity. This process takes about 8-10 hour to ensure saturation in the specimen. Before the seepage test, it need to check the position of the water level of the upper tank, seepage cell and three standpipes to assure initial water pressure for the specimens. The level of water head at the upper tank is changed to suit with the imposed hydraulic gradient. The hydraulic gradient of 0.1-0.2 increased for each step. For each step, the test process is kept approximately 20-30 min to ensure the internal erosion process completed. That means the velocity of water flow is stable. A flow velocity was directly measured using a graduated cylinder (accuracy is 10 ml). Test observation is performed by X-ray CT scanner with small apparatus and a camera system with large apparatus. In addition, visual observation is carefully realized also to check the flow turbidity, the transportation of fine particles and jumping of discharge water rate. The test process is continued until the specimen becomes instability (Boiling phenomenon). Finally, all test result is collected to the computer to analyze the internal erosion phenomenon of the specimen.

In this study, the onset of internal instability was primarily estimated on the basis of three attributes, namely the change in differential coefficient of the relationship among flow velocity (v) and hydraulic gradient (i), visual observation and using X-ray CT

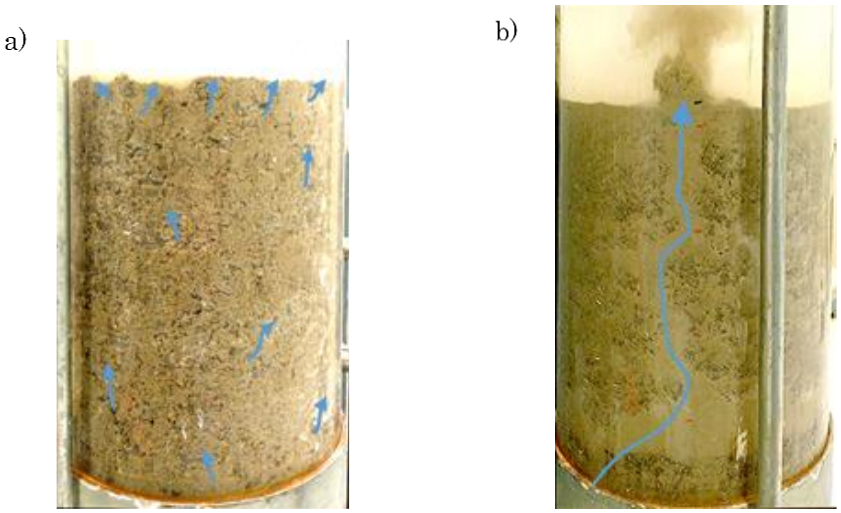

Figure.4.10 Observed particle migrations (a) Piping phenomenon, (b) Boiling phenomenon

scanner. The minimum hydraulic gradient at which the first sign of fine particles moved out of the top was defined as “piping phenomenon”, thereafter the behavior at which both coarse and fine particles migrated from the bottom to the top was defined as “boiling phenomenon”. Figure.4.10 shows typical photos for piping and boiling phenomena in the seepage test.

4.5 Summary

The program of testing was performed on six gradations of Komaoka volcanic soil. Geotechnical conditions of test materials such as grain size distribution and fines content and compaction conditions (degree of compaction, initial water content) are used for assessing piping mechanisms of volcanic coarse grained soils. Those conditions are shown in Figure 4.9 and Table 4.1. In each test, a mixing specimen preparation and compacted method was used for yielding a saturated and homogeneous specimen. A total of 75 tests on Toyoura sand and Komaoka volcanic soils were performed in either a small apparatus or a large apparatus, both of which were operated using a principle of head seepage control. Almost tests were performed by large apparatus to analyze the piping phenomenon occurring in the samples such as K_{soil}, $K_{1.9}$, $K_{8.5A}$, $K_{8.5B}$, K_{40A}, and K_{40B}. Furthermore, the small apparatus was used combination with an X-ray CT scanner to observe the detail deformation of particles in K_{soil} sample under seepage flow. The process of analyzing images obtained from X-ray CT scanner was performed by 2-dimensional Digital Image Correlation analysis, 2DIC to calculate deformation of soil particles. As a result, the piping phenomenon on volcanic coarse grained soils is revealed. Finally, the calculation procedure was then executed to assess the onset of piping and onset of boiling into relation with hydro mechanical properties.

CHAPTER 5:

RESULTS AND DISCUSSIONS

In the field observation of a full-scale embankment constructed by Komaoka volcanic coarse grained soil in Sapporo, Japan (2012), traces of exudation routes of water during field monitoring were realized, as shown in Figure.2.26 and Figure.2.27. Therefore, the evaluation of internal stability of volcanic soils by empirical geometric criteria was required. Subsequently, a series of seepage tests was conducted using both the small apparatus and the large apparatus. Following some engineering definitions, The results obtained from total six test materials adopted in empirical geometric criteria and in the experiments in the laboratory are presented herein.

5.1 Stability evaluation of test materials based on empirical criteria

In order to evaluate internal stability of Komaoka volcanic soils, a geotechnical evaluation on piping phenomenon has been conducted using empirical geometric criteria. Firstly, internal instability by the literature and current study was investigated, information on internal stability tests on 81 different soils was collected. The information includes geometric characteristics of the soils and testing results such as internal stable or unstable, etc. The details of geometric information of each soil are summarized in Table 5.1 and Table 5.2. Subsequently, internal erosion of those soils is assessed by five currently available methods proposed by Kezdi (1979), Kenney and Lau (1985, 1986), Burenkova (1993), Skempton and Brogan (1994) and Chang and Zhang (2013). The main contents of these criteria are represented in Chapter 2. In addition, investigation on each criteria is performed for evaluation of six kinds of volcanic soil from experimental results.

Table 5.1 shows evaluation on internal instability on 81 different soils under Kezdi method and Kenny and Lau method. Geometric index $(D'_{15}/D'_{85})_{max}$ and $(H/F)_{min}$ of all soils were taken from literature such as Usace(1953); Kenney and Lau (1985); Burenkova (1993); Skempton and Brogan (1993); Honjo et al. (1996); Khan (2003); Mao (2005); Liu (2005); Li (2008); Chang and Zhang (2011); Marot et al. (2011); Salehi

Sadafhiani and Witt (2011); Lin ke and Akihiro Takahashi (2012). According to Kezdi criterion, 52 of 54 unstable soils, which have stability index $(D'_{15}/D'_{85})_{max}>4$, are classified as internally unstable soil. However, 20 of 27 stable soils are correctly evaluated by this method. Therefore, unstable soils can be successfully assessed according to the Kezdi criterion. Furthermore, based on geometric index $(H/F)_{min}$ of 81 different soils, all unstable soil gradations collected from the literature are classified as unstable by the Kenney and Lau method, on the other hand, 19 of 27 stable soils, which have stability index $(H/F)_{min}$ >1, are correctly evaluated by this criterion (see Table 5.1). Therefore, the method might successfully predict the potential for internal stability in soils.

In addition, by comparing Kezdi and Kenny and Lau criteria, Li & Fannin (2008) suggested that "limit values to stability of $D'_{15}/D'_{85} = 4$ and $H/F = 1$ yield a unique point on the gradation curve where both criteria converge at F=15%". As a result, the criterion summarized by two criteria is examined internal instability for Komaoka volcanic soil in this study, the results are shown in Figure.5.1. Particularly, the curves describing relation between mass fraction smaller than (F) and mass fraction between D and 4D (H) were calculated based on the chart about grain size distribution of test materials. Therefore, it was apparent that K_{soil} classified into "well graded type (WG)" under the original condition was judged to an unstable grading because its portion of shape curve lay in unstable area. Conversely, the shapes of curves of $K_{8.5A}$ and $K_{8.5B}$ material located on stable zone of internally stable soil, as shown in Figure.5.1.

On the other hand**,** Table 5.2 shows internal instability of 81 soils samples which are evaluated by the Burenkova method. Based on two ratios called conditional factors of uniformity D_{90}/D_{60} and D_{90}/D_{15} of these soils, 49 of 54 unstable soils and 16 of 27 stable soils are correctly evaluated by the Burenkova criterion. These results suggest that the method appears much conservative in evaluating the potential for stable soil. On the other hand, unstable soils can be successfully predicted according to the Burenkova criterion. In addition, using the Burenkova method to evaluate internal instability of Komaoka volcanic soil (K_{soil}; $K_{1.9}$; $K_{8.5A}$; $K_{8.5B}$) is examined (see Figure 5.2). Based on the comparing between the uniformity conditional factors ratios of Komaoka volcanic soil and boundary proposed by Burenkova indicates that $K_{soil,}$ $K_{1.9,}$ and $K_{8.5B}$ are internally stable soil. Contrarily, $K_{8.5A}$ is assessed internally unstable soil, as shown in Figure 5.2.

According to Chang and Zhang criterion, test materials in this study are classified. In particular, $K_{8.5A}$ and $K_{8.5B}$ with $F_c = 8.5$ % of less than 10% and the gap ratio equal to 40 of gap-graded soil is classified as internally unstable. In another case, $K_{1,9}$ with $F_c = 1.9$ % and filter index $(H/F)_{min} = 0.3$ of well-graded soil is deemed to be internally unstable. Contrarily, well-graded soils K_{soil} and K_{40A} having $F_c = 27\%$ and 40%,

respectively are assessed as internal stable soil. In addition, a gap-graded soil K_{40B} with F_c = 40% is deemed to be internally stable by Chang and Zhang criterion.

On the other hand, according to Skempton & Brogan (1994), if finer fractions of soils exceed about 35%, coarse particles float in a matrix of fine grains. As a result, they cannot act as a filter for the fines. In the cases of K_{40A} and K_{40B}, coarse particles can be floated in a matrix of fine grains. Therefore, internal instability of soils might proceed gradually by moving of volcanic fine particles having a low specific gravity under seepage flow (see Figure.5.3).

Evaluation results of the potential internal erosion of test materials in the laboratory are examined and summarized under Kezdi (1979), Kenny and Lau (1986), Burenkova (1993), and Chang and Zhang (2013) criteria, as shown in Table 5.3. These results show that the assessment of internal stability of Komaka volcanic coarse grained soils has difference between empirical theories and test results. This may be due to the soils investigated by most of these authors are sand gravels free of silty fines. The

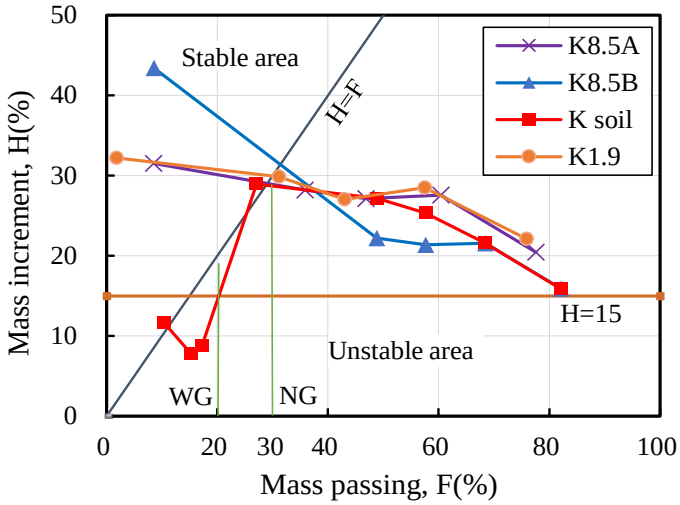

Figure 5.1. Internal stability assessment for Komaoka soils based on the Kezdi's and Kenney & Lau's criteria (Li & Fannin, 2008).

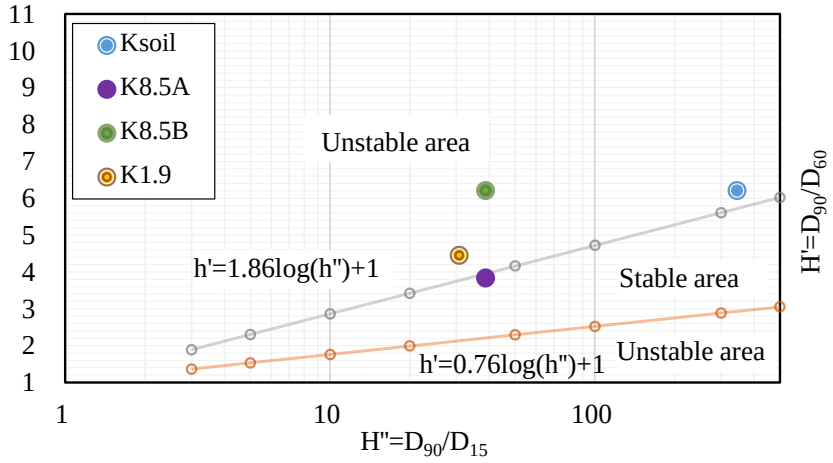

Figure 5.2. Internal stability assessment for Komaoka soils based on the Burenkova's criteria (1993).

exception is Burenkova (1993) who investigated silt-sand-gravel soils but tested them under maximum particle size up to 100mm and very high gradients. Besides, volcanic coarse grained soils in this study contain a significant amount of fine particles with low plasticity, especially containing void inside of constitutive particles. In addition, it is necessary to examine the potential internal erosion of volcanic coarse grained soils under geotechnical conditions (grain size distribution and fines content etc.) and compaction conditions (degree of compaction). These conditions directly affect to stability of volcanic embankment during construction and operation.

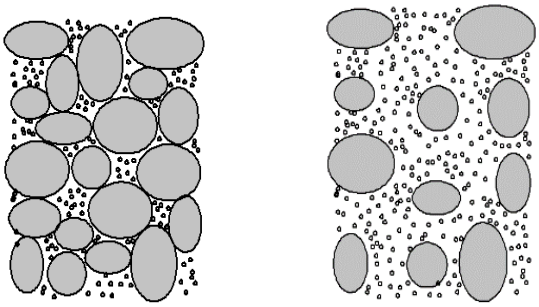

Figure 5.3. Grains distribution of Komaoka soils: (a) K soil, $K_{8.5A,}$ $K_{8.5B}$ and $K_{1.9}$; (b) K_{40A}, $K_{40B.}$

Table 5.1. Evaluation of internal stability of soils by Kezdi (1979) and Kenney and Lau (1986) methods

Sample name	Soil gradation	$(D'_{15}/D'_{85})_{max}$	$(H/F)_{min}$	Kezdi	Kenny and Lau	Laboratory	References
A	WG	3.7	0.55	S	U	S	Usace(1953)
B	WG	3.1	1.6	S	S	S	
C	WG	2.4	1.5	S	S	S	
D	WG	8.2	0.75	U	U	U	
A	WG	3.6	0.48	S	U	U	Kenney and Lau (1985)
D	WG	6.8	0.48	U	U	U	
X	WG	51	0.7	U	U	U	
Y	WG	6.5	0.6	U	U	U	
Y_s	WG	8	0.85	U	U	U	
A_s	WG	3.5	0.95	S	U	U	
D_s	WG	4.1	2.9	U	S	S	
K	WG	3.1	3.5	S	S	S	
1	WG	2.5	1.15	S	S	S	
2	WG	2.4	1.5	S	S	S	
3	WG	3.5	1.25	S	S	S	
20	WG	1.5	1.93	S	S	S	

21	WG	1.6	2.0	S	S	S	
23	WG	2.1	1.9	S	S	S	
1	WG	82	0.16	U	U	U	Burenkova (1993)
2	WG	13.5	0.55	U	U	U	
3	WG	45.0	0.28	U	U	U	
4	WG	37.0	0.19	U	U	U	
11	WG	16	1.6	U	S	S	
12	WG	11	0.35	U	U	S	
13	WG	11.5	0.36	U	U	S	
14	WG	8.5	0.42	U	U	S	
A	GG	10.3	0.16	U	U	U	Skempton and Brogan (1994)
B	WG	9.8	1.0	U	U	U	
C	WG	4.7	1.5	U	S	S	
D	WG	4.0	2.75	S	S	S	
G3-a	GG	5.4	0	U	U	U	Honjo et al. (1996)
G3-b	GG	5.2	0	U	U	U	
G3-c	GG	5.2	0.3	U	U	U	
G4-a	GG	7.4	0	U	U	U	
G4-b	GG	7.4	0	U	U	U	
G4-c	GG	7.4	0.3	U	U	U	
G1-a	GG	3.7	1.42	S	S	S	
G1-b	GG	3.7	1.0	S	S	S	
G1-c	GG	3.7	0.85	S	U	S	
G1-d	GG	3.7	0.8	S	U	S	
G2-a	GG	2.6	2.5	S	S	S	
G2-b	GG	2.6	1.5	S	S	S	
G2-c	GG	2.6	1.4	S	S	S	
4.4S25	GG	4.5	0.31	U	U	U	Khan (2003)
5.9S25	GG	6	0.31	U	U	U	
7.4S25	GG	7.4	0.31	U	U	U	
8.7S25	GG	8.65	0.31	U	U	U	
a	WG	6	0.6	U	U	U	Mao (2005)
b	WG	4.75	0.75	U	U	U	
c	WG	6.5	0.82	U	U	U	
d	WG	22	0.3	U	U	U	
A	GG	45.70	0	U	U	U	
B	GG	41.38	0.35	U	U	U	
C	GG	30.57	0.35	U	U	U	
D	GG	22.85	0.35	U	U	U	

T0	GG	13.7	0.34	U	U	U	Moffat (2005)
T5	GG	14.3	0.6	U	U	U	
C-20	WG	7.7	0.67	U	U	U	
C-30	WG	10	0.42	U	U	U	
1	WG	34	0.47	U	U	U	Liu (2005)
2	WG	18	0.43	U	U	U	
3	WG	35	0.50	U	U	U	
4	WG	9.9	0.35	U	U	U	
29B	WG	9.1	0.39	U	U	U	
4’	WG	25.00	0.31	U	U	U	
26	WG	13	0.85	U	U	U	
5’	WG	7.5	0.70	U	U	S	
6	WG	3.3	1.02	S	S	S	
FR7	GG	7.3	0	U	U	U	Li (2008)
FR8	GG	8.0	0	U	U	U	
HF01	GG	10.5	0.13	U	U	U	
HF03	GG	5.0	0.4	U	U	U	
HF05	GG	5.7	0.6	U	U	U	
HF10	WG	15.5	0.7	U	U	S	
A	GG	11	0.85	U	U	U	Chang and Zhang (2011)
F	GG	17.8	0	U	U	U	Marot et al. (2011)
A	GG	12	0.45	U	U	U	Salehi Sadafhiani and Witt (2011)
Specimen A	GG	8.67	0.1	U	U	U	Lin ke and Akihiro Takahashi (2012)
Specimen B	GG	10	0.2	U	U	U	
Specimen C	GG	8.67	0.2	U	U	U	
Specimen D	GG	31.7	0.3	U	U	U	
K_{27}	WG	11.3	0.2	U	U	U	Current study
$K_{8.5A}$	GG	2.7	0.5	S	S	U	
K_{40A}	WG	-	-	-	-	U	
$K_{8.5B}$	GG	2.7	0.5	S	S	U	
K_{40B}	GG	-	-	-	-	U	
$K_{1.9}$	WG		0.3	S	S	U	

WG: Widely graded soils; GG: Gap-graded soils; U: Unstable soils; S: Stable soils

Table 5.2. Evaluation of internal stability of soils by Burenkova method (1993)

Sample name	Soil gradation	D_{90}/D_{15}	D_{90}/D_{60}	Assessment	Laboratory	References
A	WG	37	2.11	U	S	Usace(1953)
B	WG	38.4	4.92	U	S	
C	WG	20.77	4.58	U	S	
D	WG	15.2	1.68	U	U	
A	WG	36.16	1.90	U	U	Kenney and Lau (1985)
D	WG	22.88	1.7	U	U	
X	WG	16.33	1.81	U	U	
Y	WG	90.06	2.34	U	U	
Y_s	WG	47.98	2.14	U	U	
A_s	WG	21.77	1.79	U	U	
D_s	WG	4.24	1.87	S	S	
K	WG	3.98	1.40	S	S	
1	WG	11.68	1.49	U	S	
2	WG	36.22	3.62	S	S	
3	WG	13.42	1.57	U	S	
C_u=3	WG	5.2	1.93	S	S	
C_u=6	WG	14.7	2.93	S	S	
C_u=12	WG	41.57	4.44	U	S	
1	WG	5.2	1.28	U	U	Burenkova (1993)
2	WG	4.5	1.45	U	U	
3	WG	8.63	1.41	U	U	
4	WG	15.08	1.527	U	U	
11	WG	20.72	2.69	S	S	
12	WG	35.63	3.49	S	S	
13	WG	49.35	4.13	S	S	
14	WG	67.96	4.38	S	S	
A	GG	19.13	1.54	U	U	Skempton and Brogan (1994)
B	WG	7.46	1.54	U	U	
C	WG	7.1	1.54	U	S	
D	WG	3.88	1.45	S	S	
G3-a	GG	11.66	1.47	U	U	Honjo et al. (1996)
G3-b	GG	13.61	1.55	U	U	
G3-c	GG	14.48	1.67	U	U	
G4-a	GG	16.49	1.48	U	U	
G4-b	GG	19.25	1.56	U	U	
G4-c	GG	20.48	1.68	U	U	
G1-a	GG	2.38	1.42	S	S	

G1-b	GG	8.37	1.48	U	S	
G1-c	GG	9.77	1.56	U	S	
G1-d	GG	10.39	1.68	U	S	
G2-a	GG	5.82	1.47	S	S	
G2-b	GG	6.80	1.55	S	S	
G2-c	GG	7.24	1.67	S	S	
4.4S25	GG	11.96	1.54	U	U	Khan (2003)
5.9S25	GG	12.68	1.30	U	U	
7.4S25	GG	20.04	1.55	U	U	
8.7S25	GG	20.71	1.40	U	U	
a	WG	31.66	1.86	U	U	Mao (2005)
b	WG	56.47	2.83	S	U	
c	WG	14.69	1.58	U	U	
d	WG	10.19	1.41	U	U	
A	GG	45.70	1.34	U	U	
B	GG	41.38	1.32	U	U	
C	GG	30.57	1.30	U	U	
D	GG	22.85	1.34	U	U	
T0	GG	242.63	4.03	S	U	Moffat (2005)
T5	GG	242.63	4.03	S	U	
C-20	WG	140.72	9.22	U	U	
C-30	WG	175.16	8.06	U	U	
1	WG	22.29	1.25	U	U	Liu (2005)
2	WG	71.62	1.4	U	U	
3	WG	191.83	2.75	U	U	
4	WG	79.56	2.40	U	U	
29B	WG	100.61	1.24	U	U	
4’	WG	140.48	1.65	U	U	
26	WG	24.56	2.62	S	U	
5’	WG	220.98	4.30	S	S	
6	WG	158.12	7.13	U	S	
FR7	GG	14.57	1.38	U	U	Li (2008)
FR8	GG	14.36	1.34	U	U	
HF01	GG	26.67	1.69	U	U	
HF03	GG	37.71	2.77	S	U	
HF05	GG	124.14	8.87	U	U	
HF10	WG	35.12	2.26	S	S	
A	GG	35.24	1.95	U	U	Chang and Zhang (2011)
F	GG	2.77	1.29	U	U	Marot et al. (2011)

A	GG	12.09	0.86	U	U	Salehi Sadafhiani and witt (2011)
Specimen A	GG	16.15	1.17	U	U	Lin ke and Akihiro Takahashi (2012)
Specimen B	GG	15	1.17	U	U	
Specimen C	GG	10.5	1.17	U	U	
Specimen D	GG	2.65	1.17	U	U	
K_{27}	WG	344.4	6.2	U	U	Current study
$K_{8.5A}$	GG	38.75	3.83	S	U	
K_{40A}	WG	442.86	10.69	-	-	
$K_{8.5B}$	GG	38.75	6.2	U	U	
K_{40B}	GG	442.86	6.2	-	-	
$K_{1.9}$	WG	30.78	4.44	U	U	

Table 5.3 Assessment of test specimens to internal stability by empirical theories

Sample notation	Test results in the laboratory	Assessment of internal stability			
		Kezdi (1979)	Kenney, Lau (1985,1986)	Burenkova (1993)	Chang, Zhang (2013)
K_{soil}	U	U	U	U	S
$K_{1.9}$	S	S	S	U	U
$K_{8.5A}$	S	S	S	S	U
$K_{8.5B}$	U	S	S	U	U
K_{40A}	U	-	-	-	S
K_{40B}	U	-	-	-	S

Note: U means unstable and S means stable;

5.2 Seepage flow test on Toyoura sand.

Before commencing discussions of piping phenomenon for Komaoka volcanic soils, a reliability of test apparatus used in this study was confirmed on Toyoura sand (see Figure 5.4). In order to accomplish the purpose, the upward seepage test on Toyoura sand was performed in the test apparatus of laboratory with the same test condition in the seepage apparatus shown in Yoshimi data (See Figure 5.5). Test results of Toyoura sand reported by Yoshimi et al. (1975) and current laboratory are shown in Figure 5.6. In the figure, linear relationships between hydraulic gradient and flow velocity are recognized at the first stage. This is accordance with Darcy's law indicating that the rate of flow is proportional to the hydraulic gradient. Additionally, the velocity of seepage flow in Toyoura sand with D_r=28% of relative density was almost the same as that of D_r=32% (Yoshimi et al. 1975). The calculated critical hydraulic gradients for Toyoura sand with D_r=32% and D_r=28% by Terzaghi's equation are 0.9 and 0.88, and the experimental

values are 0.9 and 1, respectively. The piping phenomenon was also not observed in Toyoura sand until boiling phenomenon occurred for this study. Therefore, the reliability of the apparatus at current laboratory was confirmed.

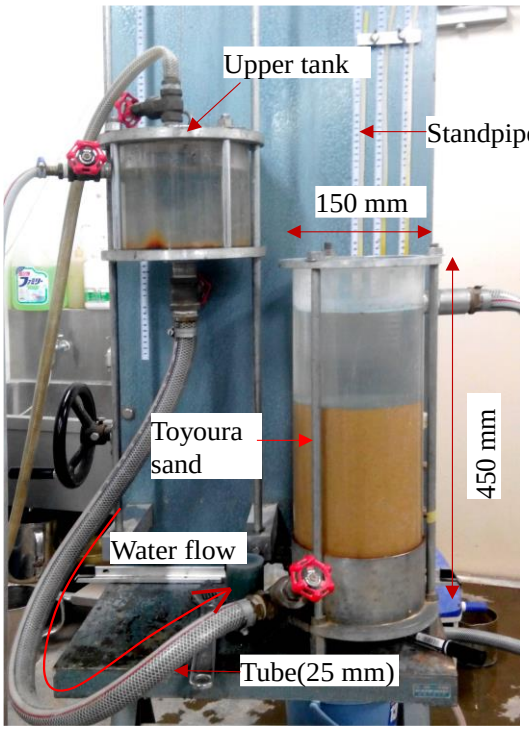

Figure 5.4. Apparatus for seepage test (Current laboratory)

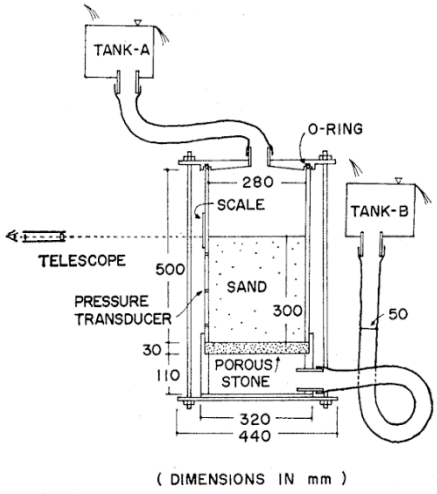

Figure 5.5 Apparatus for seepage test (Yoshimi et al., 1975)

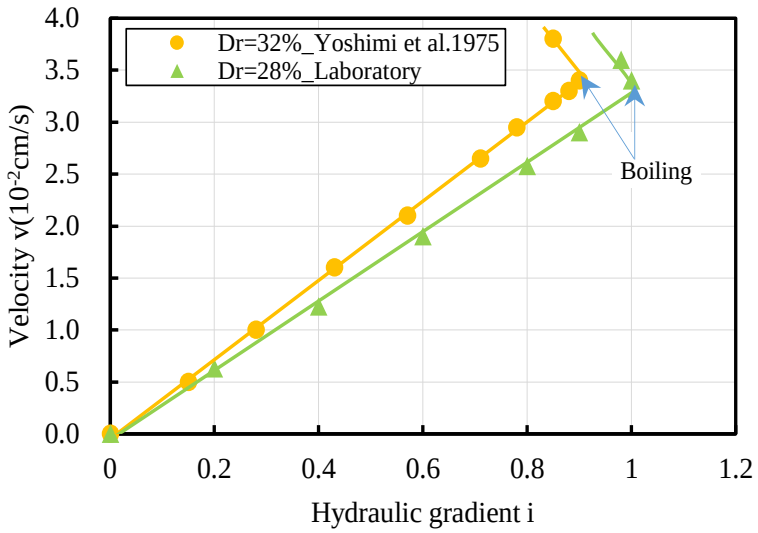

Figure.5.6 Results of test on Toyoura and with Dr=32% (Yoshimi et al., 1975) and Dr=28% (Laboratory).

5.3 Piping phenomenon in Komaoka volcanic soils.

To assess the piping phenomenon on test materials in this study, a small apparatus with 10cm in diameter and X-ray CT scanner device are used in the laboratory. The piping phenomenon was investigated on original Komaoka volcanic soil (K_{soil}). Test material and test procedure is performed in the laboratory as represented at Chapter 4. The results of seepage test are presented as follows.

Firstly, a flow velocity was directly measured using a graduated cylinder. Subsequently, the result of the piping test on original Komaoka volcanic soil (K_{soil}) with the degree of compaction is 85% is represented in Figure.5.7. At the first stage of the test process, the slope of curve showing the relationship between hydraulic gradient and flow velocity was changed. In particular, at hydraulic gradient (i) equal 0.1, the permeability of K_{soil} suddenly decrease (see Figure.5.7 (b)). This means that movement of particles occurs in the sample and changes soil structure. Under seepage flow, a part of fine particles fill into void of coarse particles leading to decreasing effective porosity of the test sample. Subsequently, the permeability of K_{soil} gradually increases until i=0.6. At i=0.7 the boiling phenomenon occurred in the sample in which velocity of water flow suddenly increased, as shown in Figure.5.7 (a).

Additionally, microscopic particles behavior in K_{soil} under seepage flow was observed by X-ray CT scanner. In this study, choosing eight representative sections to analyze deformation of particles in seepage test were depicted as Figure.5.8. Based on these sections, deformation of soil particles was calculated by comparing changes of image pairs at different hydraulic gradients such as i=0.0, 0.1, 0.2, 0.3, 0.4, 0.5 and 0.6 in

which the 2-dimensional Digital Image Correlation analysis, DIC (White et al. 2003) was used. The image processing conducted during the experiment to measure the displacement of soil particles between a pair of digital images is shown schematically in Figure.5.9. The first image is divided into a grid of test patches. Each test patch, $I_{test}(U)$, consists of a sample of the image matrix, I(U), of size 50x50pixels (approximately 3.72 x 3.72 mm square). To find the displacement of the test patch between images 1 and 2, a search patch $I_{search}(U + S)$ is extracted from the second image. This search patch extends beyond the test patch by a distance S_{max} = 20 pixels, in the Z and Y directions, defining the zone in which the test patch is to be searched for (Figure.5.9). The cross-correlation of $I_{test}(U)$ and $I_{search}(U + S)$ is evaluated, and normalized by the square root of the sum of the squared values of $I_{search}(U + S)$ over the range of U occupied by the test patch. The correlation operations are conducted in the frequency domain by taking the fast Fourier transform (FFT) to reduce the computational requirement. The procedure described above for evaluating a single displacement vector is repeated for the entire grid of test patches that were located on a grid with 20 pixels spacing (approximately 1.488 mm), producing the displacement field between the pair of images.

Total images collected from X-ray CT machine are about 1000 images which correspond to cross and longitudinal sections of XY, YZ, and XZ axes, as shown in Figure.5.10. The typical result of deformation vectors of particles at imposed hydraulic gradient values were represented from analyzing X-ray CT images are shown in Figure.5.11. In particular, these Figures depict distribution of deformation vectors of particles calculated using the images at hydraulic gradient i = 0.0, 0.1, 0.2, 0.3, 0.4, and 0.6 of eight representative slice images by the DIC analysis, as shown in Appendix. Based on these Figures, it is clear that the upward deformations of particles due to water flow are increased with the increase in hydraulic conductivity. In particular, at i=0.1 slight movement of particles was seen in the whole area of the specimen. Similarly, at i=0.2 and i= 0.3 the movement of particles was still slight but at between of compaction layers of the sample, particles movement was larger. At i=0.4 and i= 0.5 particles strongly moved in the middle of the top layer (layer 1) and between of compaction layers 2 and 3. In addition, slight movement of particles occurred on the other area of the sample. At i=0.6 strong movement of particles occurred on the whole area of the sample until the internal erosion was completed in the sample, that means boiling phenomenon, at i=0.7.

Based on Figures shown deformation vector of particles, synthesizing displacement of soil particles from eight sections of the X-ray CT images of speciment (K_{soil}) was performed. As a result, evaluating the movement of particles in the model test with Ksoil is clarified, as shown in Figure.5.12. For example, when the value of hydraulic gradient(i) is 0.1, a slight movement of fine particles occurred, particularly 95% particles

moved with distance less than 0.1mm and 5% particles moved with distance more than 0.1mm. At i=0.2, 98% particles moved with distance less than 0.1mm and 2% particles moved with distance more than 0.1mm. Therefore, movement of particles is decreased when the value of hydraulic gradient increase from 0.1 to 0.2. These results analyzed vector deformation phenomenon coincides with the result shown in Figure.5.7. The permeability decrease corresponds with an increase from 0.1 to 0.2 of hydraulic gradient. Movement of fines at i=0.1 deems to induce the changes of pore structures and to prevent internal erosion process of the sample under seepage flow. This coincides with the suggestion of Kenney and Lau (1985), loose particles move from pore to pore of coarse particles, if they encounter smaller constrictions, their movement will be halted and they will act as parts of the filter fabric. At i= 0.3 velocity of flow increases, fine particles move over the whole area of model test with percentage ratio at movement distance of particles (A) >0.1mm is 21%. Then, Fine particles washed up through the sample at i=0.3 trapped by the filter at i=0.4. A relative of low permeability and 19% of percentage ratio at A>0.1% prove lift of filter. The crack open again at i=0.5 and 0.6, percentage ratio of particles movement at A > 0.1mm were 79%, and 92%, respectively. The fine particles are washed out by seepage flow. This leads to be an increase in hydraulic conductivity. At i=0.7, there was boiling of fine particles and a fast increase in velocity of flow at the same hydraulic gradient.

In addition, based on the maximum size of fine particles in the test material the movement of particles of K_{soil} was tracked in the range of 0 to 0.075mm and more than 0.075mm by analyzing images from X-ray CT and using the DIC program. From Figure.5.13, it is evident that fine particles at the first stage of *i*=0.1 to 0.2 were gradually moved by water flow in the specimen. For example, 76.9%-84% of particles were moved for the range of 0 <A< 0.075 mm and A>0.075mm. Thus, piping phenomenon occurred in model test at around *i*=0.1. It is also clear from *i*=0.3 to *i*=0.6 that migration of particles due to water flow increased with the increase in hydraulic conductivity. At i=0.5 and 0.6, percentage ratio of particles movement at A > 0.075mm were 87.2%, and 94.5%, respectively. The fine particles are washed out by seepage flow, leading to an increase in hydraulic conductivity. At i=0.7, there was boiling of soil particles this means a fast increase in velocity of flow at the same hydraulic gradient.

Based on analyzing images from X-ray CT scanner, it indicated that using X-ray CT method for evaluating internal erosion on soils is really useful, specially for soils having large fine particles such as volcanic soils in this study.

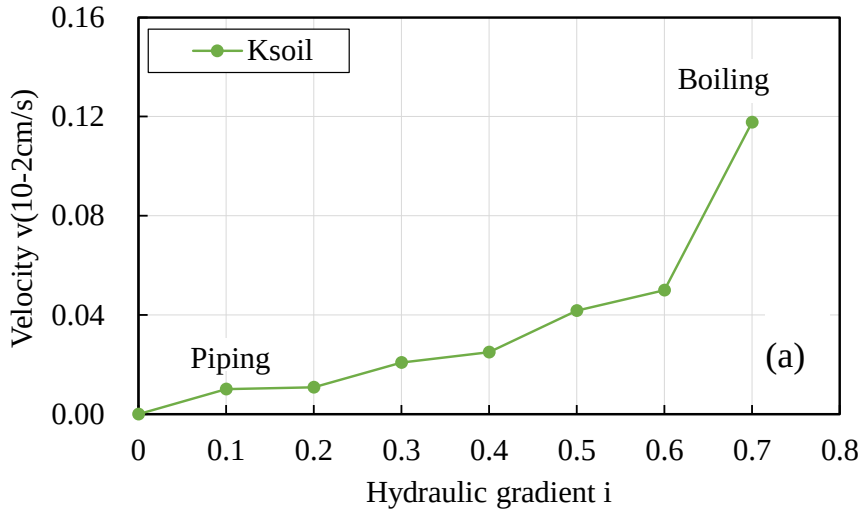

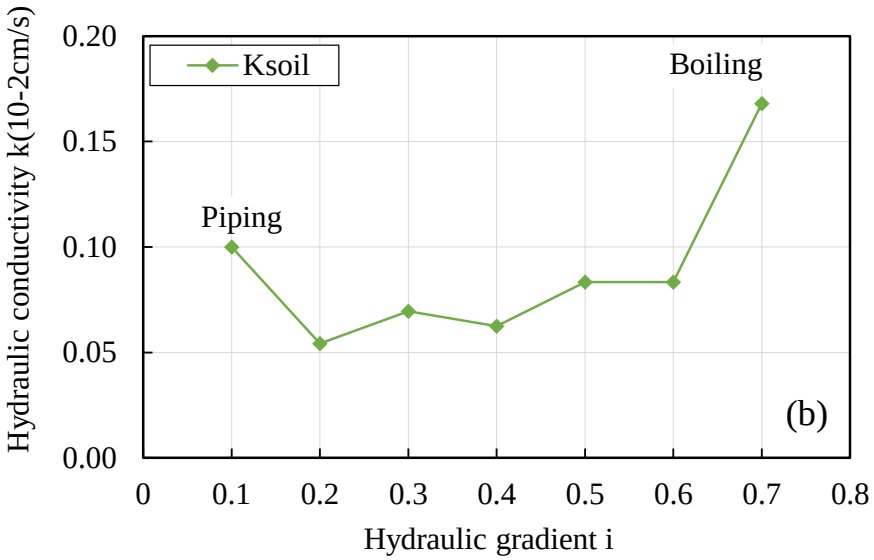

Figure.5.7 Test results of K soil with small apparatus:
(a) velocity, (b) hydraulic conductivity

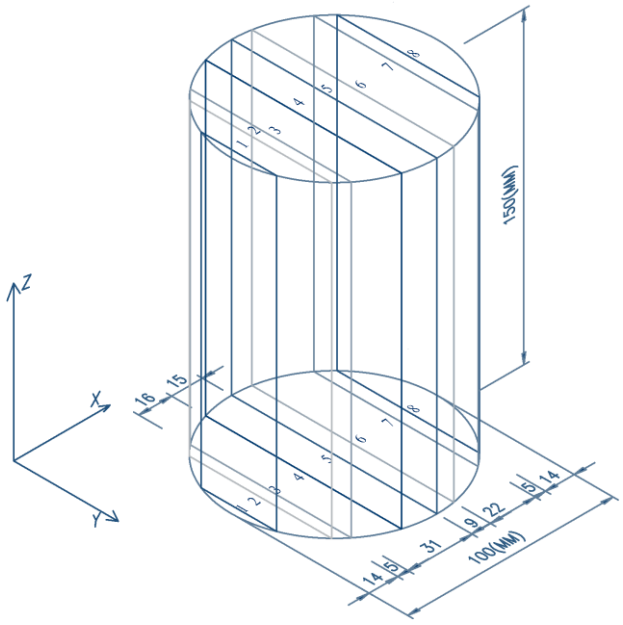

Figure.5.8 Schematic vertical section of CT images

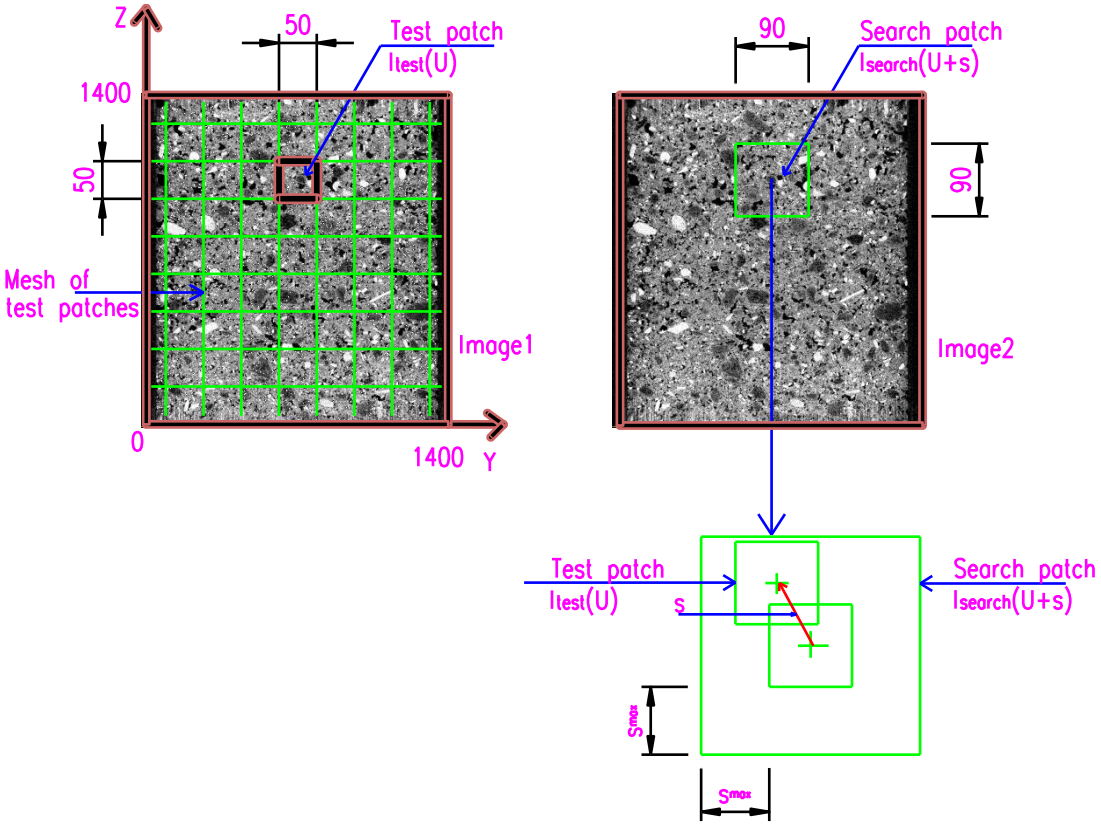

Figure.5.9 Processing deformation vector analysis from CT images

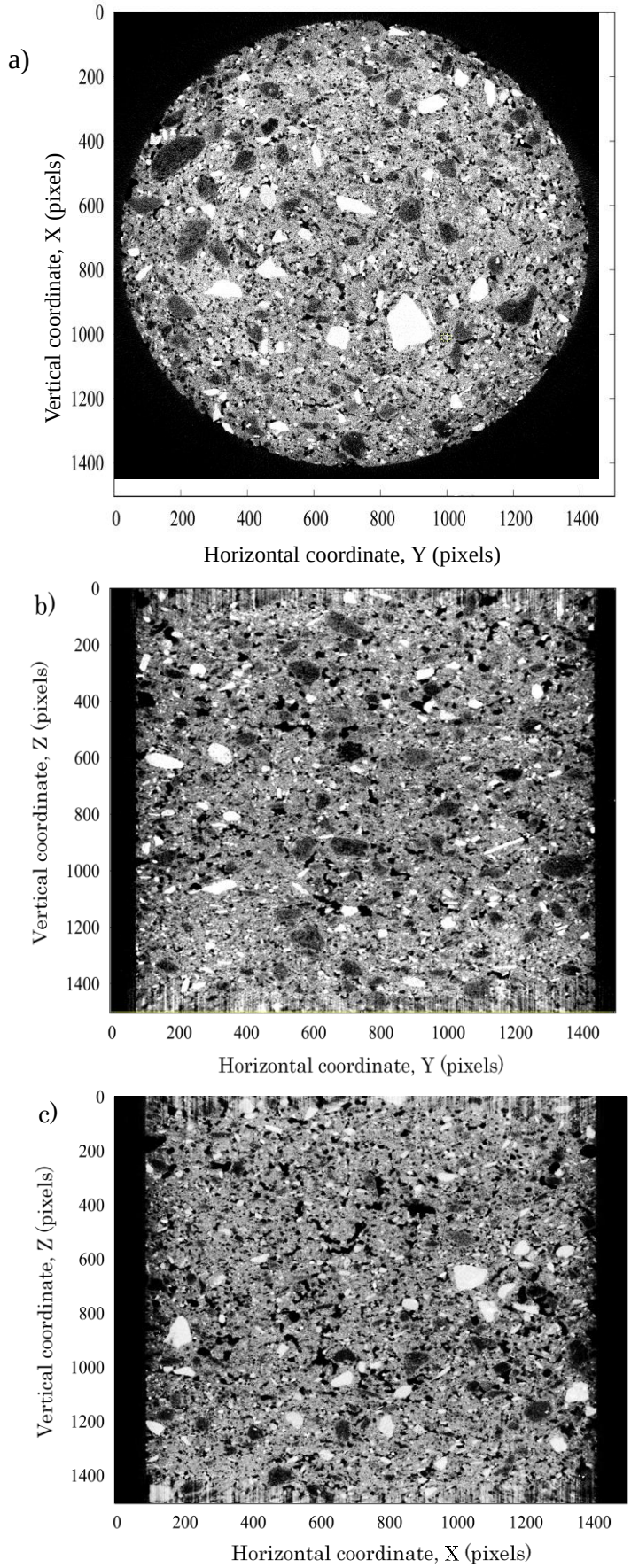

Figure.5.10 X-ray CT images: (a) XY Cross section, (b) YZ Longitudinal section (c) XZ Longitudinal section

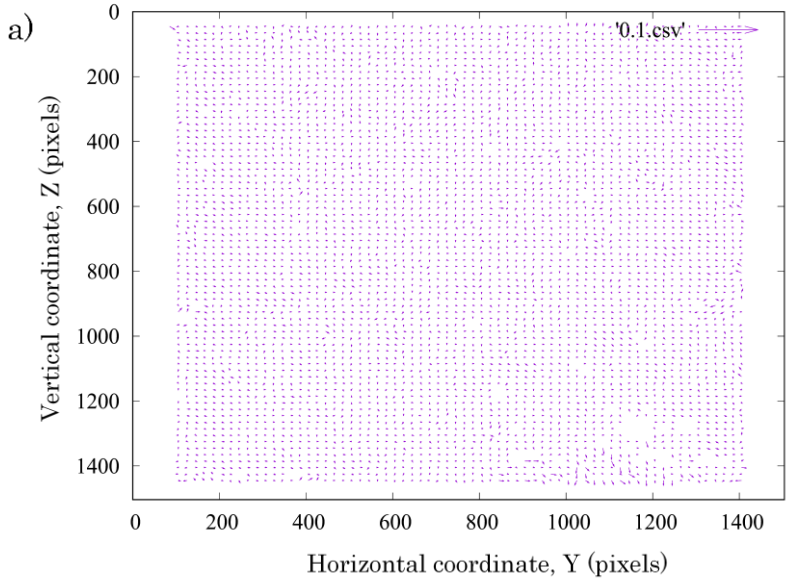
a)
'0.1.csv'
Vertical coordinate, Z (pixels)
Horizontal coordinate, Y (pixels)
0
200
400
600
800
1000
1200
1400

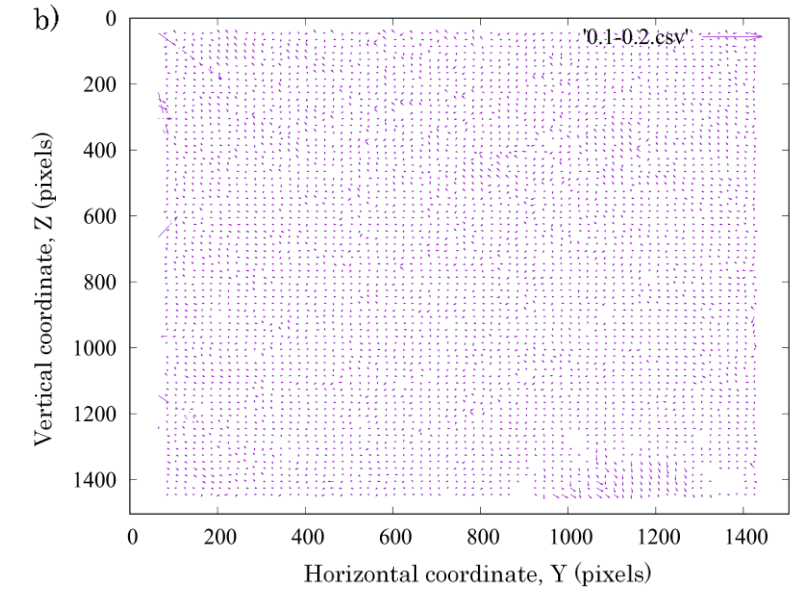
b)
'0.1-0.2.csv'
Vertical coordinate, Z (pixels)
Horizontal coordinate, Y (pixels)
0
200
400
600
800
1000
1200
1400

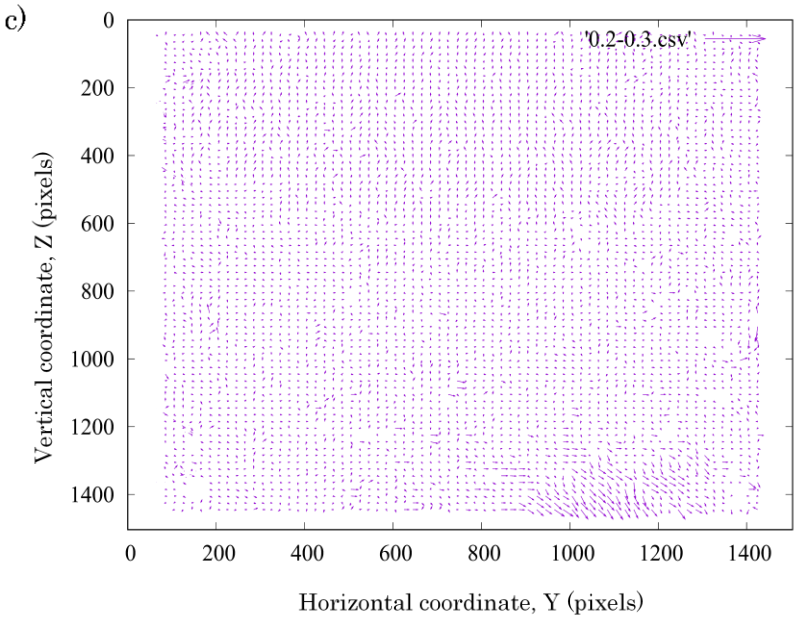
c)
'0.2-0.3.csv'
Vertical coordinate, Z (pixels)
Horizontal coordinate, Y (pixels)
0
200
400
600
800
1000
1200
1400

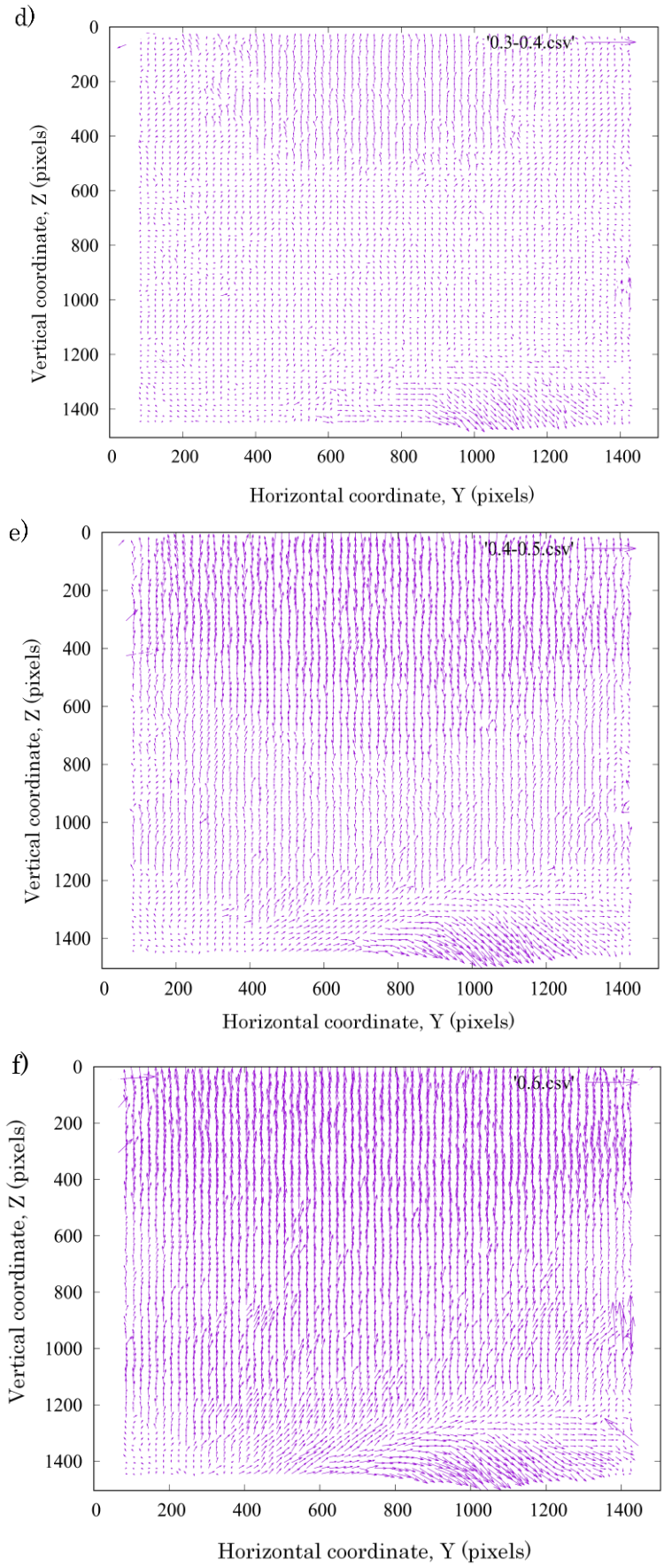

Figure.5.11 Particles deformation depicted vector deformation by DIC: (a) i=0.1, (b) i=0.2, (c) i=0.3, (d) i=0.4, (e) i=0.5, (f) i=0.6

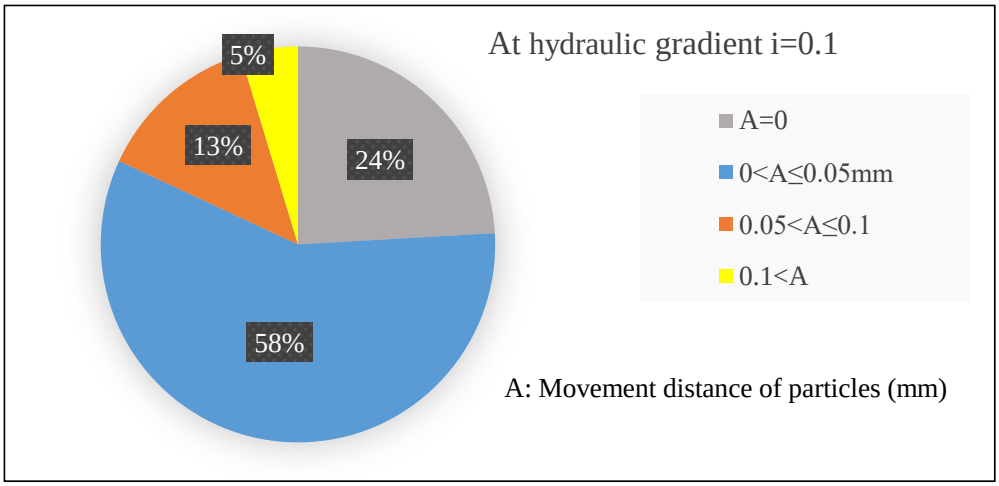
At hydraulic gradient i=0.1
5%
13%
24%
58%
A=0
0<A≤0.05mm
0.05<A≤0.1
0.1<A
A: Movement distance of particles (mm)

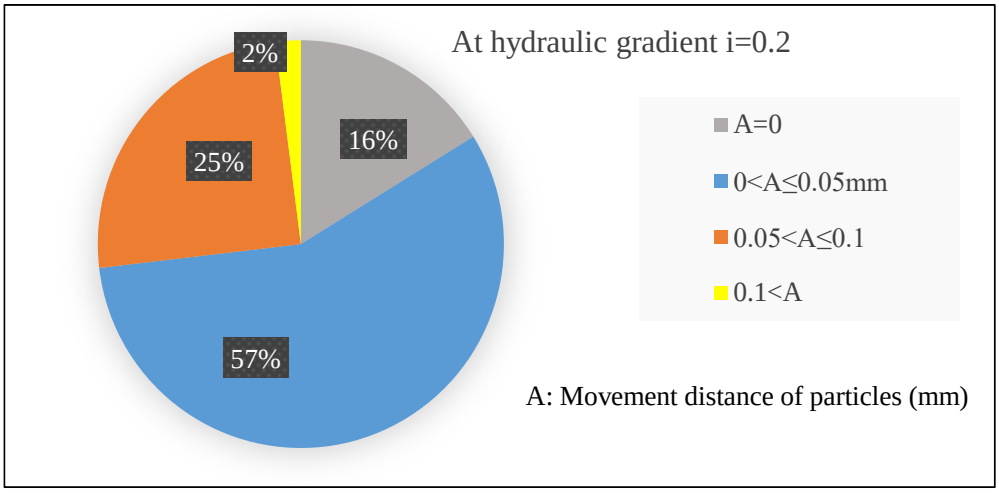
At hydraulic gradient i=0.2
2%
25%
16%
57%
A=0
0<A≤0.05mm
0.05<A≤0.1
0.1<A
A: Movement distance of particles (mm)

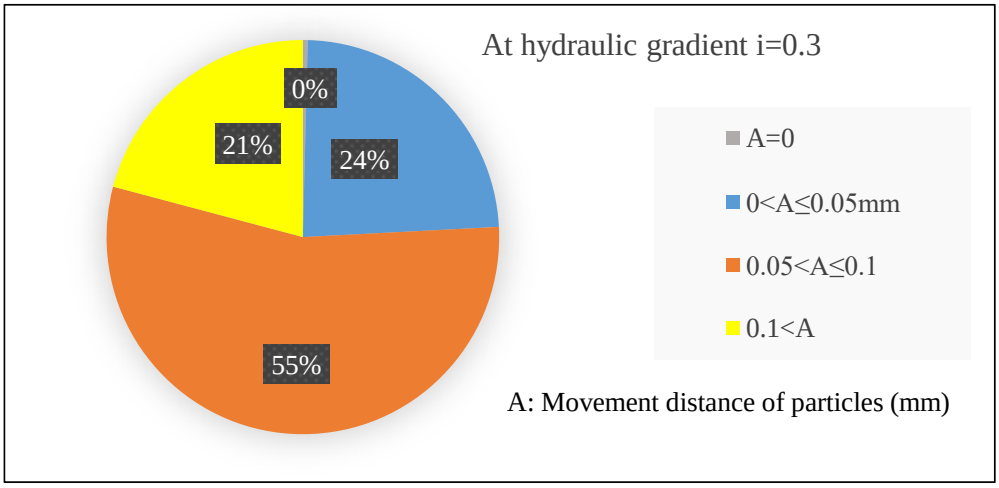
At hydraulic gradient i=0.3
0%
21%
24%
55%
A=0
0<A≤0.05mm
0.05<A≤0.1
0.1<A
A: Movement distance of particles (mm)

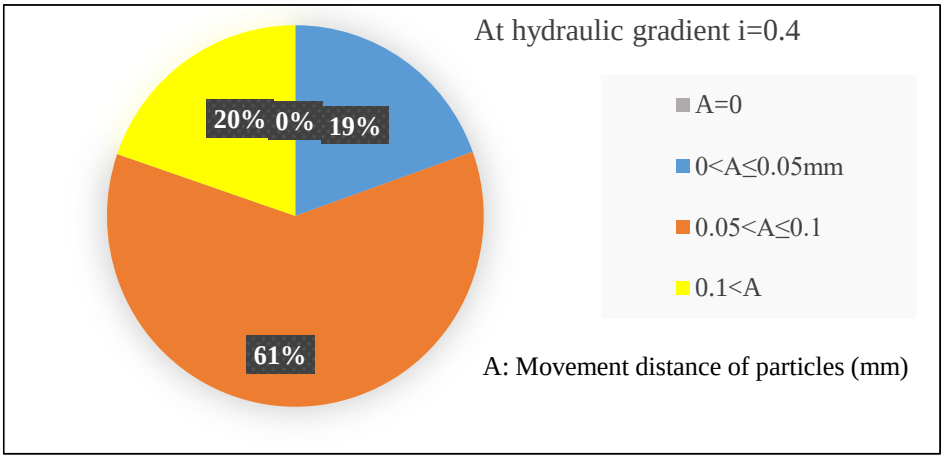

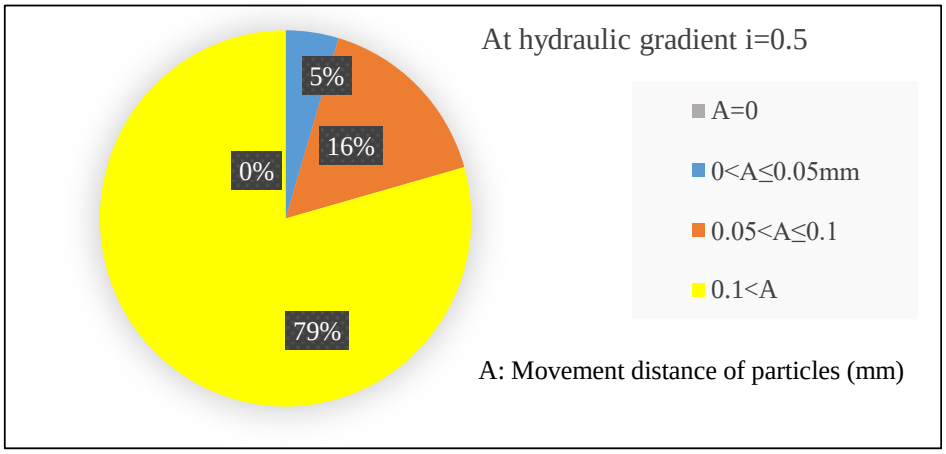

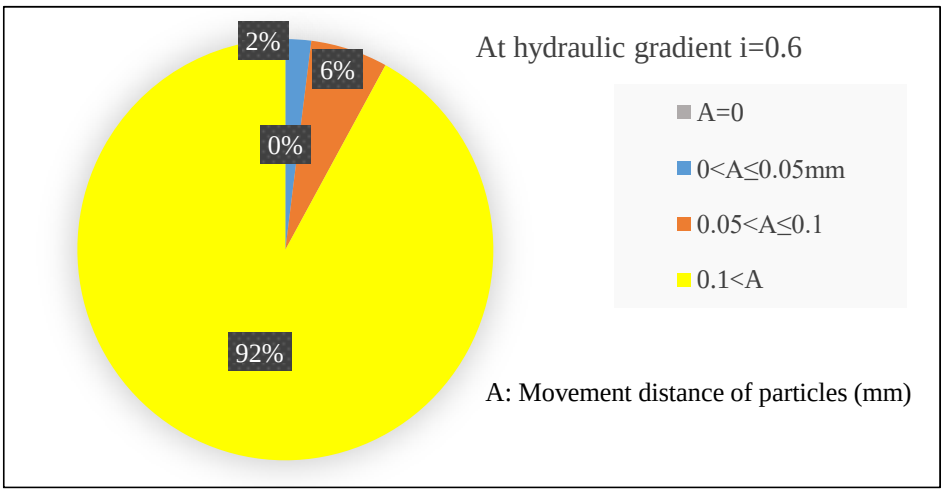

Figure.5.12 Analyzing particles movement from images of X-ray CT

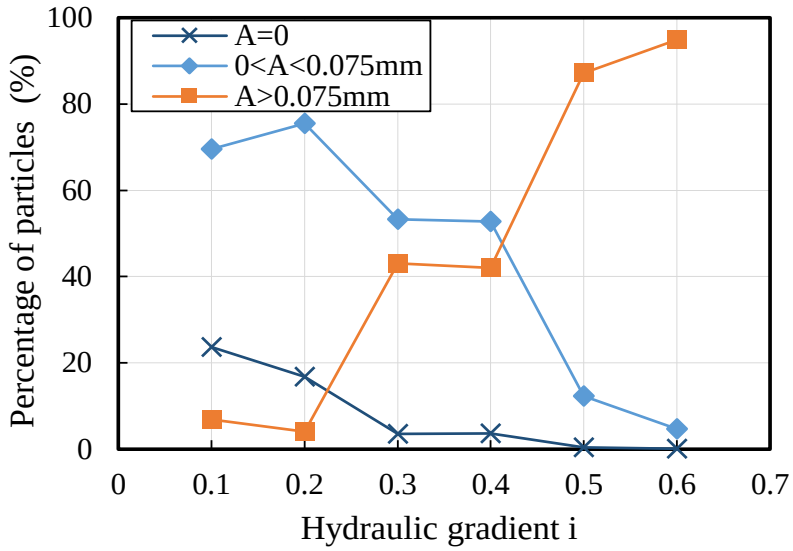

Figure.5.13 Diagram of distance of particle movement, a based on DIC analysis

5.4 Internal erosion of compacted volcanic soils

The large apparatus with 150mm in diameter was used in these experiments. In specimen reconstitution process, the value of initial water content (W_0) was equal to 37% in all samples. In addition, compaction effort imposed on samples was different depending on the degree of compaction of samples. In particular, the number of compaction per each layer of the sample is 42, 75 and 120 times corresponding to the degree of compactions (D_c) are 83%, 88%, and 95%. The degree of compaction was controlled by the index of dry density (ρ_d) of the specimen in the container. For example, K_{soil} with D_c=83%, 88%, and 95% correspond to ρ_d=0.918g/cm^3, 0.972 g/cm^3, and 1.048 g/cm^3. Subsequently, the saturation process is conducted with slow water flow into the sample. It takes around eight hours for this step until the top surface of the sample is submerged, test results are presented in Figure.5.14. This figure shows the relationship between hydraulic gradient and flow velocity, hydraulic conductivity (permeability) of K_{soil} with the different degree of compactions are 83%, 88%, and 95%, as shown in Table 4.1. At i=0.2, internal erosion occurred in all the samples. The erosion process generates the movement of fine particles within pores of coarse particles. In the K_{soil} with 83% of compaction degree, a little fine particle was lost from the test specimen at i=0.2. This induces the increase of void ratio, with increasing of hydraulic conductivity until i=0.4. From i=0.4 to i=0.8, an approximate linear relationship between hydraulic gradient and hydraulic conductivity was recognized at this stage, and internal erosion was not observed at that time. Contrarily, the permeability of the K_{soil} with 88% and 95% of compaction degree is decreased until i=0.4. This might be due to the compacted soil process lead to a strong decrease in pore size of the samples, halting travel of fine particles and making them as parts of the filter fabric. Over i= 0.4, fine particles were washed out by seepage

flow. As a result, this was leading to an increase in effective porosity, namely an increase of permeability (see Figure.5.14(b)). Finally, “boiling” occurred.

These results indicate that the degree of compaction can affect the performance of primary fabric of samples constructed by Komaoka volcanic soil (K_{soil}). The primary fabric acts as a filter for fine particles which is transferred by seepage flow. Furthermore, it is clear to see that there is a boundary value between the degree of compaction Dc = 83% and Dc = 88% influencing on the different behavior of internal erosion for K_{soil}. Especially, the difference of compaction degree at D_c=83% and D_c=88% was leading to the difference of constriction of coarse particles which affect the moving fine particles under water flow at the first stage of internal erosion. In addition, the tendency of internal erosion process of compacted materials with D_c>88% is almost the same. The influence of compaction degree on critical hydraulic gradient for internal erosion is shown in

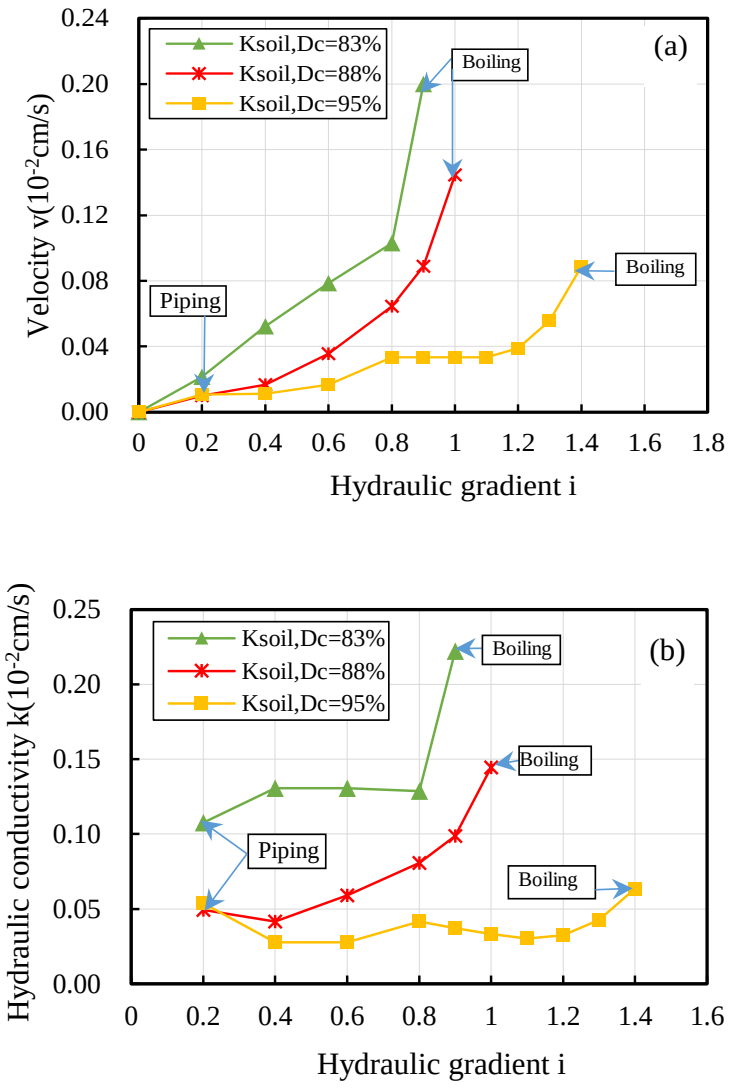

Figure.5.14 Change in results of K_{soil} with different compaction degrees: (a) velocity, (b) hydraulic conductivity.

Figure.5.15. A large degree of compaction for the sample with the same volcanic soil leads to a large value of critical hydraulic gradient for the onset of boiling.

During monitoring in the laboratory, the separation between compaction layers was observed when boiling phenomenon was induced. Particularly, the delamination phenomenon occurred at the boundary of compacted layer 1 and layer 2. The cause was due to weak connection of soil particles at the boundary of compacted layers. Simultaneously, the distance from compacted layer 2 to layer 4 is large, as a result, fine particles was slowly washed out under the seepage flow velocity. Consequently, these layers act as part of the filter fabric. The seepage force strongly concentrates at between compacted layer 1 and layer 2 and induces the delamination phenomenon, as shown in Figure.5.16. This indicates a significant sign to influence internal instability of man-made earth structures in the field.

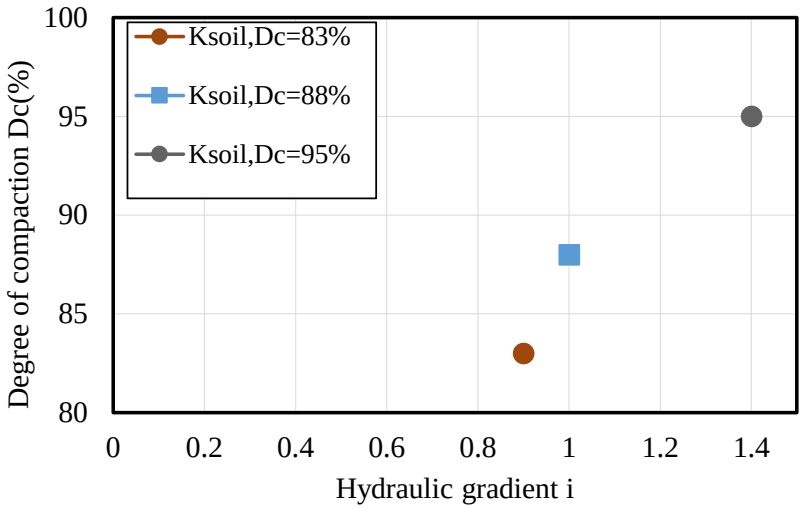

Figure.5.15 Relationship between D_c and i at the onset of boiling

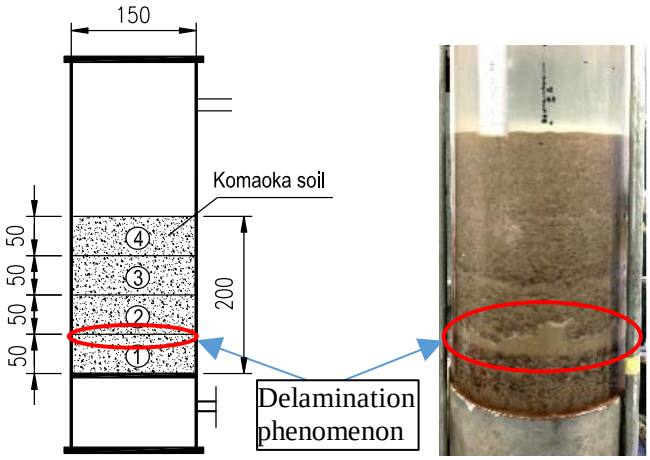

Figure.5.16 Observed delamination of K_{soil} at the onset of boiling.

5.5 Influence of fines on piping phenomenon

Particle crushing of volcanic coarse grained soils is significant for evaluation of mechanical behavior of man-made soil structures. In this study, the influence of particle breakage on seepage performance of volcanic soil was examined. Actually, it has been reported that fines content for Komaoka volcanic soils under original conditions ranges from 26.0% to 42.6%, and volcanic soils generated from Shikotsu caldera indicate a high crushability (Kawamura et al., 2015; Miura et al., 2003). If particle crushing is induced due to external forces, fine particles will increase gradually. In order to clarify an influence of fine particles on the piping phenomenon, a series of seepage flow test was also performed on $K_{1.9}$, $K_{8.5A}$, $K_{8.5B}$, K_{40A}, K_{40A} and K_{soil} soils which have different initial fines content and compaction conditions, as illustrated in Figure.3.3 and Table 4.1.

In this part, all tests were prepared in the large apparatus. During reconstitution process of test samples, a tamping tool was used for compacting the soil to the required height. The dry density and initial water content of samples were controlled at the same value 0.972g/cm^3 and 37%, respectively. Subsequently, saturation of the samples was performed in a container. This process takes around 5-10h, which depend on amount of fine particles of soil sample, to ensure saturation quality. Finally, the seepage tests were conducted in the laboratory, as described in the test procedure part of this study.

Figure.5.17 shows the results of each test case. As shown in the figures, the directional curve change of relationship between hydraulic conductivity and hydraulic gradient of these samples, in accordance with Darcy's law, indicate that all the test samples showed internal erosion phenomenon. Except for $K_{1.9}$ sample, the hydraulic behavior such as the relationship between seepage velocity and hydraulic gradient of these samples is similar for each other. In addition, an increment of fine particles in the Komaoka soil affects seepage performance of the compacted soils. For example, the piping phenomenon early occurs in the samples (at i=0.2 with K_{40A}, $K_{8.5A}$, K_{soil} and at i=0.8 with $K_{1.9}$), and its critical hydraulic gradient at boiling phenomenon for $K_{1.9}$, $K_{8.5A}$, K_{soil} and K_{40A} is 1.4, 1.4, 1, and 0.6, respectively (see Figure.5.17(a)). This is due to the difference in the degree of compaction because the maximum value of dry density (ρ_{dmax}) of the compacted soils is changed depending on the amount of fines content (see Figure.3.5, Figure.3.6 and Table 3.3). In addition, variation in hydraulic conductivity is confirmed for $K_{1.9}$, $K_{8.5A}$, K_{40A} and K_{soil} (see Figure.5.17(b)), this is due to that fine particles are clogged into coarse grained particles and then are released. Consequently, the loss of fine particles seems to increase or decrease hydraulic conductivity. At the piping test for $K_{1.9}$ sample, the velocity of flow is much higher than other cases. The reason is that pore network in coarse particles cannot hunt fine particles, as shown in Figure.5.17(a).

On the other hand, there are differences in velocity and hydraulic conductivity for $K_{8.5A}$, K_{40A} compared to those for $K_{8.5B}$, K_{40B} (see Figure.5.18). This indicates an influence of an absence of intermediate particle sizes leading to an increase in the constriction in the pore network of the primary fabric of volcanic soil. Then, water flowing through the pore network will wash out fine particles from the sample. This shows more clearly at the volcanic soil with a high amount of fine particles such as K_{40A} and K_{40B}. The loss of fine particles lead to the increase in permeability and internal instability of the sample. Consequently, the onset of boiling phenomenon early occurs and the $K_{40A,B}$ samples reach the stage of zero effective stress at critical hydraulic gradient i_c =0.6. The variance in the critical hydraulic gradient for soil instability with the different initial fine contents for the test specimens is shown in Figure.5.19. From the results, it can be said that the estimations of the amount of fine particles and grain distribution curves are very important, especially for volcanic soils including soil particles with low specific gravity.

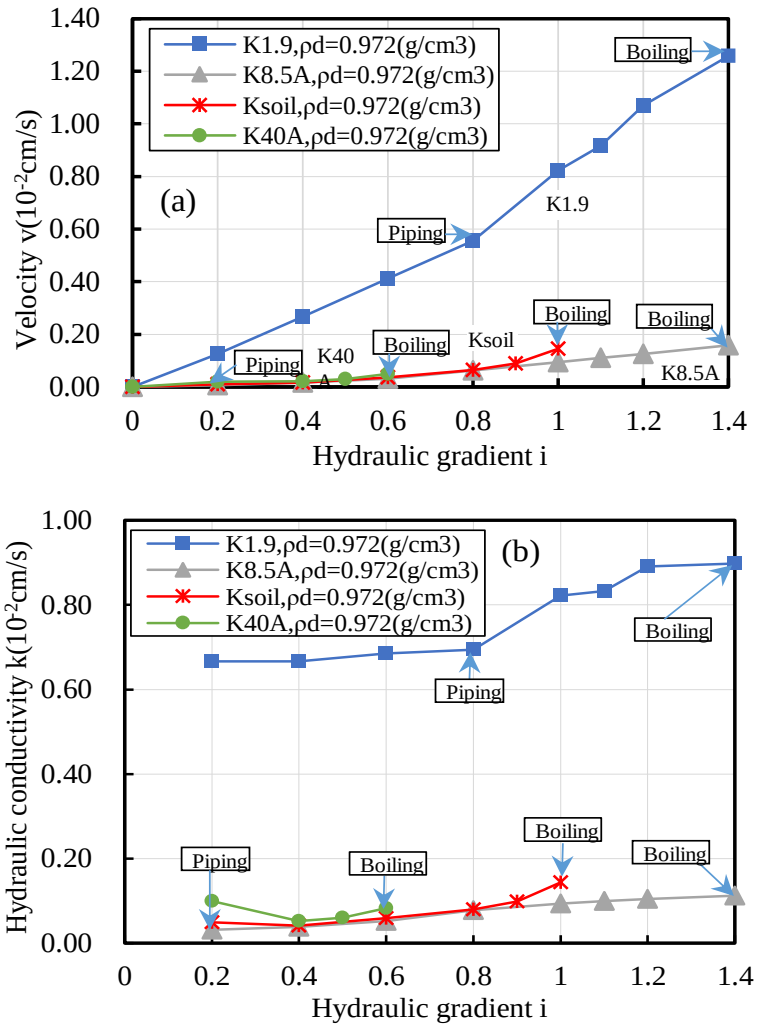

Figure.5.17 Test results of K_{soil}, $K_{1.9}$, $K_{8.5A}$ and K_{40A}: (a) velocity, (b) hydraulic conductivity.

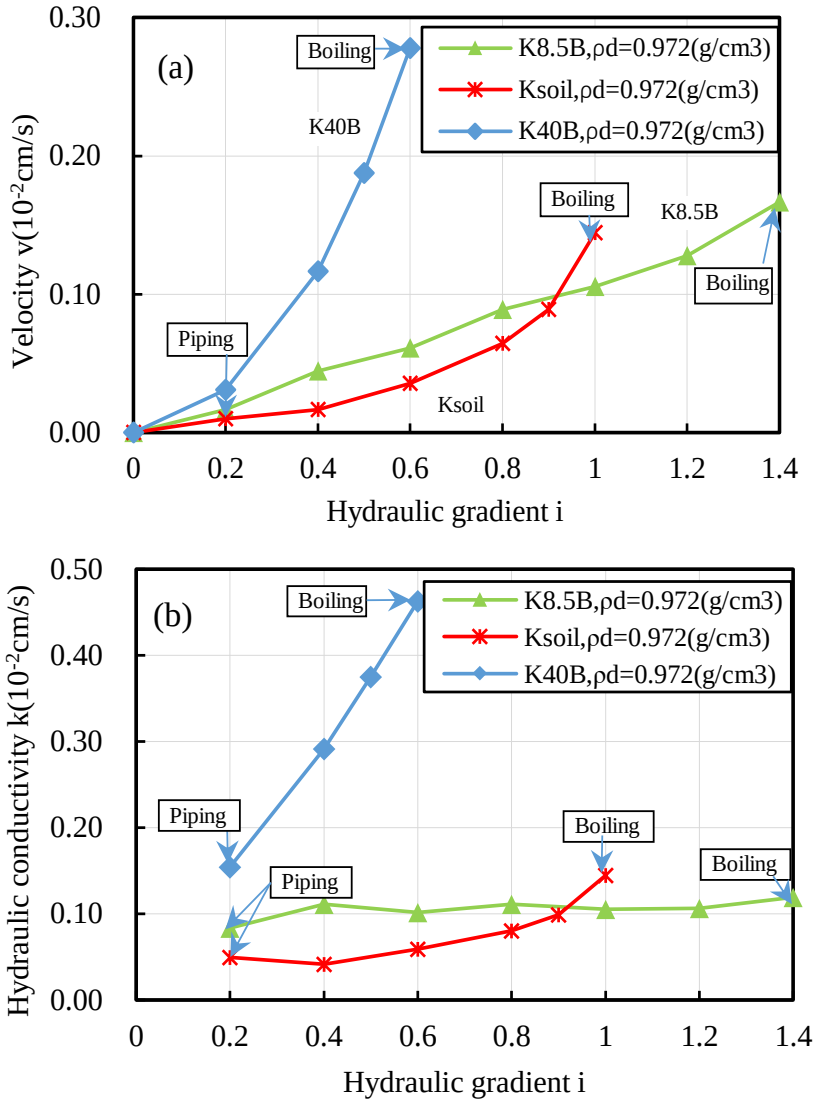

Figure.5.18 Test results of K_{soil}, $K_{8.5B}$ and K_{40B}: (a) velocity, (b) hydraulic conductivity.

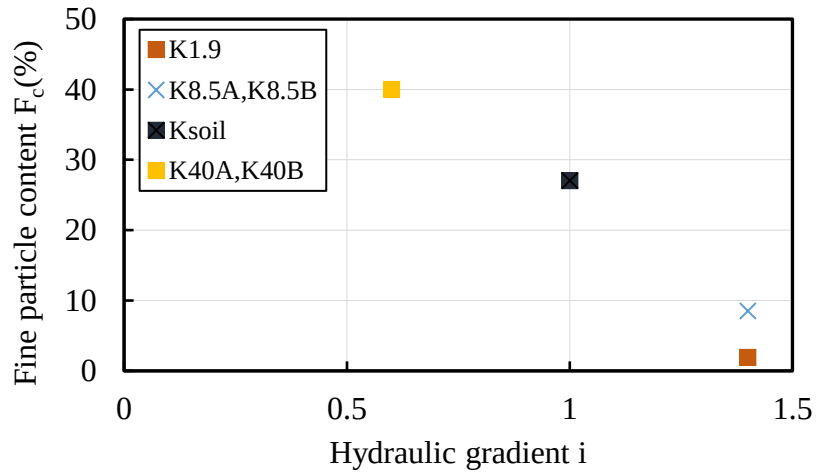

Figure.5.19 Relationship between F_c and i at the onset of boiling

5.6 Evaluation of internal stability of volcanic soils using critical void ratio

Seepage performance of Komaoka volcanic soils was clarified as described above. In this study, a simple method was proposed on volcanic coarse grained soils.

In general, a number of volcanic soils contain a relatively high amount of pumice soil particles. Nakata and Miura (2007) investigated that particles breakage features of volcanic coarse grained soils to characterize its mechanical properties. They revealed that in the volcanic soils, both inter-particle void and intra-particle void was simultaneously existed. In particular, volcanic soil particles containing void inside were modeled, as shown in Figure.5.20 and 5.21. According to their results, volcanic coarse grained soils in Hokkaido were composed of "opening intra-particle void" under a high rate, which leads to be particle breakage and changes in seepage performance. Therefore, it is important to evaluate the effect of critical void ratio on hydraulic mechanical properties of volcanic coarse grained soils. Furthermore, Kimura et al., 2010 indicated the relationship between opening intra-particle void ($e_{\text{intra-o}}$) and dry density of Komaoka volcanic soil (*Spfl*).

Based on their results, the actual void ratio was evaluated for internal stability of Komaoka volcanic soils under seepage flow. The following Eqs. to calculate soil parameters on void ratios for Komaoka volcanic soils are proposed;

$$\begin{aligned} e &= e_{inter} + e_{intra-o} + e_{intra-c} \\ &= \left(V_w + V_{pc} + V_{po}\right)/\left(V_f + V_s\right) \end{aligned} \tag{5.1}$$

where e is void ratio, $e_{\text{intra-o}}$ is opening intra-particle void, $e_{\text{intra-c}}$ is closing intra-particle void, as shown in Figure.5.20 and 5.21. Evaluation of both opening and closing intra-particle voids will be significant for piping phenomenon. In this study, an effective void ratio e' was adopted under seepage flow.

$$e' = e_{inter} = e - e_{intra-o} - e_{intra-c} \tag{5.2}$$

According to Kimura et al., (2010), these parameters was empirically given as follows;

$$\begin{aligned} &e = 1.78(\rho_d)^{-0.652}; e_{intra-c} = 0.04; \\ &e_{intra-o} = 1.49(\rho_d)^{-0.195} \end{aligned} \tag{5.3}$$

where ρ_d is dry density of soil (g/cm^3). As a result, effective critical hydraulic gradient is expressed follows;

$$i_{c\_intra} = \frac{G_s - 1}{1 + e'} \tag{5.4}$$

From Eq. (4), it is apparent that the effective critical hydraulic gradient i_{c_intra} is larger than those for theoretical ones, as shown in Table 5.4.

Based on test results, an experimental critical hydraulic gradient i_{c_exp} for each test case is summarized in Table 5.4 compared with theoretical critical hydraulic gradient i_c and effective critical hydraulic gradient i_{c_intra}. As shown in Table 5.4, i_c in some cases (K_{40A} and K_{40B}) is almost the same i_{c_exp}. On the other hand, i_{c_intra} of K_{soil}, $K_{1.9}$, $K_{8.5A}$, and $K_{8.5B}$ are similar to i_{c_exp}. From the results, it can be said that effective void ratio is available for evaluation of boiling phenomenon for the cases less than 40% of finer contents. For more than 40%, the theoretical method will be useful. At any rate, several evaluations will be required for investigation of stability of volcanic soil structures such as embankments.

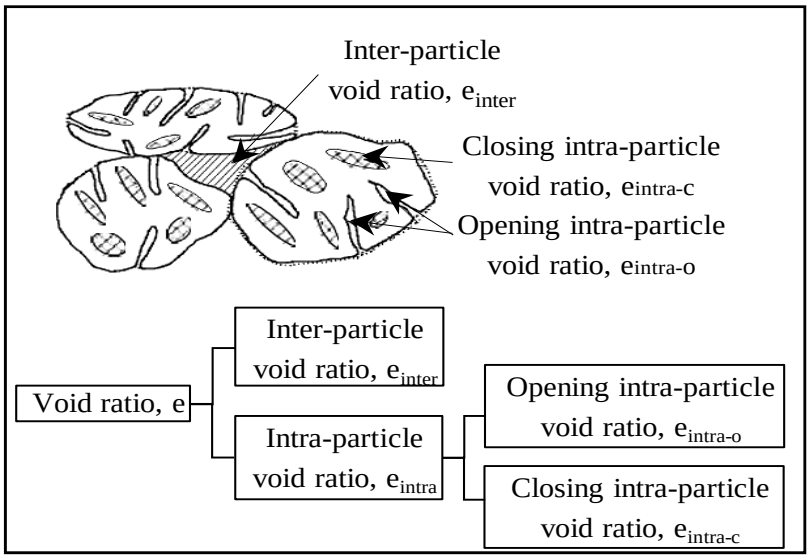

Figure.5.20 Schematic diagram of void ratio in volcanic soil
(revision of Nakata and Miura 2007)

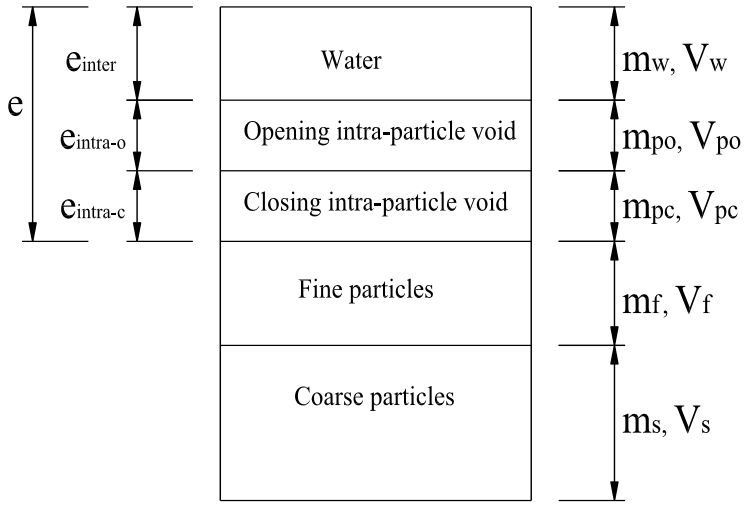

Figure.5.21 Schematic diagram of saturated volcanic soil model

Table 5.4 Critical hydraulic gradient for each case.

Sample name	Void ratio (e)	Effective void ratio (e')	Effective critical hydraulic gradient (i_{c_intra})	Theoretical critical hydraulic Gradient (i_c)	Experimental critical hydraulic gradient (i_{c_exp})
K soil	1.81	0.27	1.17	0.53	1.0
	1.73	0.25	1.18	0.54	1.4
	1.89	0.37	1.08	0.51	0.9
$K_{1.9}$	1.81	0.27	1.17	0.54	1.4
$K_{8.5A}$	1.81	0.27	1.17	0.54	1.4
$K_{8.5B}$	1.81	0.27	1.17	0.54	1.4
K_{40A}	1.81	0.27	1.17	0.54	0.6
K_{40B}	1.81	0.27	1.17	0.54	0.6

5.7 Summary

In this chapter, four commonly used geometric criteria, those of Kezdi (1979), Kenney and Lau (1986), Burenkova (1993) and Chang and Zhang (2013), are assessed using an experimental database of 81 gradations. It is found that unstable soils can be successfully assessed according to the Burenkova and Kezdi criteria. On the other hand, Kenny and Lau might successfully predict the potential for internal stability in soils. In addition, 2 of 7 test volcanic soils in the laboratory are correctly evaluated by Chang and Zhang criterion. Accordingly, the evaluation of Chang and Zhang and Burenkova are not almost in complete agreement with the outcome of the laboratory tests. However, Burenkova method can be used for assessing internal instability of volcanic soils with an absence of intermediate particle sizes such as $K_{8.5B}$ sample. Contrarily, the Kezdi method and the Kenney and Lau method proves relatively more successful in the evaluation of internal instability of volcanic soils with well-graded type (WG). Therefore, a combination of the Kezdi and the Kenney and Lau methods proposed by Li and Fannin are used in this study to evaluate internal instability of volcanic soils with well-graded type. Simultaneously, Burenkova criterion is used for evaluating internal erosion of volcanic soils with an absence of particle sizes under water flow.

A series of upward seepage tests was performed on Komaoka volcanic soils to investigate the internal stability under seepage flow. Firstly, test apparatus used in this study confirmed on Toyoura sand. Secondly, the piping phenomenon in Komaoka

volcanic soil (K_{soil}) is performed on small apparatus, then, deformation of particles under seepage flow are tracked by analyzing images collected from Xray-CT scanner. As a result, it is confirmed that the piping phenomenon early occurred in Komaoka volcanic soil at i=0.1. Subsequently, the seepage tests are performed on large apparatus to elucidate the effect of amount of fine particles and compaction conditions to piping phenomenon on test materials. The results indicate that the degree of compaction affects the performance of primary fabric of samples constructed by Komaoka volcanic soil. Simultaneously, it is found that the increasing amount of fine particles influences the internal stability in volcanic soils. Therefore, the estimation of the amount of fine particles and grain size distribution is very important for volcanic coarse grained soils. In addition, the detachment phenomenon between compacted layers occurs at the onset of boiling was observed in the test process. Thus, it is important to examine the connection of compacted layers in the soil structure construction such as embankment. Finally, based on amount of fine particles and critical void ratio, a simple method is proposed to calculate the critical hydraulic gradient on volcanic coarse grained soils. Particularly, volcanic soil having finer fraction (Fc) more than 40% is related to the effective void ratio with intra-particles void. Contrarily, theoretical void ratio is applied for the case of F_c less than 40% while calculating the critical hydraulic gradient.

CHAPTER 6:

A FRAMEWORK FOR EVALUATION OF INTERNAL INSTABILITY OF VOLCANIC SOIL

Internal erosion leads to a local failure in the inner part of embankment. It occurs when water flows through widely graded or gap graded cohesionless soils. The small particles of soil are transported by the seepage flow through the pores of the coarser particles. The coarser particles are not transported and the effective stresses are largely transferred through the matrix of the coarser particles. Physical characteristics play important role in the development of internal erosion such as grain size distribution, density, distribution of pores size, soil structure and permeability.

This study aims at clarifying mechanisms of internal erosion in volcanic embankment. In order to accomplish the purposes, the evaluation of the internal instability of volcanic soils are conducted based on two processes and a framework are proposed.

(1) Based on geometric characteristics of soils: Internal erosion is initiated when pores of the coarse particles have to be sufficiently large to allow fine particles to pass through, and the amount of finer soil particles must be less than enough to fill the voids of the basic skeleton formed by the coarser particles

(2) Based on hydraulic condition: the flow velocity has to be sufficient to detach the particles and also to transport them.

In the first condition, comparative sizes of finer particles (D_f) and pore size constrictions of coarser particles (D_p) should be examined, as shown in Figure.2.3. The filter coefficient 4 was established by considering correlative geometric of coarser particles (D_s) and finer particles (D_f). As a result, if diameter of coarser particles (D_s) is

less than 4 times diameter finer particles (D_f), the fine particles have not potential to be transported by seepage flow, the volcanic soil deem to be stable soil. Conversely, water flowing through the pore network of coarser particles will tend to move loose finer particles. However, if the fine particles encounter smaller pore constrictions, their movement will be clogged in the pore network of coarse particles. Therefore, stability indexes of Kedzi (D'_{15}/D'_{85}) and Kenny and Lau ($(H/F)_{min}$) criteria are necessarily examined for volcanic soils with widely graded particles. Simultaneously, conditional factors of uniformity d_{90}/d_{60} and d_{90}/d_{15} of Burenkova's method are used for evaluating internal stability of gap graded volcanic soils, the particular contents are presented in Chapter 5. The framework for evaluating internal erosion of volcanic soils is shown in Figure.6.1.

In the second condition, for potentially unstable materials, a gradient in excess of a critical value (i_c) is necessary to initiate movement of particles ($i > i_c$). According to Terzaghi's equation, the calculated critical hydraulic gradient for zero effective stress is defined as

$$i_c = \frac{G_s - 1}{1 + e} \tag{6.1}$$

In this study, the critical hydraulic gradient of volcanic soil is assessed based on a finer fraction (F_c) and affecting intra-particles void on void ratio (e). In particular, if $F_c \geq 40\%$, the void ratio (e) in equation 6.1 should be calculated with theoretical value as follows:

$$e = \frac{\rho_s}{\rho_d} - 1 \tag{6.2}$$

On the other hand, if $F_c < 40\%$ intra-particles void will affect to seepage characteristic of volcanic soil. Thus, when calculating critical hydraulic gradient should examine the effective void ratio of test materials. In particular, void ratio (e) in equation 6.1 can be expressed as

$$e = e_{inter} = e - e_{intra-o} - e_{intra-c} \tag{6.3}$$

where $e_{intra\text{-}o}$ is opening intra-particle void, $e_{intra\text{-}c}$ is closing intra-particle void, these parameters were given by Kimura et al. (2010). The evaluation process of internal erosion with volcanic soils is shown in Figure.6.1. According to this procedure, it is easily evaluate internal erosion of volcanic soil.

In the study, experiments were performed on Komaoka volcanic coarse grained

soil. The specimen was specified into Shikotsu pumice flow deposit (Spfl). Consequently, the result of research only apply to volcanic soil with flow deposit including specific characteristics such as non-plastic, low specific gravity and containing intra-particle void ratio. Besides, experiments were performed on homogeneous volcanic specimen containing amount of fine particles (Fc) of 1.9%; 8.5%; 27% and 40%. Therefore, the evaluation method of this study is used for stability evaluation on internal erosion of homogeneous embankments and amount of fine particles is range of 1% to 40%. A flowchart showing the main steps in assessing the stability of volcanic embankment is presented in Figure 6.2.

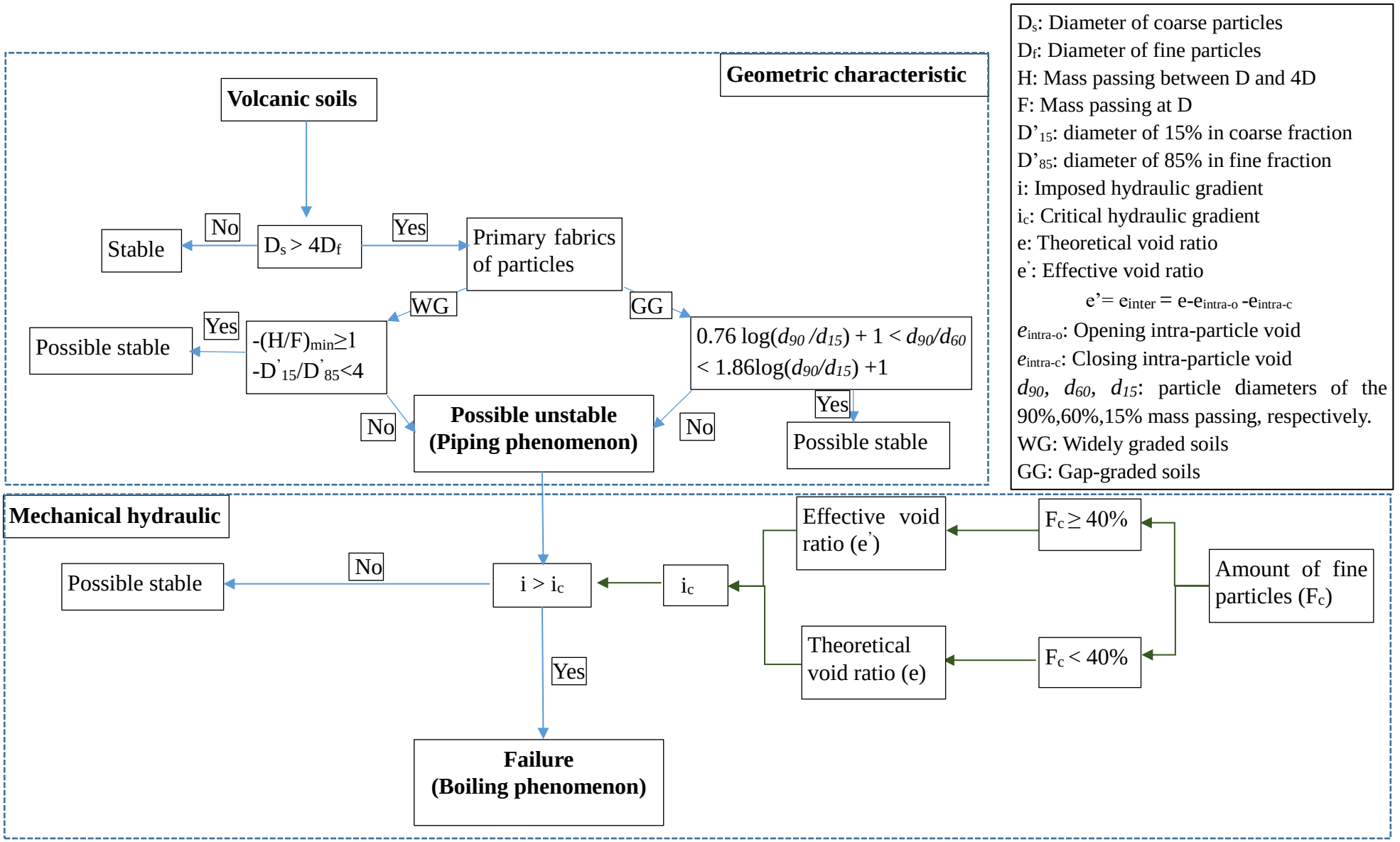

Figure.6.1 A framework for evaluation of internal instability in volcanic soils

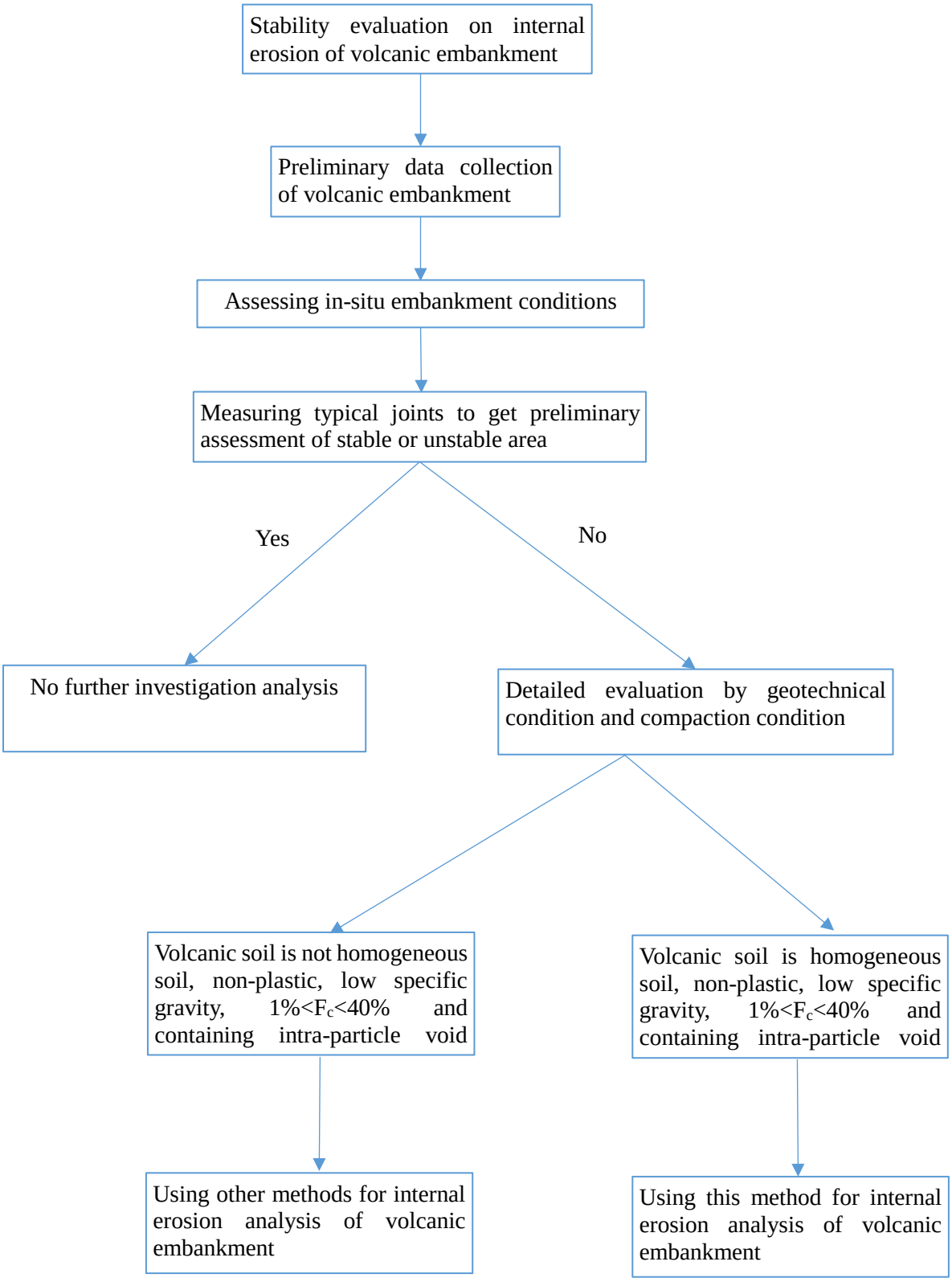

Figure 6.2 Flowchart for volcanic embankment stability assessment

CHAPTER 7:

CONCLUSIONS AND RECOMMENDATIONS

7.1 *Conclusions*

Internal erosion of volcanic soils has been investigated based on field observation of a full-scale embankment was firstly carried out. Thereafter, a series of upward seepage test was conducted to grasp features of seepage behavior in volcanic soils. Consequently, onset of internal instability (piping phenomenon) and failure (boiling phenomenon) are governed by (1) grain size distribution curve of a soil, and (2) a combined effects of amount of fine particles and intra-particles void ratio on critical hydraulic gradient value. Based on comparing four criteria about internal instability, the relative evaluation of empirical criteria is examined so that confidence is improved in using them in the engineering practice. According to the criteria, internal stability of volcanic soils is classified. Then, a series of upward seepage tests was performed on Komaoka volcanic soils to elucidate the effect of amount of fine particles and compaction conditions to piping phenomenon. In addition, a hydromechanical criteria, which is deepened on the relation between critical hydraulic gradient and finer fraction, is defined based on investigation of inside void in volcanic particles. A summary of the findings is presented below that addresses the field and experimental observations, geometric indices, compaction conditions and hydraulic index in evaluating internal erosion of volcanic soils.

1) From the results of the in-situ monitoring of the full-scale embankment constructed by Komaoka volcanic soil, traces of exudation routes of water during field monitoring were observed. This phenomenon occurred along embankment boundaries. According to the in-situ observation, fine particles were flowing out. This means that piping and exudation routes might be easily generated in volcanic man-made soil

structures, although the embankment was compacted by more than the degree of compaction Dc=95%. Therefore, it was pointed out that the evaluation of seepage performance is significant for volcanic man-made structures containing a significant amount of fine particles with non-plastic materials.

2) In analyses on criteria of internal stability of soils, three kinds of empirical geometric criteria which are Kezdi, Kenny and Lau and Burenkova methods are evaluated. In particular, Kezdi, and Kenney and Lau methods proposed by Li and Fannin are used for evaluating internal instability of volcanic soils with well-graded type. Simultaneously, Burenkova criterion is used for evaluating internal erosion of volcanic soils with an absence of particle sizes. As a result, Komaoka volcanic soil under the original condition classified into "well-graded type (WG)" was evaluated to an unstable grade on piping phenomenon based on empirical criteria.

3) The piping phenomenon was analyzed on original Komaoka volcanic soil (K_{soil}) in the laboratory by using a small apparatus with 10cm in diameter. Thereafter, behavior of internal erosion of K_{soil} under seepage flow was observed by X-ray CT scanner. Deformation of soils was estimated by DIC analysis on the X-ray CT images. The analytical results of seepage test indicate that piping phenomenon early occurs in the Komaoka volcanic soil ranging from i= 0.1 to i= 0.2. However, after the onset of internal erosion, movements of fine particles were clogged in pore network of particles. Thereafter, fine particles was washed out by water flow for larger hydraulic gradient.

4) Investigation of seepage performance of compacted volcanic soils was performed on the large apparatus with 150mm in diameter. Test results indicate that piping phenomenon behavior significantly differed depending on compaction conditions. Furthermore, the different behavior of internal erosion appeared for the data in degree of compaction Dc = 83% and Dc = 88%. The tendency of internal erosion process of compacted volcanic soils with D_c>88% is almost the same. In addition, detachment phenomenon between compacted layers of specimens was observed when boiling occurred. The cause was due to weak connection of soil particles at the boundary of compacted layers. This might be one of the reasons of the destabilization of man-made earth structures subjected to seepage flow.

5) In order to clarify an influence of fine particles on the piping phenomenon, a series of seepage flow test was also performed on $K_{1.9}$, $K_{8.5A}$, $K_{8.5B}$, K_{40A}, K_{40A} and K_{soil} soils. The test results show that the increasing amount of fine particles led to the high internal instability in volcanic soils. In addition, an absence of intermediate particle sizes induced increase of flow velocity and hydraulic conductivity for $K_{8.5B}$, K_{40B} compared to $K_{8.5A}$, K_{40A}. Consequently, it is important to grasp the amount of fine particles and the

shapes of grain distribution curve, especially volcanic soils including soil particles with low specific gravity.

6) The porosity and particle crushability are considered to influence the seepage performance of volcanic coarse-grained soil. From the analysis results, it can be said that effective void ratio with intra-particles void is available for evaluation of boiling phenomenon for the cases less than 40% of finer contents. For more than 40%, the theoretical method will be useful to calculate the critical hydraulic gradient of volcanic soils. At any rate, several evaluations will be required for investigation of stability of volcanic soil structures such as embankments.

7.2 *Recommendations for future studies*

In this study, the theoretical analysis and experimental evaluation are performed based on analyzing results of seepage flow tests in the upward direction. Seepage tests in the laboratory were performed on reconstituted Komaoka volcanic soil specimens, using the apparatus with the transparent plastic cylinder. In further studies, it is recommended that consideration is given to:

- Volcanic activities from the Neogene to the Quaternary were the origin of many kinds of volcanic soil deposits widely over the area of Japan. Simultaneously, the mechanical property of volcanic soil grounds vitally depends on the sedimentary structure, components, distributional area and degrees of the weathering. Therefore, it is necessary to perform seepage flow tests on other volcanic soils, in order to more broadly evaluate internal erosion in volcanic soils.
- The effects of uniformity and initial water content of specimen in preparation process on the behavior of seepage flow.
- Controlling degree of saturation of the test material before taking seepage test, in order to more accurately evaluate internal erosion in volcanic soils.
- Performing measurement of changes in effective stress and pore water pressure of the specimen due to internal erosion, in order to more exactly determine the onset of piping and boiling.
- Performing seepage flow tests on model embankments with horizontal flow, which is likely more representative of field conditions such as embankment.
- Establishing a numerical model to simulate the phenomenon of internal instability in volcanic soils.

LIST OF SYMBOLS

ρ_{dmax}	Maximum dry density obtained from compaction test (g/cm^3)
ρ_s	Soil particle density (g/cm^3)
ΔF_c	Increment of finer particle (%)
A	Distance of particle movement (mm)
C_u	Coefficient of uniformity
C_c	Coefficient of curvature
D	Diameter of specimen
D'_{15}	The diameter for 15% mass passing in the coarser fraction
D'_{85}	The diameter for 85% mass passing in the finer fraction
D_{50}	Mean grain size (mm)
D_c	Degree of compaction (%)
e	Void ratio
e'	Effective void ratio
$e_{intra\text{-}c}$	Closing intra-particle void
$e_{intra\text{-}o}$	Opening intra-particle void
F	Mass fraction smaller than D in % (Kenny and Lau, 1985 and 1986)
Gs	Specific gravity
H	Mass fraction measured between D and 4D in % (Kenny and Lau, 1985, 1986)
h	Water head (cm)
F_c	Finer content (% <75μm)
i	Hydraulic gradient
L	Length of the specimen (cm)
i_c	Critical hydraulic gradient
I_p	Plasticity index
JGS	The Japanese Geotechnical Society
JSCE	Japanese society of civil engineering
k	Hydraulic conductivity (permeability coefficient) (m/s)
K $_{original}$	Shikotsu pumice flow deposit with the original grain size distribution sampled in Komaoka district, Makomanai, Hokkaido
$K_{1.9}$	K soil with the controlled grain size distribution of F_c = 1.9 %
$K_{8.5A}$	K soil with the controlled grain size distribution of F_c = 8.5 %
$K_{8.5B}$	K soil with the controlled grain size distribution of F_c = 8.5 % and D_{50}
K_{40A}	K soil with the controlled grain size distribution of F_c = 40 %
K_{40B}	K soil with the controlled grain size distribution of F_c = 40 % and D_{50}
K_{soil}	Shikotsu pumice flow deposit with the cut grain size distribution (< 9.5 mm) sampled in Komaoka district, Makomanai, Hokkaido

n	Porosity of a soil
NG	Narrowly graded soil
NP	Non plastic soil
S	Stable soil
Spfl	Shikotsu pumice flow deposit
S_r	Degree of saturation (%)
U	Unstable soil
U_c	Uniformity coefficient
v	Discharge velocity (cm/s)
w_f	Water content at failure (%)
WG	Widely graded soil
w_L	Liquid limit (%)
w_P	Plastic limit (%)
d_{90}	Particle diameter of the 90% mass passing
d_{60}	Particle diameter of the 60% mass passing
d_{15}	Particle diameter of the 15% mass passing
WG	Widely graded soils
GG	Gap-graded soils

LIST OF TABLES

LIST OF FIGURES

ACKNOWLEDGEMENTS

Firstly, I would like to express my sincere gratitude to my advisor Associate Professor Shima Kawamura for the continuous support of my Ph.D study and related research, for his atience, motivation, and immense knowledge. His guidance helped me in all the time of research and writing of this thesis.

Besides my advisor, I would like to thank the rest of my thesis committee: Professor Yukihiro Kohata, and Professor Makoto Nakatsugawa for their insightful comments and encouragement, but also for the hard question which incented me to widen my research from various perspectives.

My gratitude extends to Dr. Satoshi Matsumura and all the staffs at Port and Airport Research Institute, who provided me an opportunity to join their team as intern, and have given helpful advices about various things. Without this precious support it would not be possible to conduct this research.

I thank my fellow labmates in for the stimulating discussions, for the everyday we were working together, and for all the fun we have had in the three years. In particular, thanks are extended to Mr. Ryoichi Yamada, Mr. Koki Fukutsu, Mr. Yuuki Kishimoto, Mr. Yuki Tsuchida and Mr. Yunzheng Lan for their cooperation in experimental works.

I am grateful to all the staffs of the Centre for International Relations, Muroran IT, Mr. Jinro Endo, Ms. Hatsuki Noda, Ms. Naoko Naito, Mr. Sangyub Baek and Ms. Nanae Chiba for making my life in Hokkaido really comfortable and enjoyable. Especially thanks to Associate Professor Naoko Yamaji, who taught Japanese language that help me to integrate into the life in Japan.

Further, I also sincerely thank Associate Professor Le Anh Dung and Associate Professor Vu Ngoc Anh of the Hanoi Architectural University (HAU) for offering me recommendation letters to apply for the doctor course. I also thank to technology and construction management Department, Civil Engineering Faculty and HAU for creating good conditions to study at Muroran IT. Thanks are also extended to Dr. Duong Quang Hung for his introduction and recommendation to Muroran Institute of Technology and Associate Professor Kawamura before I applied for doctor course here.

Last but not the least, I would like to thank my family: my parents, my wife and family members for their constant encouragement and support over the course of this study.

REFERENCES

[1] Chang DS and Zhang LM, "Extended internal stability criteria for soils under seepage", Soils and Foundations, Vol. 53, No. 4, 2013, pp. 569-583.

[2] Chang, D.S., Zhang, L.M., 2011. A stress-controlled erosion apparatus for studying internal erosion in soils. Geotechnical Testing Journal 34 (6), 579–589.

[3] Chapuis, R.P. (1992), Similarity of internal stability criteria for granular soils. Canadian Geotechnical Journal, 29: 711-713.

[4] Dao MH, Kawamura S, Matsumura S and Lan Y, "Piping phenomenon of embankments constructed by volcanic soils and its evaluation", Geotechnical Special Publication, No,280, ASCE, 2017, pp. 688-698.

[5] Dao, M. H., Kawamura, S. and Matsumura, S. (2017). "Internal erosion of volcanic coarse grained soils and its evaluation", International Journal of GEOMATE, Vol.13 Iss.38, pp.165-173.

[6] Fell, R., Foster, M., Davidson, R., Cyganiewicz, J., Sills, G. and Vroman, N. (2008). *A Unified Method for Estimating Probabilities of Failure of Embankment Dams by Internal Erosion and Piping.* UNICIV Report R 446, The School of Civil and Environmental Engineering, University of New South Wales, Sydney, Australia 2052.ISBN:85841 413 9

[7] Fell,R. Fry,J.J. 2007. Internal erosion of dams and their Fundations. Taylor & Francis ed.

[8] Foster M., Fell R. (2000) Use of event trees to estimate the probability of failure of embankment dams by internal erosion and piping ICOLD Beijing Congress Q76 R16.

[9] Foster, M., Fell, R. and Spannagle, M. (2000a): The statistics of embankment dam failures and accidents, Can. Geotech. J., 37, 1000–1024.

[10] Foster, M., Fell, R. and Spannagle, M. (2000b): A method for as- sessing the relative likelihood of failure of embankment dams by piping, Can. Geotech. J., 37, 1025–1061.

[11] Foster, M., Spannagle, M. and Fell, R. (1998). Report on the analysis of embankment dam incidents. *UNICIV Report No.R374, School of Civil and Environmental Engineering*, University of New South Wales ISBN: 85841 349 3; ISSN 0077-880X.

[12] Foster, M.A. and Fell, R. (1999b). *A Framework for Estimating the Probability of Failure of Embankment Dams by Piping Using Event Tree Methods*. UNICIV Report No. R377. School of Civil and Environmental Engineering, The University of New South Wales. ISBN 85841 343 4

[13] Fry.J.J. 2016. Lessons on internal erosion in embankment dams from failures and

physical models. International conference on Scour and Erosion, ICSE-8, 12-15 September 2016, Oxford, UK, P41.

[14] Fujisawa K, Murakami A and Nishimura S, “Numerical analysis of the erosion and the transport of fine particles within soils leading to the piping phenomenon”, Soils and Foundations, Vol.50 (4), 2010, pp. 471–482.

[15] Hokkaido branch of the Japanese Geotechnical Society (2010) : Volcanic soil for geo-engineer, geotechnical characteristics, design, construction and disaster case (in Japanese).

[16] Honjo, Y., Haque, M.A., Tsai, K.A., 1996. Self-filtration behaviour of broadly and gap-graded cohesionless soils. In: Proceedings of the 2nd International Conference on Filters and Drainage in Geotechnical and Environmental Engineering, Geofilters 1996, Montreal, pp. 227-236.

[17] ICOLD (1974). *Lessons from Dam Incidents*. International Commission on Large Dams, Paris.

[18] ICOLD (2015). Bulletin 164 Internal erosion of existing dams, levees and dikes, and their foundations, Volume 1: internal erosion processes and engineering assessment (19 February 2015). Go to: icold-cigb.org/bulletins

[19] Japanese Geotechnical Society [JGS]. (2004). Reconnaissance report of the 2003 Tokachi-oki Earthquake, The Reconnaissance Committee of 2003 Tokachi-oki Earthquake (in Japanese).

[20] Japanese Geotechnical Society, Hokkaido Branch. (2011). "Volcanic soils for engineers" - characteristics, design, construction and disasters -, The Research Committee in Hokkaido Branch, JGS, 1-130. (in Japanese)

[21] Japanese Geotechnical Society. (2004). "Reconnaissance report of the 2003 Tokachi-oki Earthquake", The Reconnaissance Committee of 2003 Tokachi-oki Earthquake, JGS. (in Japanese)

[22] Japanese Geotechnical Society.: Test method for soil compaction using a rammer (JGS 0711-2009), Standards of Japanese Geotechnical Society, JGS, 2009.

[23] Jones JAA (1981) The nature of soil piping: a review of research. BGRG research monograph 3. Geo Books, Norwich

[24] JSCE, “The disaster investigative report of the Typhoon 10th (2003),” Committee on Hydroscience and Hydraulic Engineering, pp. 1–95, 2004 (Japanese).

[25] JSSMFE, “The disaster investigative report of the 1993 Kushiro-oki Earthquake and Notohanto-oki Earthquake,” The 1993 Earthquake Disaster Investigative Committee, 1995.

[26] Kawamura, S. and Miura, S. (2013). "Rainfall-induced failures of volcanic slopes subjected to freezing and thawing", Soils and Foundations, Vol.53 No.3,

443-461.

[27] Kawamura, S. and Miura, S. (2014). "Stability of volcanic slopes in cold regions", Journal of Geography and Geology, Vol.6 No.3, pp.34-54.

[28] Kawamura, S. and Tsuchida, Y. (2017). "Wave-induced failure of volcanic embankments subjected to cyclic loadings such as seismic loadings and its evaluation", Journal of Coastal Engineering, JSCE, Vol.73, No.2/B2. (in Japanese) (in Press)

[29] Kawamura, S., & Miura, S. (2011). Stability evaluation of slope subjected to rainfall and freeze-thaw actions based on field monitoring. Advances in Civil Engineering (Online Access Journal), 2011, 14 pages. Hindawi Publishing Corporation. http://dx.doi.org/10.1155/2011/867909.

[30] Kawamura, S., Miura, S. and Matsumura, S. (2015). "Stability evaluation of full-scale embankment constructed by volcanic soil in cold regions." Proc., 15th Asian Regional Conf. on Soil Mechanics and Geotechnical Engineering, ISSMGE, Japanese Geotechnical Society, Special Publication, Vol.2 No.26, Fukuoka, Japan, pp.971-976.

[31] Kawamura, S., Miura, S., Dao. M. H and Yamada, R. (2016). "Rainfall-induced failure of volcanic embankments subjected to cyclic loadings in cold regions, Geotechnical Special Publication, No.257, ASCE, pp.116-123.

[32] Kawamura, S., Miura, S., Ishikawa, T., & Yokohama, S. (2010a). Rainfall-induced failure of unsaturated volcanic slope subjected to freeze-thaw action and its evaluation. Journal of Geotechnical Engineering, JSCE, C-66(3), 577-594 (in Japanese).

[33] Ke L and Takahashi A, "Strength reduction of cohesionless soil due to internal erosion induced by one-dimensional upward seepage flow", Soils and Foundations, Vol.52 (4), 2012, pp.698–711.

[34] Kenney TC and Lau D, "Internal stability of granular filters, reply", Canadian Geotechnical Journal, Vol. 23, No. 4, 1986, pp. 420–423.

[35] Kenney TC and Lau D, "Internal stability of Granular Filters", Canadian Geotechnical Journal, Vol. 22, No. 2, 1985, pp. 215-225.

[36] Kezdi A, "Soil Physics-Selected Topics", Elsevier Scientific Publishing Co., Amsterdam, 1979, 160p.

[37] Khan, A. S. (2003) Experimental Study for Evaluating the Internal Stability of Gap Graded Soils, M.A.Sc Thesis, University of British Columbia, Vancouver, BC, Canada.

[38] Khilar, K. C., Fogler, H. S. and Gray, D. H. (1985): Model for piping-plugging in earthen structures, Journal of Geotechnical En- gineering, ASCE, 111(7), 833–846.

[39] Kimura M, Nakata T, Miyaura M and Yokohama, S, “Evaluation of particle breakage on volcanic grounds for construction of snow dumping site”, Hokkaido branch of the Japanese geotechnical society, Vol.67, 2010 (in Japanese).

[40] Kudo, A. (2013). Damage and restoration for slope failure in Route 230. Tsuchi-to- Kiso, JGS, 61(3), 30-31 (in Japanese).

[41] Lane EW (1934) Security from under-seepage masonry dams on earth foundations. Trans ASCE 60(4):929–966.

[42] Leamy, M.L., 1984. Andisols of the world. In: Congresco international de Suelos Volcanicos. Communicaciones. Universida de la Laguna Secretariado de Publicacioned, serie informes 13, pp. 368-387.

[43] Li M and Fannin RJ, “Comparison of two criteria for internal stability of granular soil”, Canadian Geotechnical Journal, Vol. 45, 2008, pp. 1303-1309.

[44] Li, M., 2008. Seepage Induced Instability in Widely Graded Soils (Ph.D. thesis). The University of British Columbia.

[45] Liu, J. (2005) Seepage control of earth-rock dams: theoretical basis, engineering experiences and lessons (in Chinese), China Waterpower Press, Beijing, 219p.

[46] Mao, C.X. (2005) Study on piping and filters: Part I of piping (in Chinese). Rock and Soil Mechanics, Vol.26, No.2: 209-215.

[47] Matsumura, S.: Laboratory and in-situ studies on mechanical properties of volcanic soil embankment in cold region. Doctoral Dissertation, Graduate school of Engineering, Hokkaido University, 2014.

[48] Miura S, “Mechanical behavior and earthquake-induced failures of volcanic soils in Japan”, in Proc. of Advances in Transportation Geotechnics II, IS-Hokkaido, Sapporo, Japan, 2012, pp.13-33.

[49] Miura, S. and Yagi, K. (1997) : Particle breakage of volcanic coarse-grained soils and its evaluation, J. of Geotech. Engrg., JSCE, No.561/III-38, pp.257-269 (in Japanese).

[50] Miura, S., Yagi, K., and Asonuma, T.: Deformation-strength evaluation of crushable volcanic soils by laboratory and in-situ testing, Soils and Foundations, Vol. 43, No. 4, pp. 47-57, 2003.

[51] Miura, S.: Evaluations of problematic soils as engineering materials, General Remark, The Foundation Engineering & Equipment (Kiso-ko), Vol. 42, No. 12, pp. 2-7, 2014 (in Japanese).

[52] Moffat, R. (2005) Experiments on the internal stability of widely graded cohesionless soils, PhD thesis, the University of British Columbia, Vancouver, Canada.

[53] Nakata T and Miura S, “Change in void structure due to particle breakage of volcanic coarse-grained soil and its evaluation”, J. of Geotech. Eng, JSCE,

Vol.63, No.1, 2007, pp.224-236 (in Japanese).

[54] Reddi, L. N., Lee, In-M and Bonala, M. V. S. (2000): Comparison of internal and surface erosion using flow pump test on a sand- kaolinite mixture, Geotechnical Testing Journal, 23(1), 116–122.

[55] Richards K S and Reddy K R, "Critical appraisal of piping phenomena in earth dams", Bull. Eng. Geo. Environ, Vol.66, 2007, pp.381–402.

[56] Salehi Sadaghiani, M.R., Witt, K.J., 2011. Experimental identification of mobile particles in suffusible non cohesive soils. European Journal of Environmental and Civil Engineering 15 (8), 1155–1165.

[57] Shimizu, M. 1999. Geotechnical features of volcanic-ash soils in Japan, Proc. of the International Symposium on Problematic Soils, Vol. 2: 907–927.

[58] Skempton AW and Brogan JM, "Experiments on piping in sandy gravels", Geotechnique, Vol. 44, No. 3, 1994, pp. 449–460.

[59] Terzaghi K (1925) Erdbaumechanik. Franz Deuticke, Vienna

[60] Terzaghi K, "Soil mechanics: a new chapter in engineering science", Journal of the Institution of Civil Engineers 12, 1939, pp.106–141.

[61] Terzaghi, K. and Peck, R.B. (1948). *Soil Mechanics in Engineering Practice*. First edition,Wiley International, New York.

[62] U.S. Army Corps of Engineers (USACE), 1953. Filter Experiments and Design Criteria. Waterways Experiment Station, Vicksburg, Technical Memorandum, No. 3-360.

[63] U.S. Waterways Experiment Station, "Soil Mechanics Fact Finding Survey: Seepage Studies," Tech. Memo. No. 175-1, 1941.

[64] Wan, C.F. and Fell, R. (2002). Investigation of internal erosion and piping of soils in embankment dams by the slot erosion test and the hole erosion test. UNICIV Report No. R- 412, ISBN: 85841 379 5, School of Civil and Environmental Engineering, The University of New South Wales.

[65] Wan, C. F. and Fell, R. (2004a): Investigation of rate of erosion of soils in embankment dams, Journal of Geotechnical and Geoen- vironmental Engineering, 130(4), 373–380.

[66] Wan, C.F. and Fell, R. (2004b). Laboratory tests on the rate of piping erosion of soils in embankment dams. *Geotechnical Testing Journal*, vol.27, No.3, 295-303.

[67] Wan, C.F. and Fell, R. (2007). Investigation of internal erosion by the process of suffusion in embankment dams and their foundations. In *Internal Erosion of Dams and their Foundations.* Editors R Fell and J-J Fry. Taylor and Francis, London. 219-234.

[68] White DJ, Take WA and Bolton MD, "Soil deformation measurement using particle image velocimetry (PIV) and photogrammetry", Géotechnique, Vol.53

(7), 2003, pp.619-631.

[69] Yamazaki, T., Tomojiri, S., & Sasaki, T. (2000). Highway Technology. Research Institute, Japan Highway Public Corporation, 16, 75-81 (in Japanese).

[70] Yoshimi Y, F Kuwabara and K Tokimatsu, “One-Dimensional volume change characteristics of sands under very low confining stresses”, Soils and Foundations, Vol. 15, No. 3, 1975, pp. 51-60.

[71] Zhang LM and Chen Q, “Analysis of seepage failure of the Gouhou rockfill dam during reservoir water infiltration” Soils and Foundations, Vol.46 (5), 2006, pp. 557–568.

APPENDIX (Analizing X-ray CT images of K_{soil} in the seepage flow test)

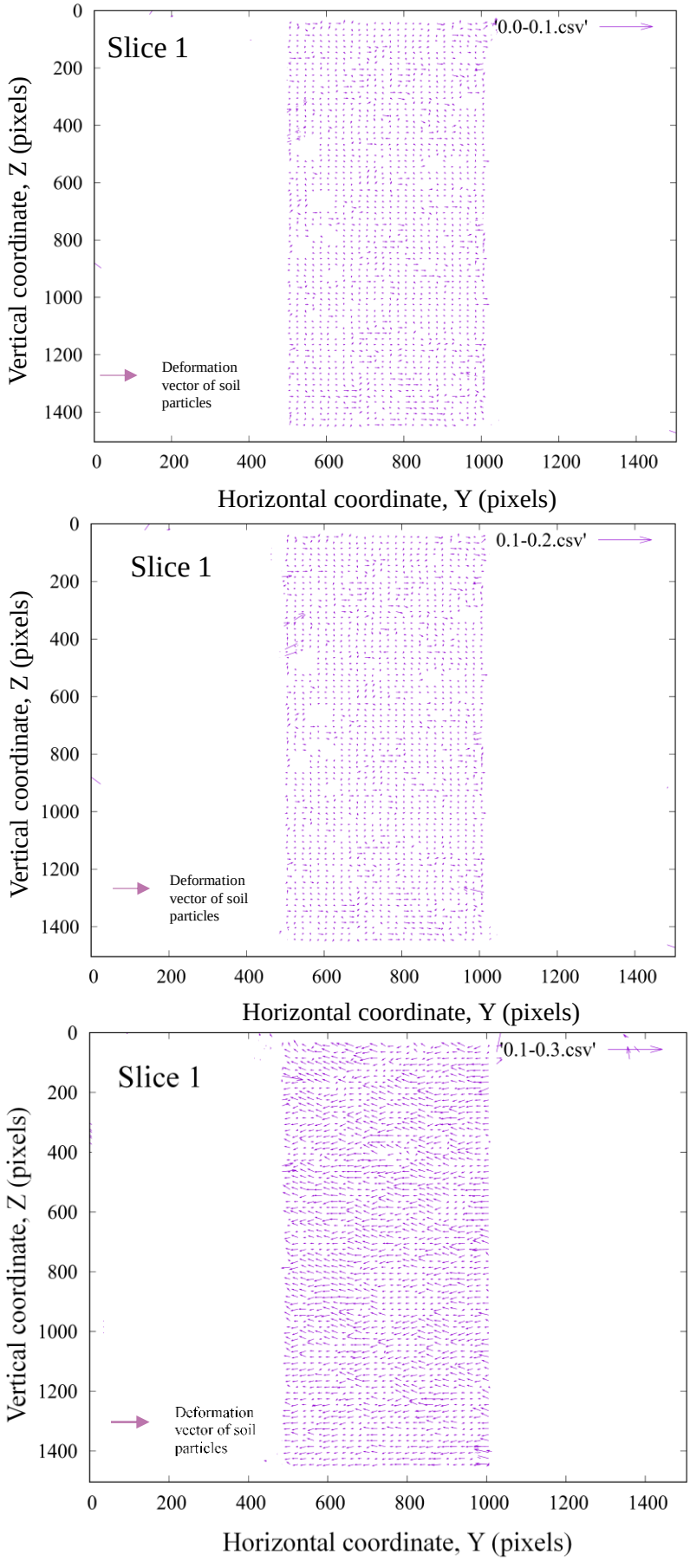

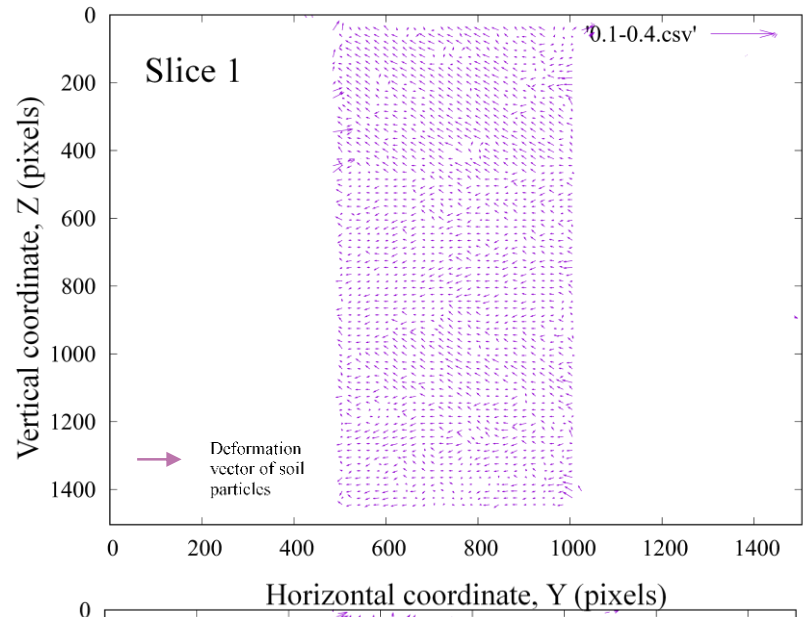
Slice 1
'0.1-0.4.csv'
Deformation vector of soil particles
Vertical coordinate, Z (pixels)
Horizontal coordinate, Y (pixels)
0
200
400
600
800
1000
1200
1400

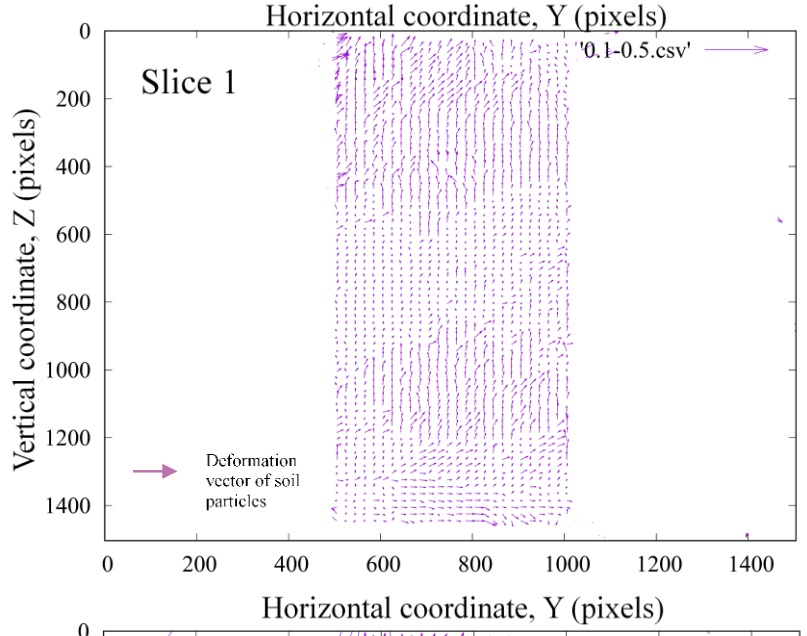
Slice 1
'0.1-0.5.csv'
Deformation vector of soil particles
Vertical coordinate, Z (pixels)
Horizontal coordinate, Y (pixels)
0
200
400
600
800
1000
1200
1400

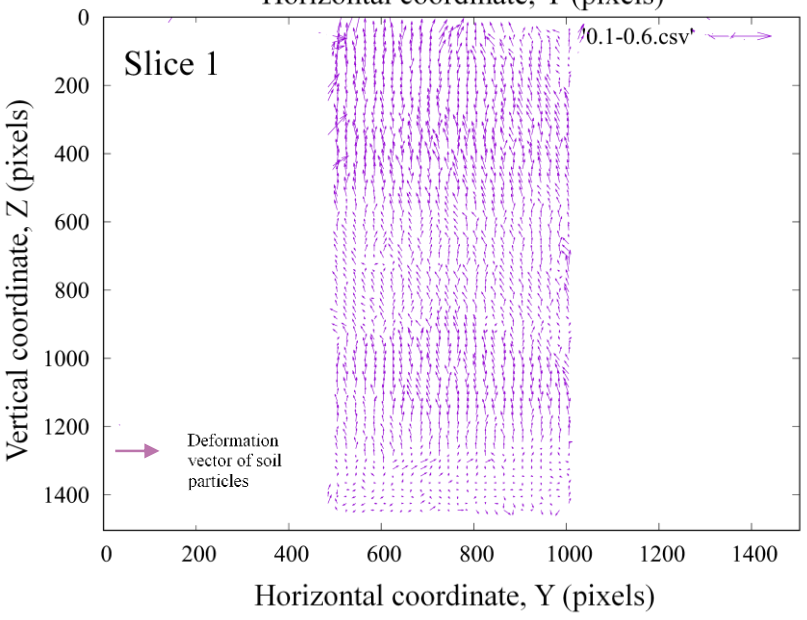
Slice 1
'0.1-0.6.csv'
Deformation vector of soil particles
Vertical coordinate, Z (pixels)
Horizontal coordinate, Y (pixels)
0
200
400
600
800
1000
1200
1400

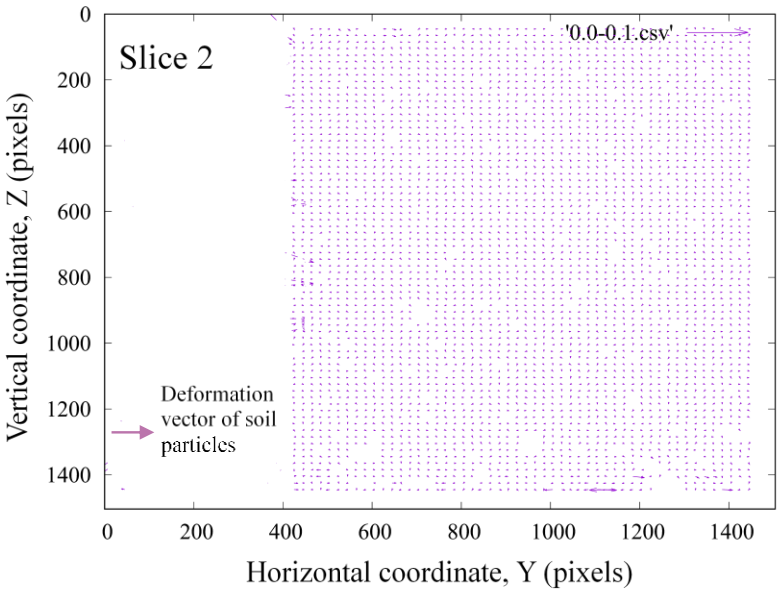
Slice 2
'0.0-0.1.csv'
Deformation vector of soil particles
Vertical coordinate, Z (pixels)
Horizontal coordinate, Y (pixels)
0
200
400
600
800
1000
1200
1400

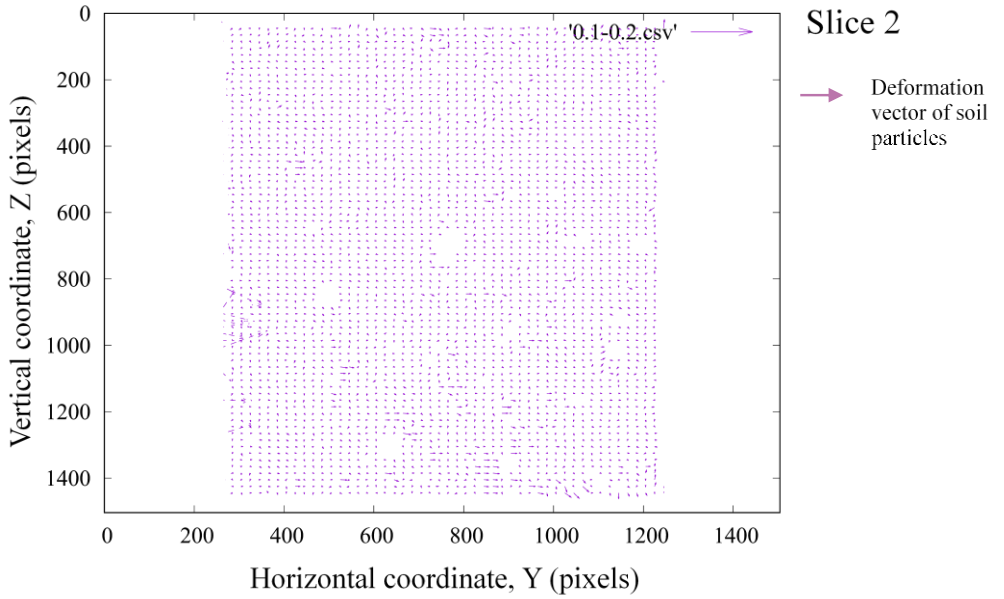
'0.1-0.2.csv'
Slice 2
Deformation vector of soil particles
Vertical coordinate, Z (pixels)
Horizontal coordinate, Y (pixels)
0
200
400
600
800
1000
1200
1400

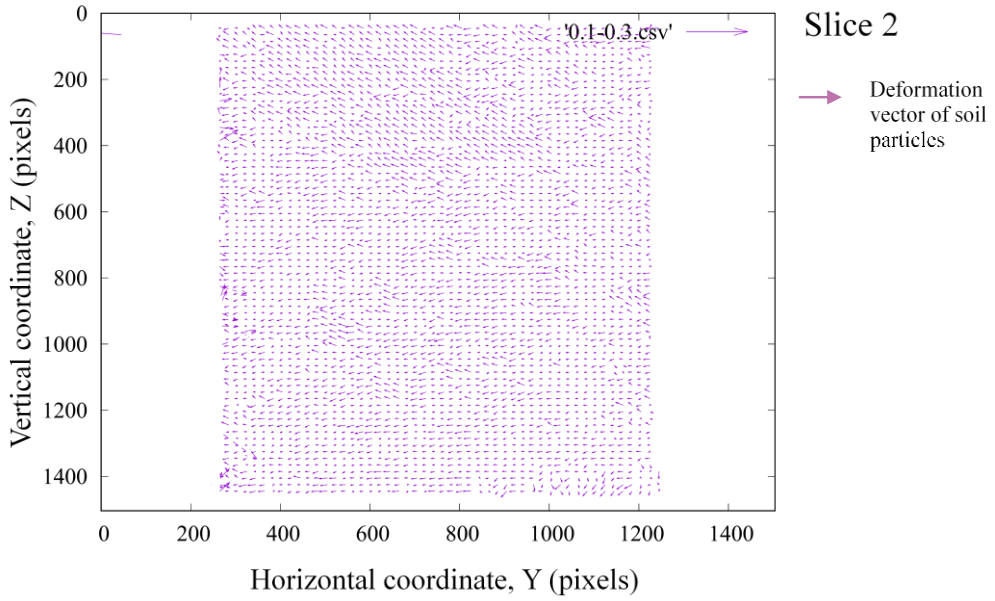
'0.1-0.3.csv'
Slice 2
Deformation vector of soil particles
Vertical coordinate, Z (pixels)
Horizontal coordinate, Y (pixels)
0
200
400
600
800
1000
1200
1400

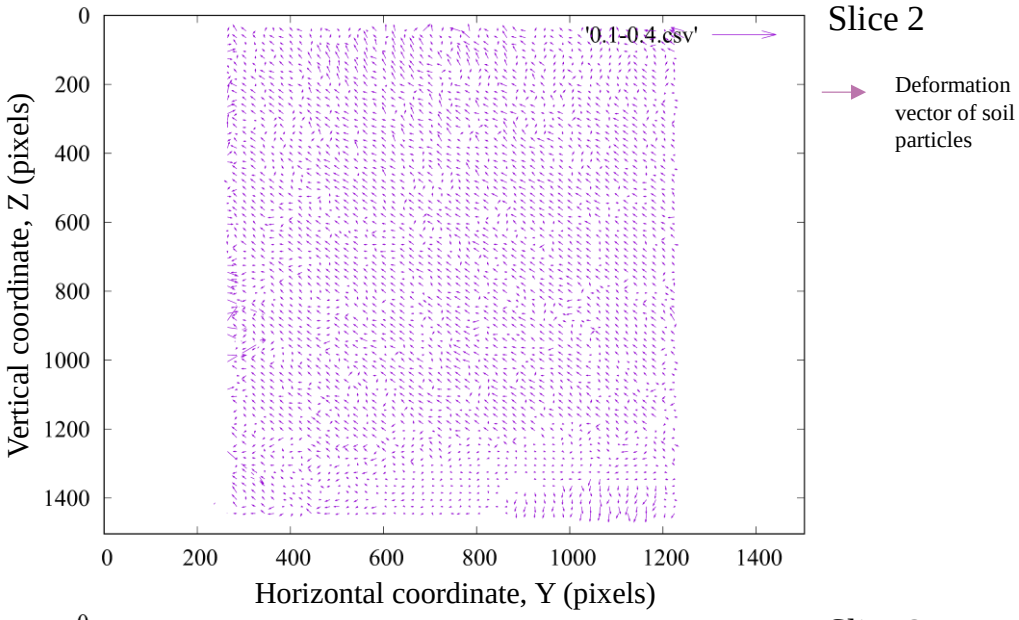
'0.1-0.4.csv'
Slice 2
Deformation vector of soil particles
Vertical coordinate, Z (pixels)
Horizontal coordinate, Y (pixels)
0
200
400
600
800
1000
1200
1400

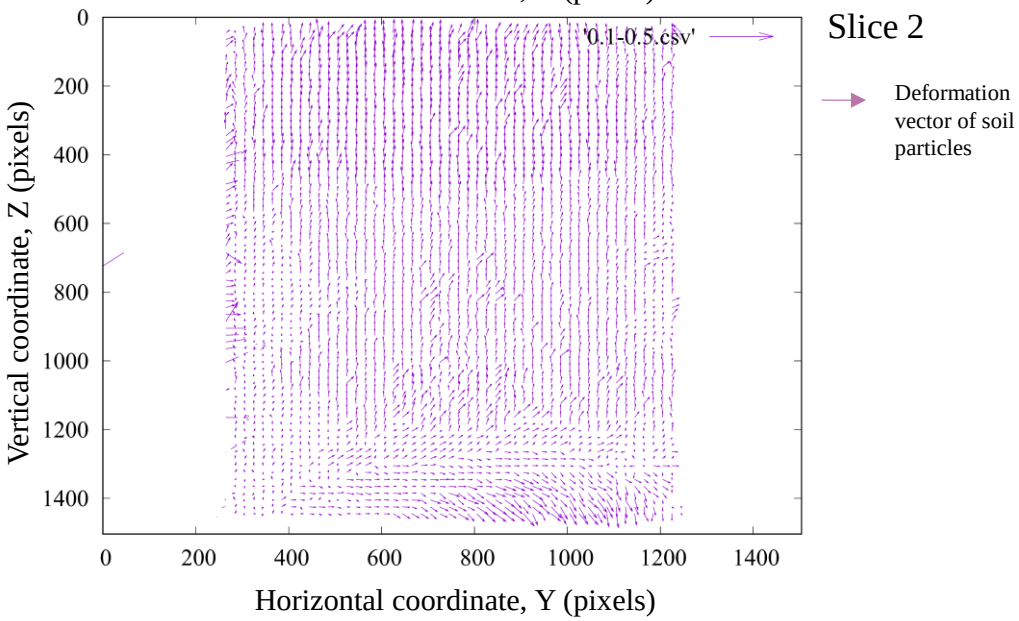
'0.1-0.5.csv'
Slice 2
Deformation vector of soil particles
Vertical coordinate, Z (pixels)
Horizontal coordinate, Y (pixels)
0
200
400
600
800
1000
1200
1400

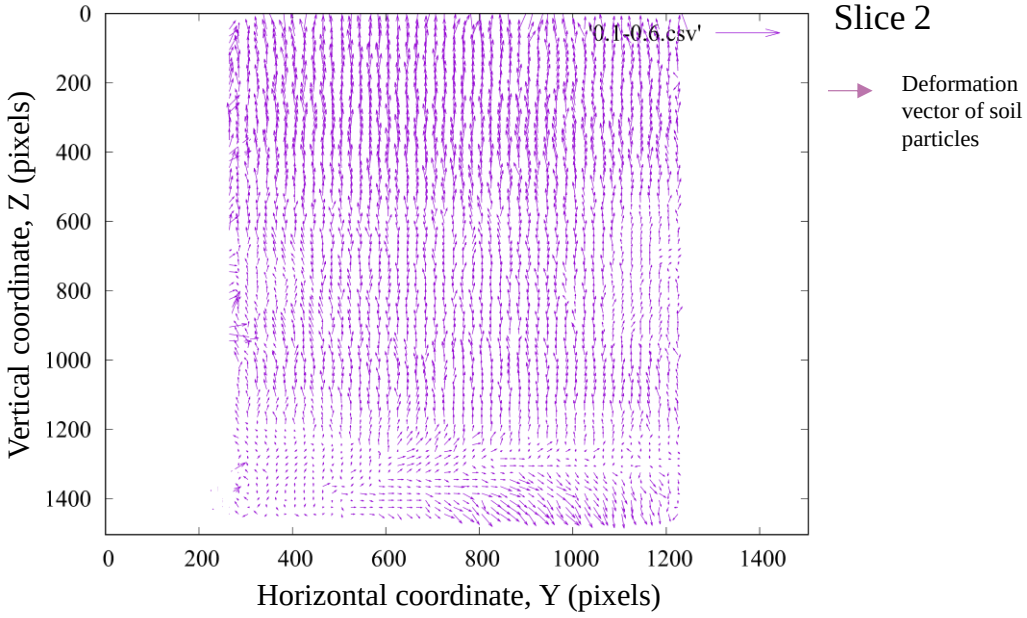
'0.1-0.6.csv'
Slice 2
Deformation vector of soil particles
Vertical coordinate, Z (pixels)
Horizontal coordinate, Y (pixels)
0
200
400
600
800
1000
1200
1400

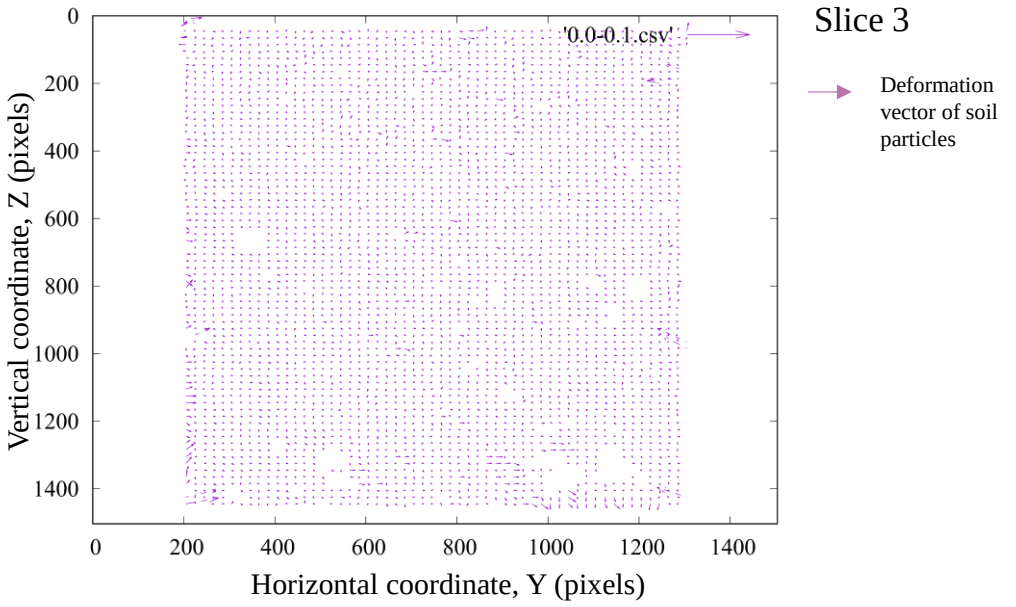
'0.0-0.1.csv'
Slice 3
Deformation vector of soil particles
Vertical coordinate, Z (pixels)
Horizontal coordinate, Y (pixels)
0
200
400
600
800
1000
1200
1400

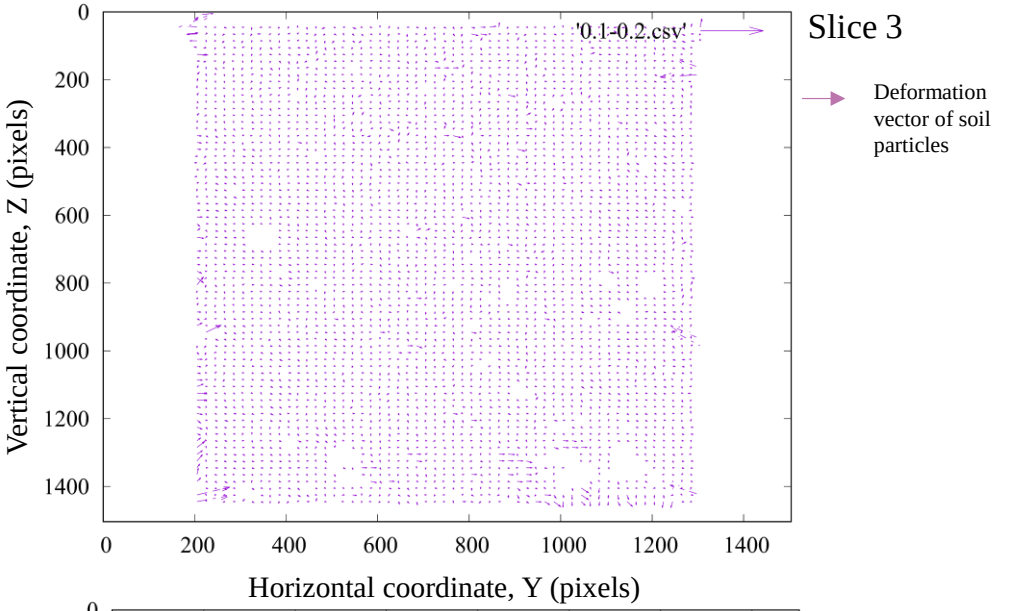
'0.1-0.2.csv'
Slice 3
Deformation vector of soil particles
Vertical coordinate, Z (pixels)
Horizontal coordinate, Y (pixels)
0
200
400
600
800
1000
1200
1400

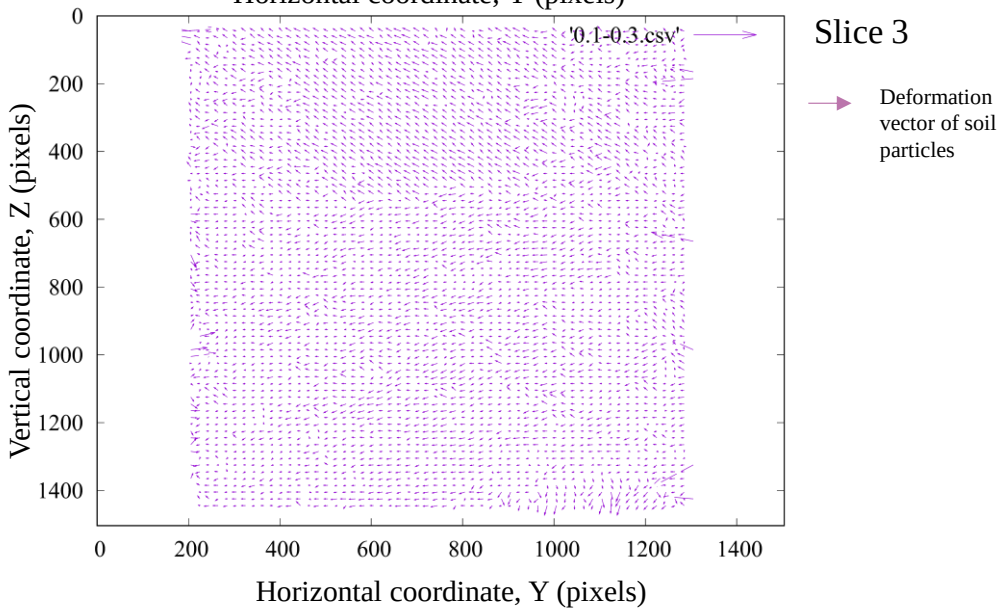
'0.1-0.3.csv'
Slice 3
Deformation vector of soil particles
Vertical coordinate, Z (pixels)
Horizontal coordinate, Y (pixels)
0
200
400
600
800
1000
1200
1400

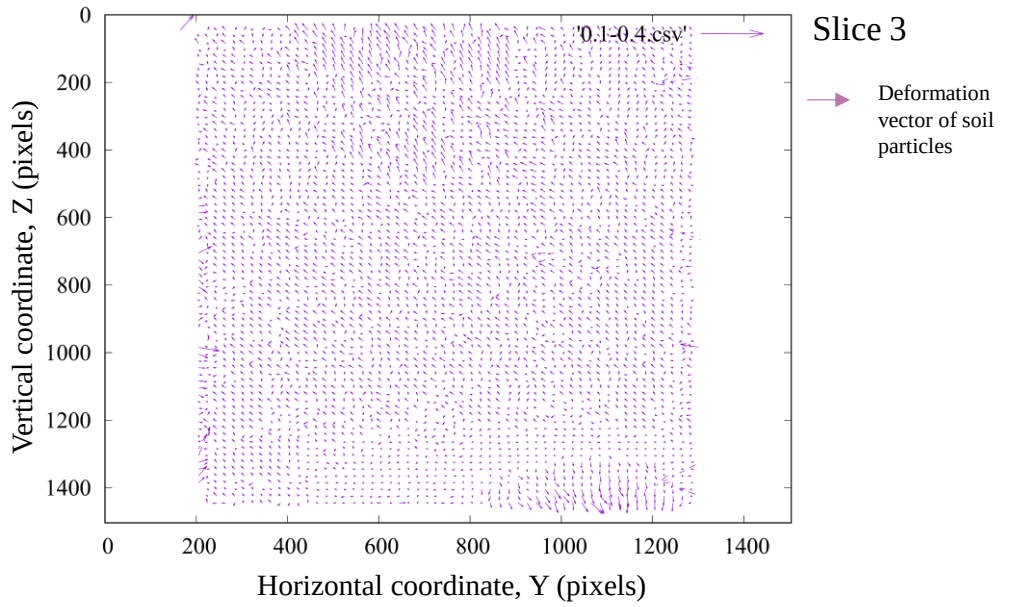
'0.1-0.4.csv'
Slice 3
Deformation vector of soil particles
Vertical coordinate, Z (pixels)
Horizontal coordinate, Y (pixels)
0
200
400
600
800
1000
1200
1400

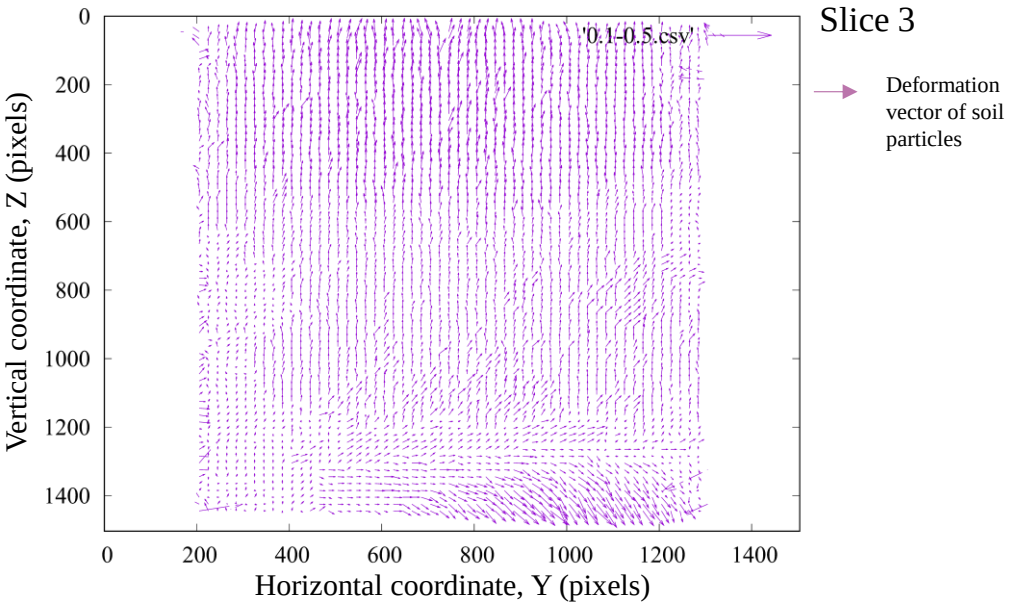
'0.1-0.5.csv'
Slice 3
Deformation vector of soil particles
Vertical coordinate, Z (pixels)
Horizontal coordinate, Y (pixels)
0
200
400
600
800
1000
1200
1400

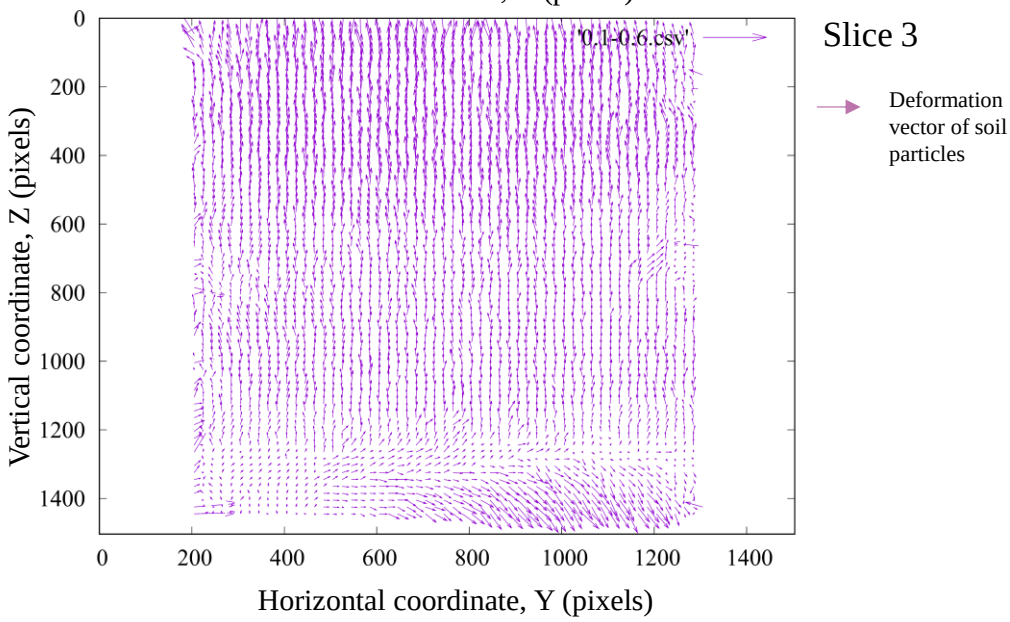
'0.1-0.6.csv'
Slice 3
Deformation vector of soil particles
Vertical coordinate, Z (pixels)
Horizontal coordinate, Y (pixels)
0
200
400
600
800
1000
1200
1400

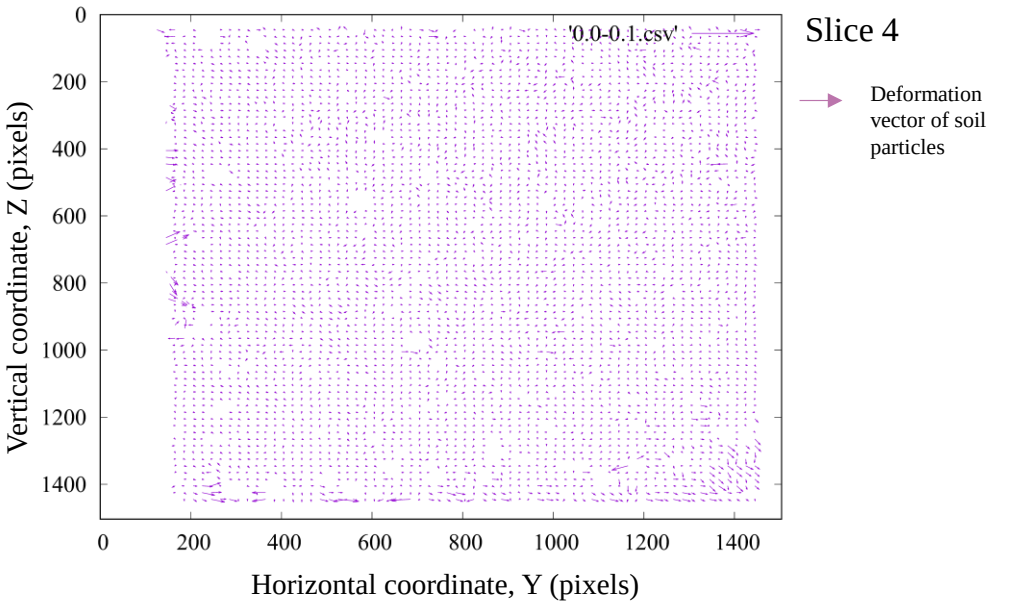
'0.0-0.1.csv'
Slice 4
Deformation vector of soil particles
Vertical coordinate, Z (pixels)
Horizontal coordinate, Y (pixels)
0
200
400
600
800
1000
1200
1400

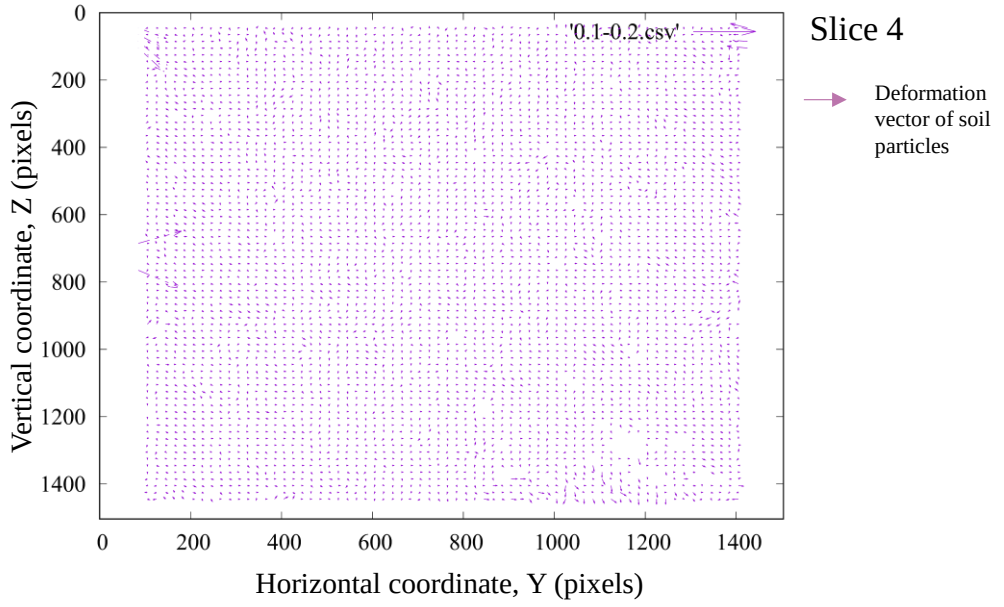
'0.1-0.2.csv'
Slice 4
Deformation vector of soil particles
Vertical coordinate, Z (pixels)
Horizontal coordinate, Y (pixels)
0
200
400
600
800
1000
1200
1400

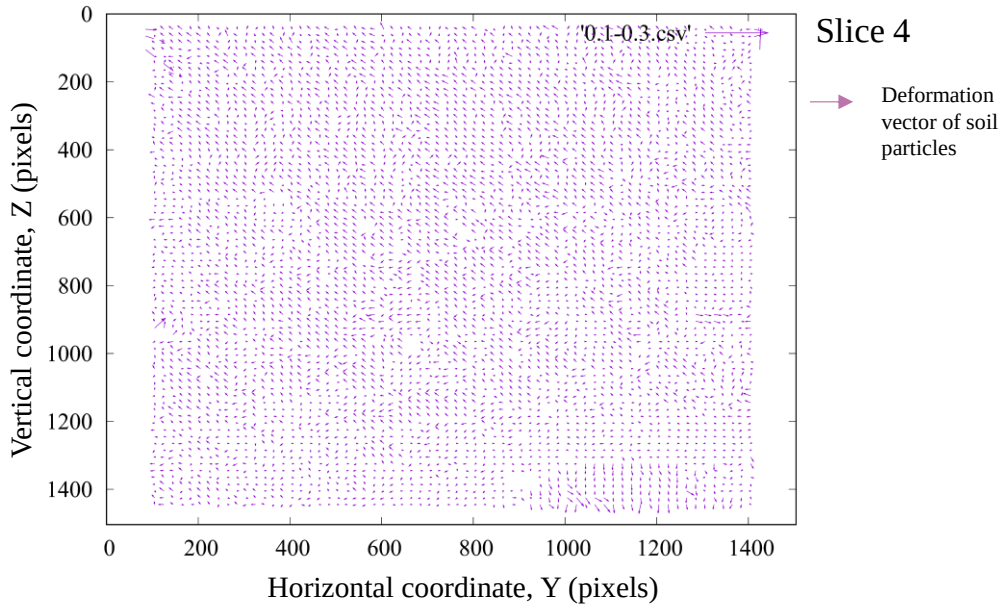
'0.1-0.3.csv'
Slice 4
Deformation vector of soil particles
Vertical coordinate, Z (pixels)
Horizontal coordinate, Y (pixels)
0
200
400
600
800
1000
1200
1400

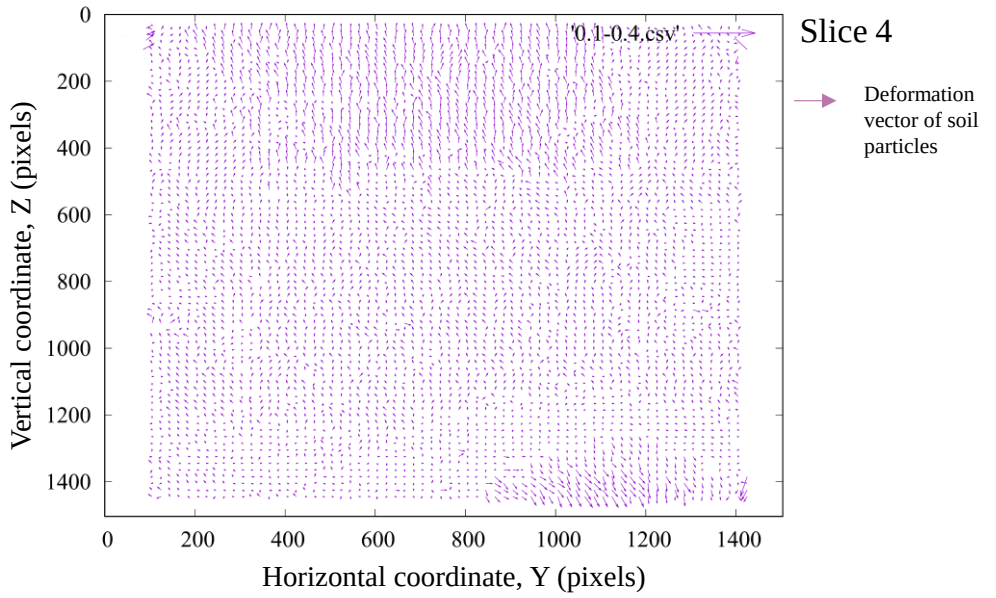
'0.1-0.4.csv'
Slice 4
Deformation vector of soil particles
Vertical coordinate, Z (pixels)
Horizontal coordinate, Y (pixels)
0
200
400
600
800
1000
1200
1400

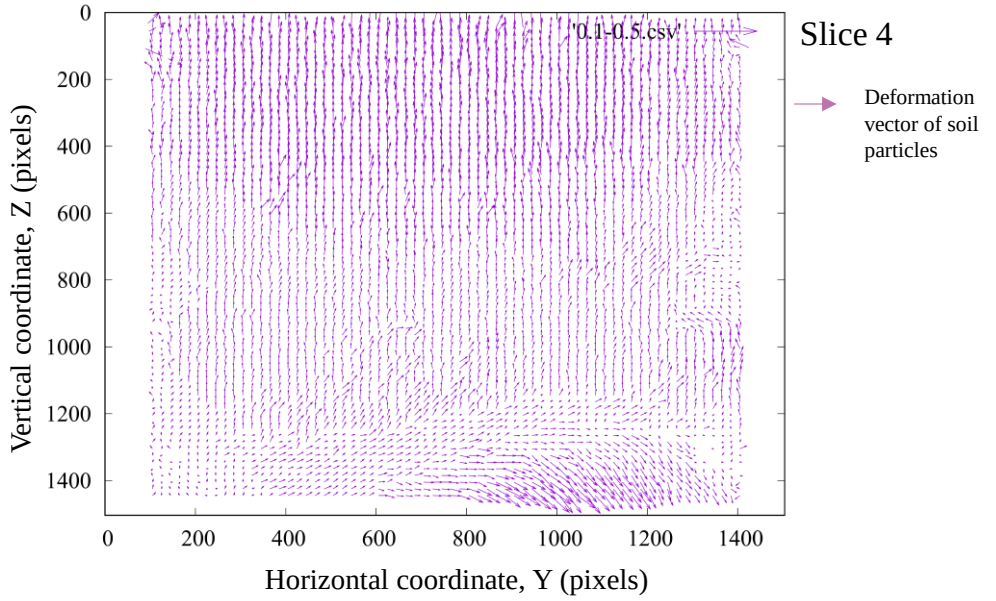
'0.1-0.5.csv'
Slice 4
Deformation vector of soil particles
Vertical coordinate, Z (pixels)
Horizontal coordinate, Y (pixels)
0
200
400
600
800
1000
1200
1400

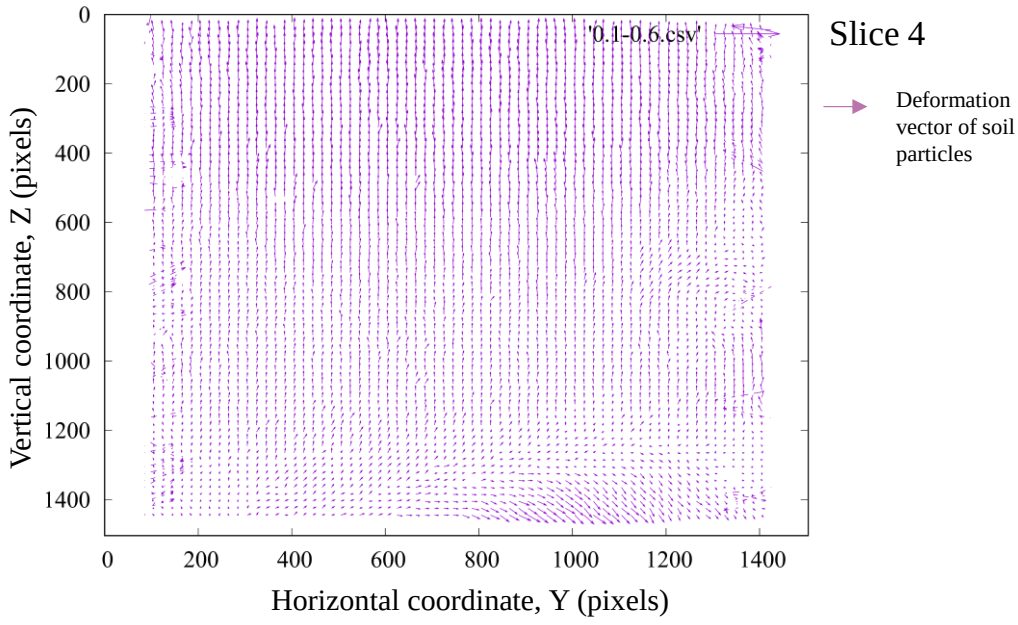
'0.1-0.6.csv'
Slice 4
Deformation vector of soil particles
Vertical coordinate, Z (pixels)
Horizontal coordinate, Y (pixels)
0
200
400
600
800
1000
1200
1400

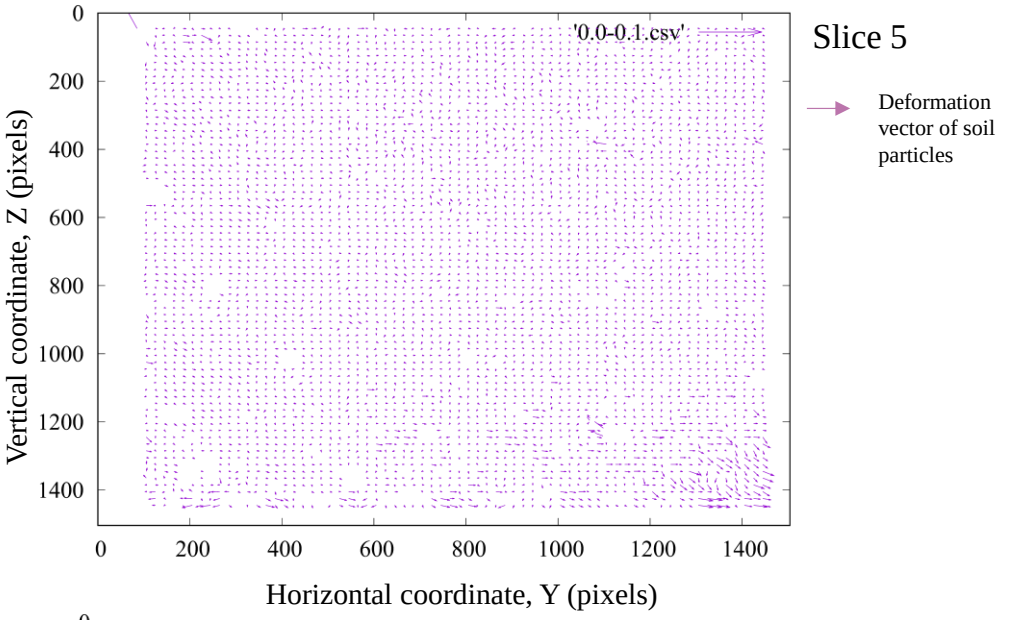
'0.0-0.1.csv'
Slice 5
Deformation vector of soil particles
Vertical coordinate, Z (pixels)
Horizontal coordinate, Y (pixels)
0
200
400
600
800
1000
1200
1400

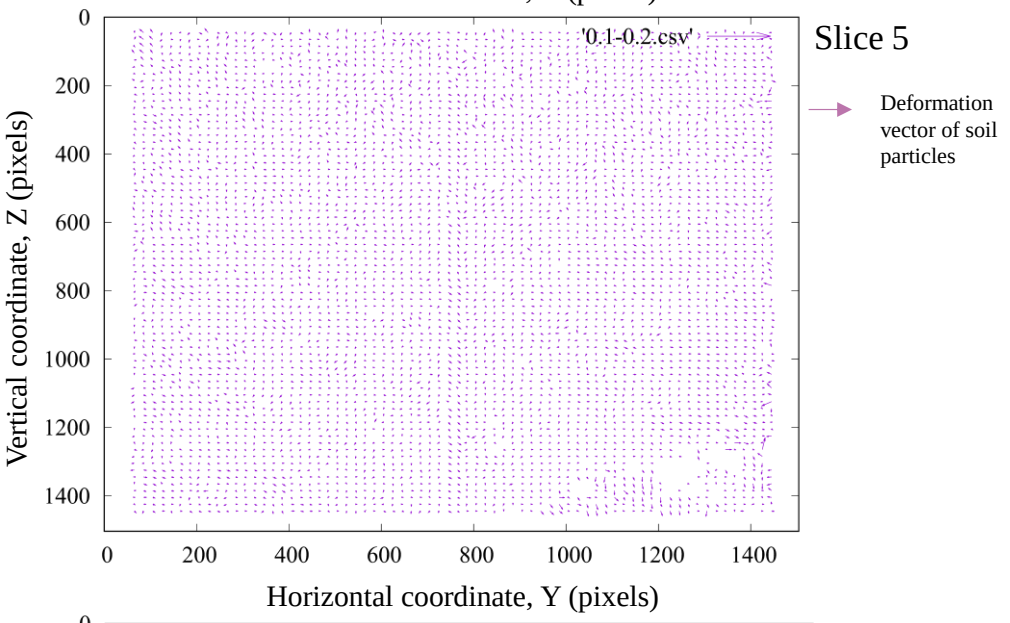
'0.1-0.2.csv'
Slice 5
Deformation vector of soil particles
Vertical coordinate, Z (pixels)
Horizontal coordinate, Y (pixels)
0
200
400
600
800
1000
1200
1400

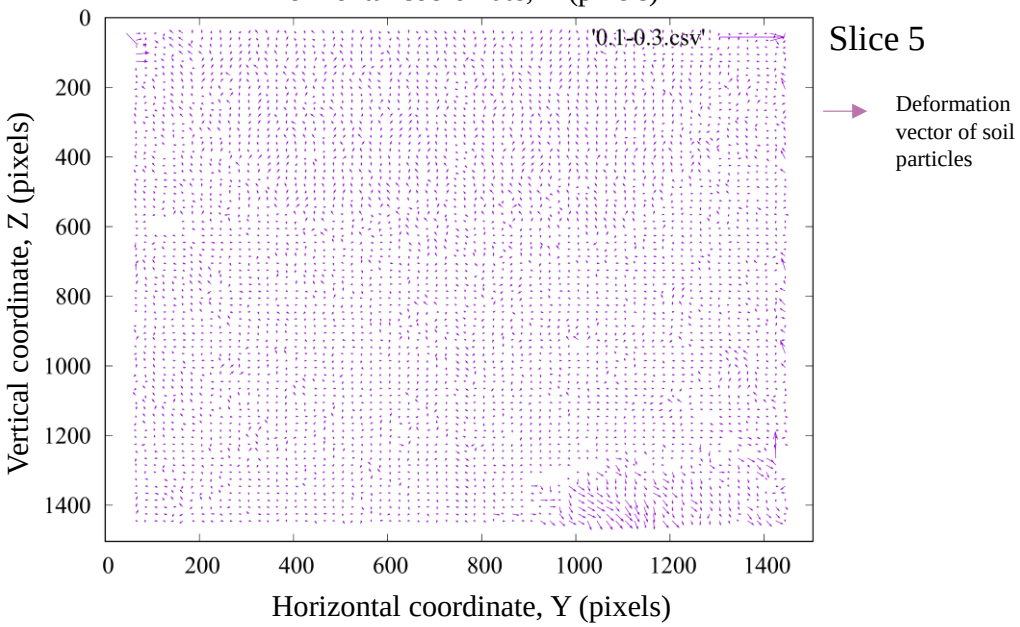
'0.1-0.3.csv'
Slice 5
Deformation vector of soil particles
Vertical coordinate, Z (pixels)
Horizontal coordinate, Y (pixels)
0
200
400
600
800
1000
1200
1400

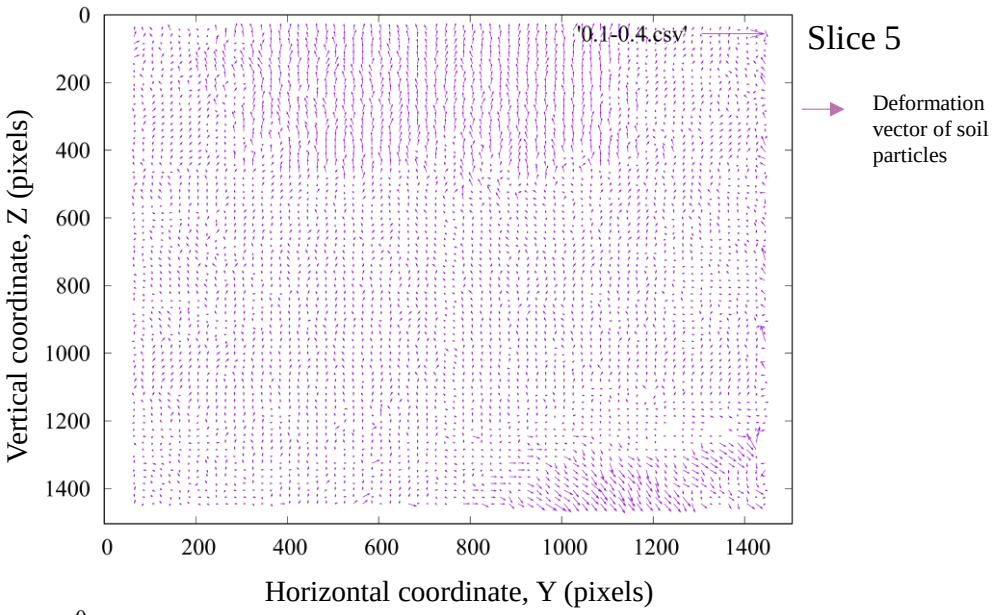
'0.1-0.4.csv'
Slice 5
Deformation vector of soil particles
Vertical coordinate, Z (pixels)
Horizontal coordinate, Y (pixels)
0
200
400
600
800
1000
1200
1400

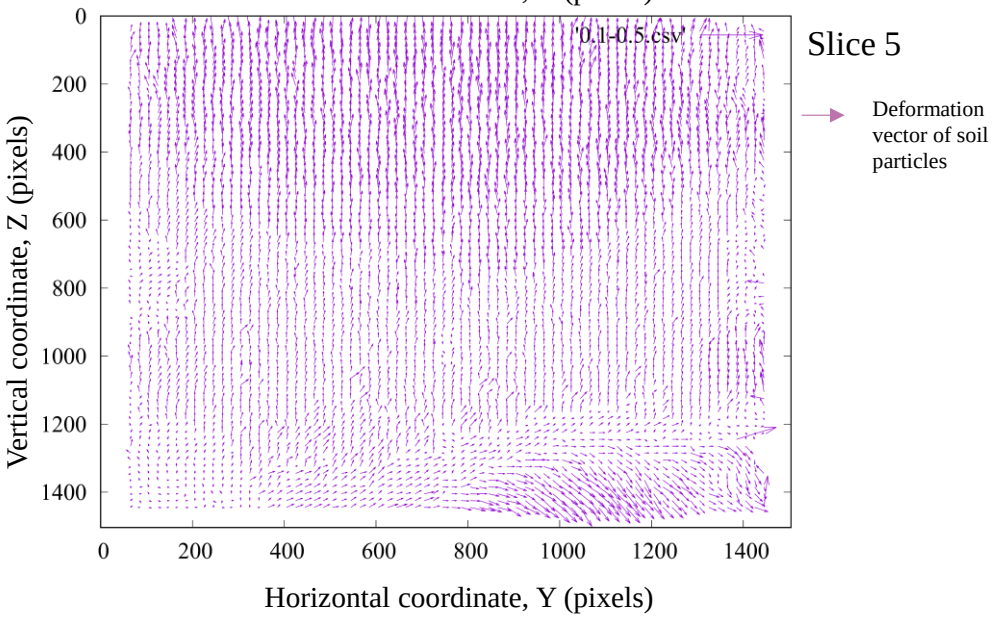
'0.1-0.5.csv'
Slice 5
Deformation vector of soil particles
Vertical coordinate, Z (pixels)
Horizontal coordinate, Y (pixels)
0
200
400
600
800
1000
1200
1400

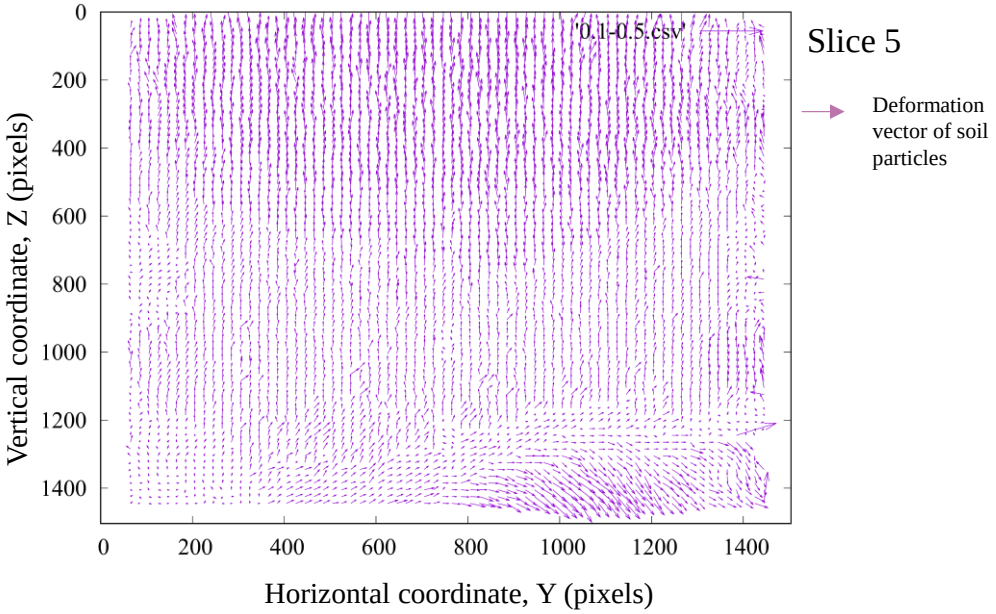
'0.1-0.5.csv'
Slice 5
Deformation vector of soil particles
Vertical coordinate, Z (pixels)
Horizontal coordinate, Y (pixels)
0
200
400
600
800
1000
1200
1400

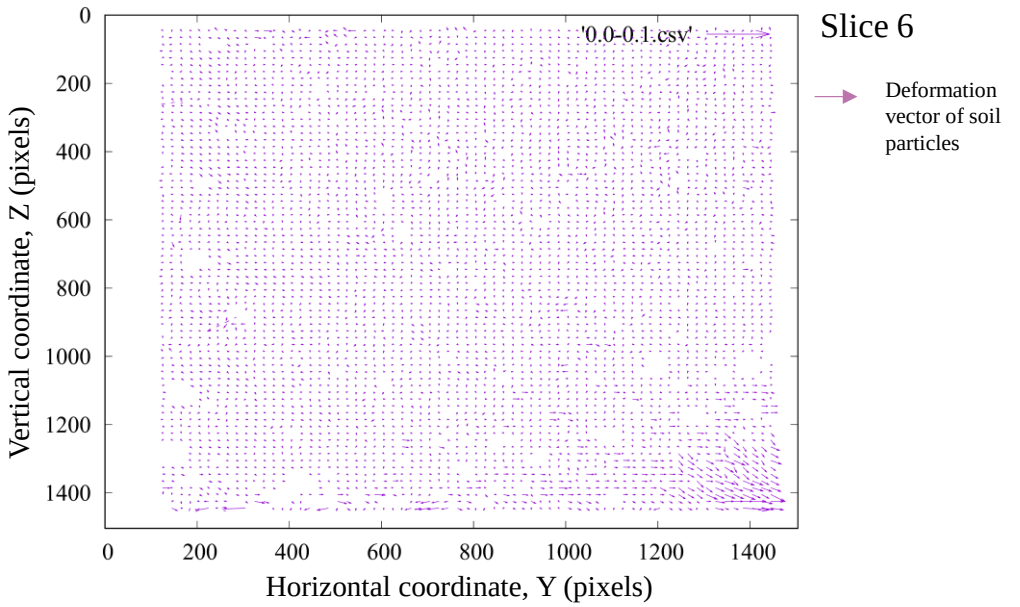
'0.0-0.1.csv'
Slice 6
Deformation vector of soil particles
Vertical coordinate, Z (pixels)
Horizontal coordinate, Y (pixels)
0
200
400
600
800
1000
1200
1400

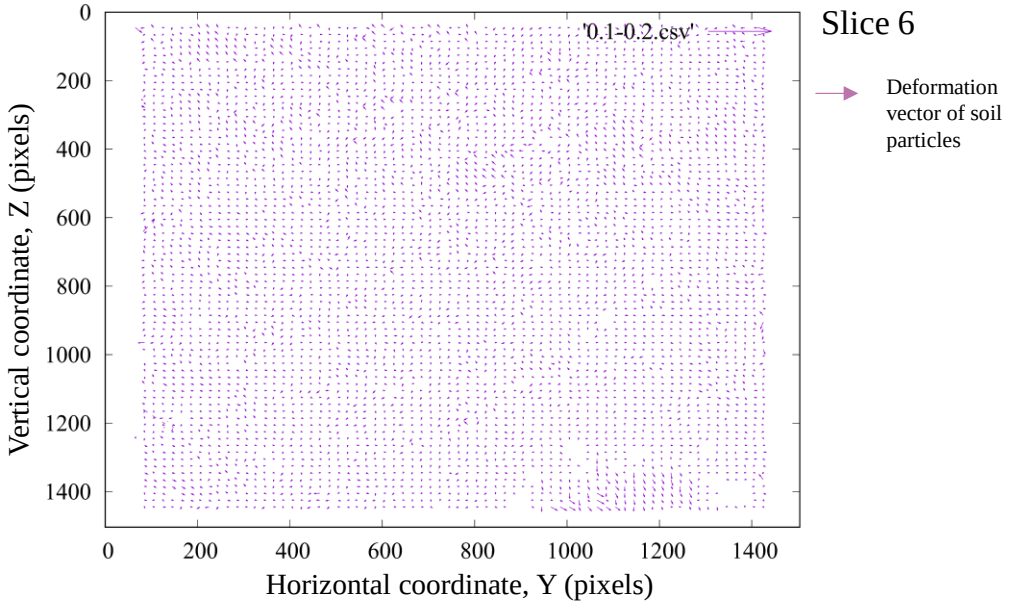
'0.1-0.2.csv'
Slice 6
Deformation vector of soil particles
Vertical coordinate, Z (pixels)
Horizontal coordinate, Y (pixels)
0
200
400
600
800
1000
1200
1400

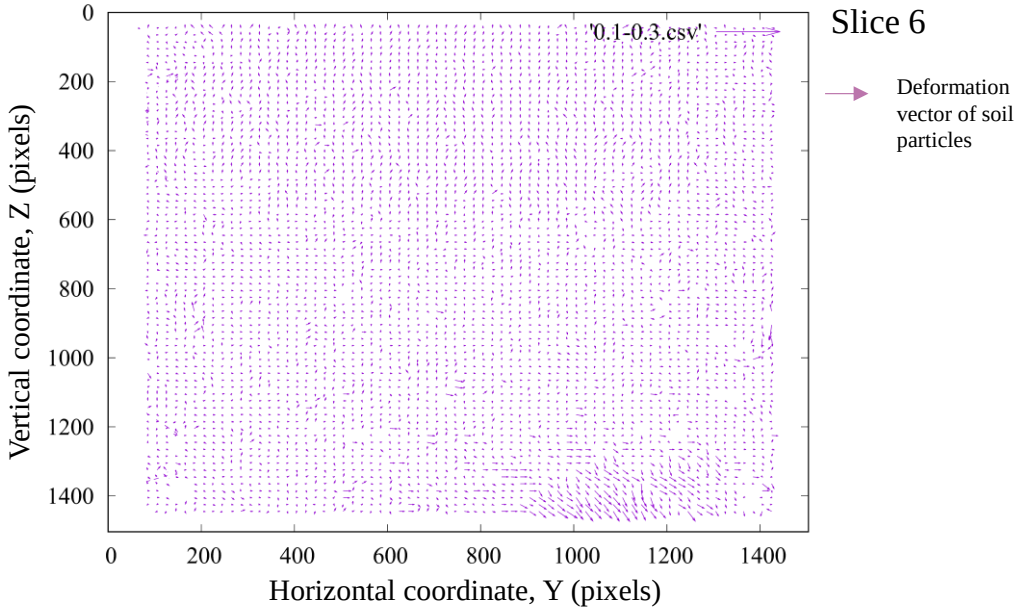
'0.1-0.3.csv'
Slice 6
Deformation vector of soil particles
Vertical coordinate, Z (pixels)
Horizontal coordinate, Y (pixels)
0
200
400
600
800
1000
1200
1400

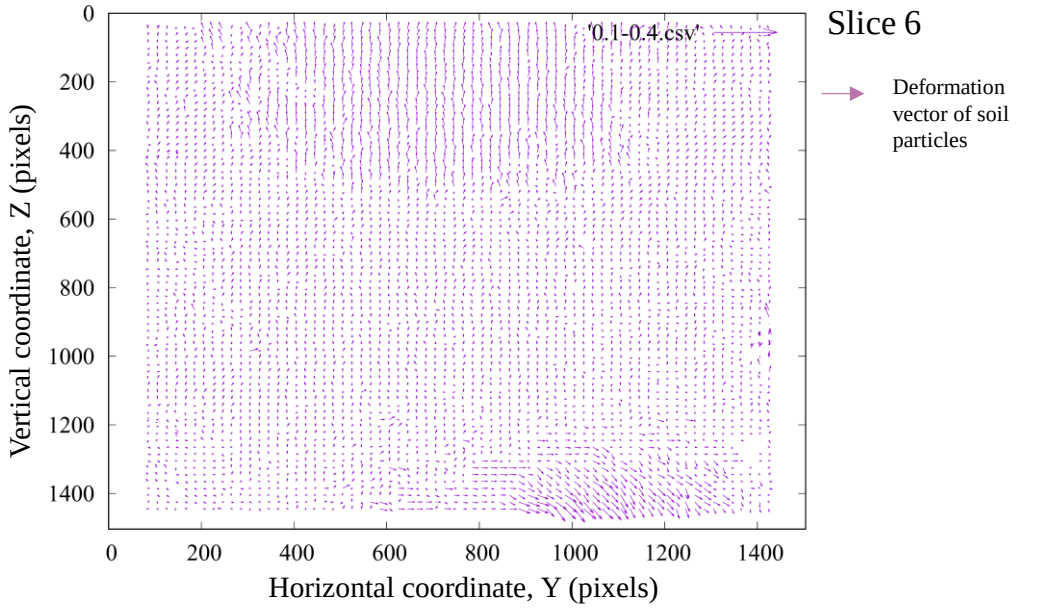
'0.1-0.4.csv'
Slice 6
Deformation vector of soil particles
Vertical coordinate, Z (pixels)
Horizontal coordinate, Y (pixels)
0
200
400
600
800
1000
1200
1400

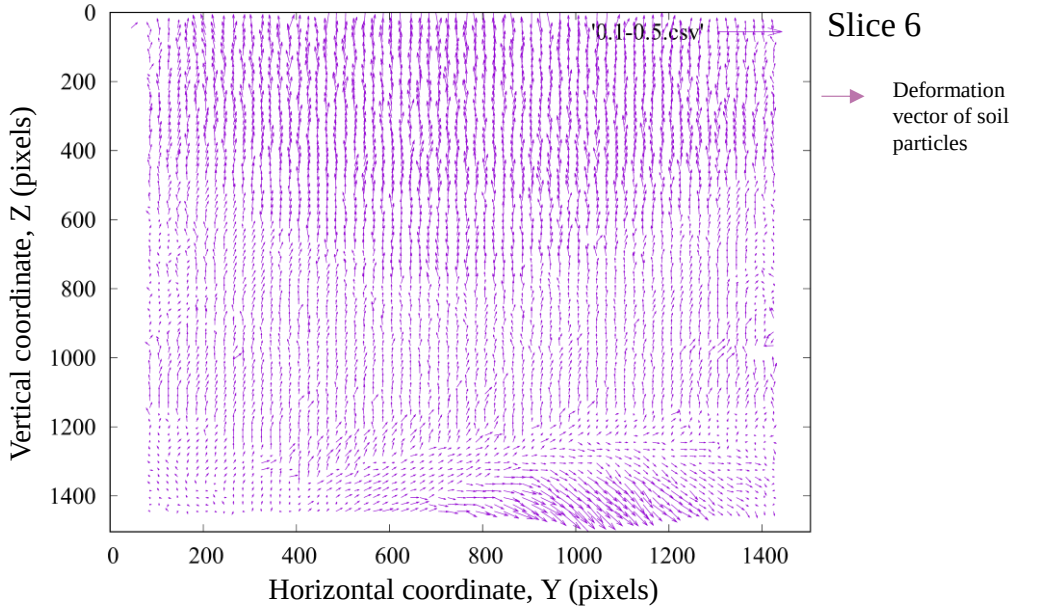
'0.1-0.5.csv'
Slice 6
Deformation vector of soil particles
Vertical coordinate, Z (pixels)
Horizontal coordinate, Y (pixels)
0
200
400
600
800
1000
1200
1400

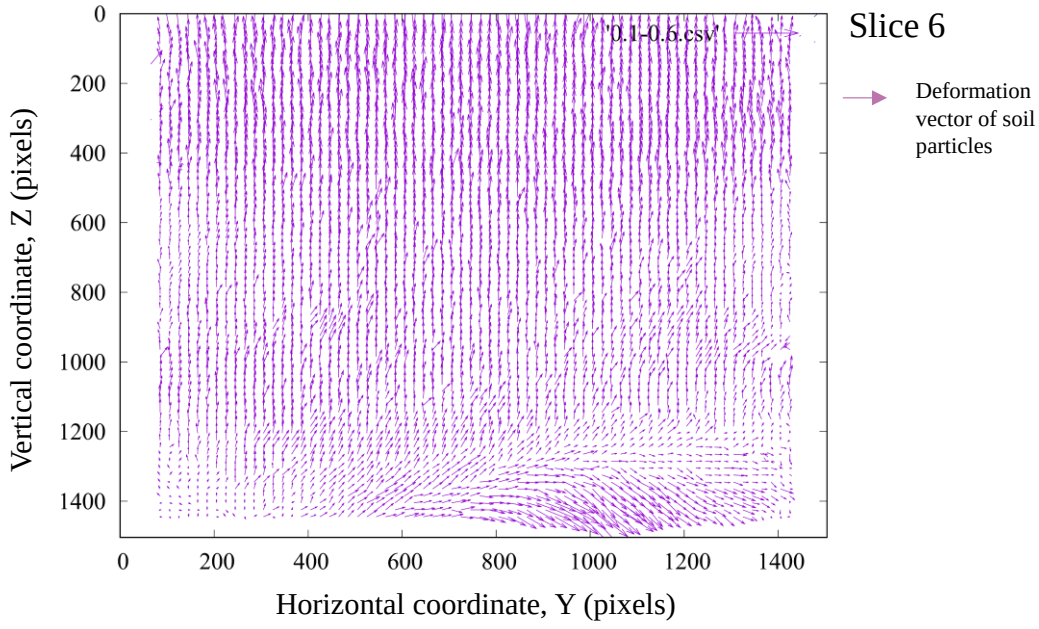
'0.1-0.6.csv'
Slice 6
Deformation vector of soil particles
Vertical coordinate, Z (pixels)
Horizontal coordinate, Y (pixels)
0
200
400
600
800
1000
1200
1400

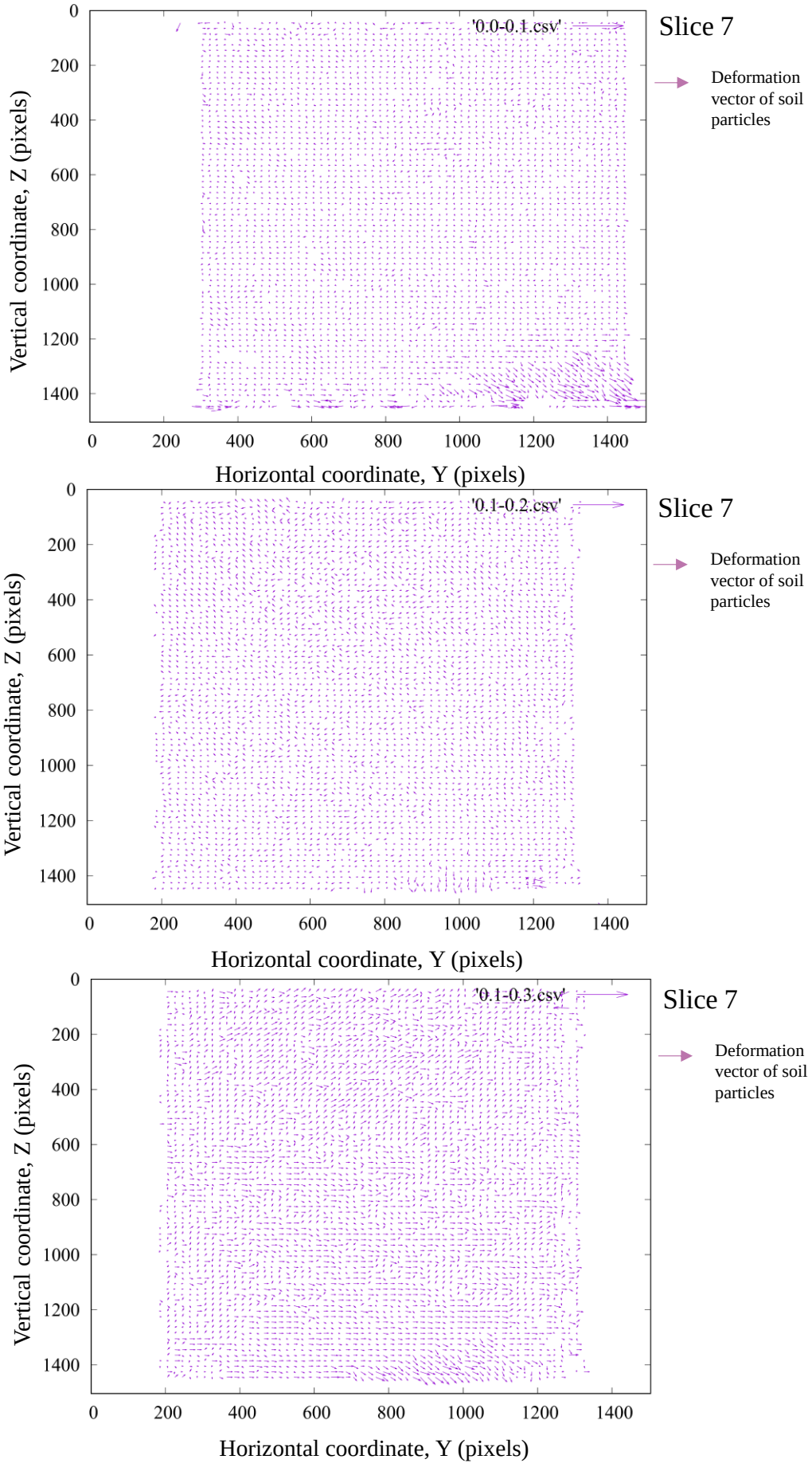
'0.0-0.1.csv'
Slice 7
Deformation vector of soil particles
Vertical coordinate, Z (pixels)
Horizontal coordinate, Y (pixels)
'0.1-0.2.csv'
Slice 7
Deformation vector of soil particles
Vertical coordinate, Z (pixels)
Horizontal coordinate, Y (pixels)
'0.1-0.3.csv'
Slice 7
Deformation vector of soil particles
Vertical coordinate, Z (pixels)
Horizontal coordinate, Y (pixels)

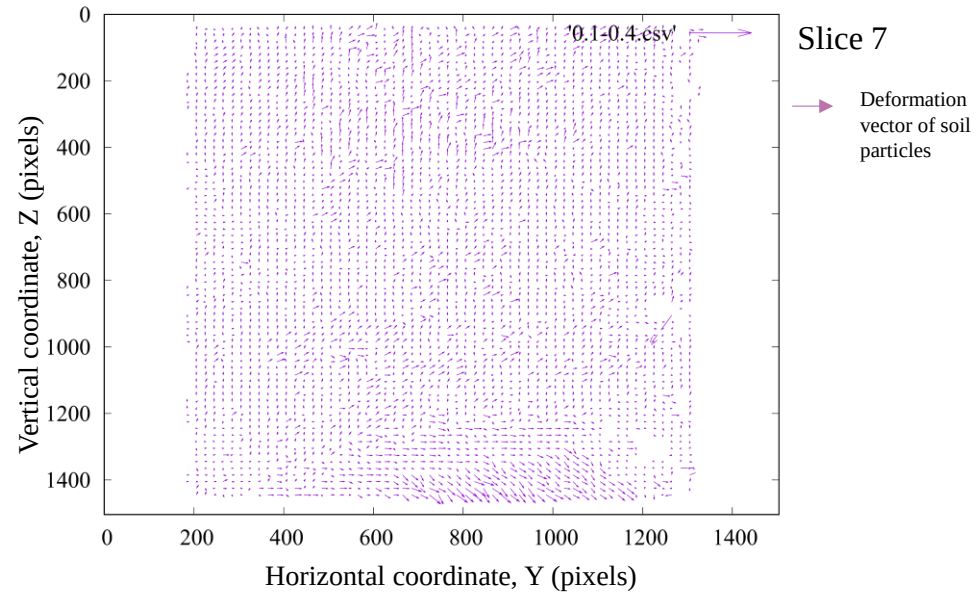
'0.1-0.4.csv'
Slice 7
Deformation vector of soil particles
Vertical coordinate, Z (pixels)
Horizontal coordinate, Y (pixels)
0
200
400
600
800
1000
1200
1400

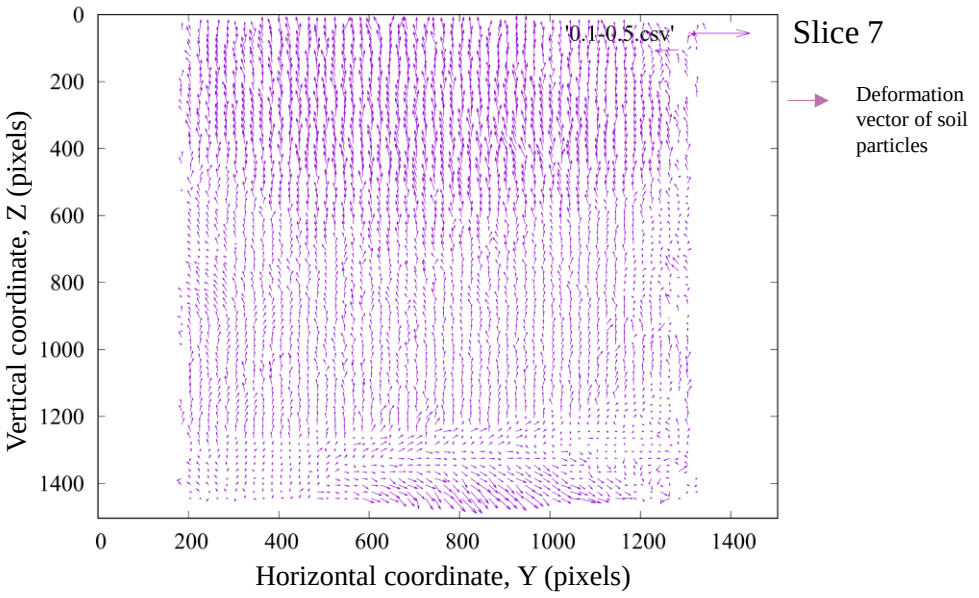
'0.1-0.5.csv'
Slice 7
Deformation vector of soil particles
Vertical coordinate, Z (pixels)
Horizontal coordinate, Y (pixels)
0
200
400
600
800
1000
1200
1400

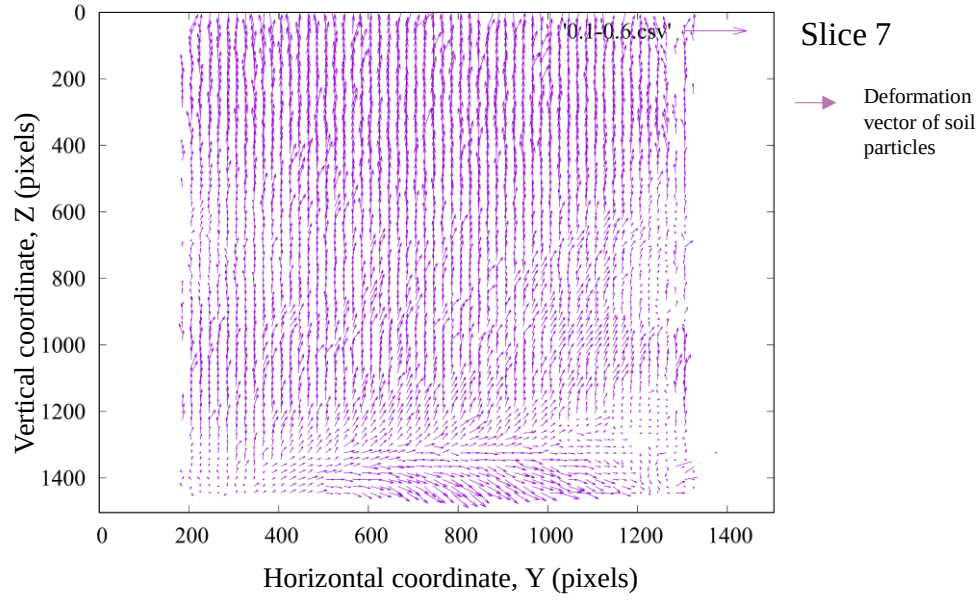
'0.1-0.6.csv'
Slice 7
Deformation vector of soil particles
Vertical coordinate, Z (pixels)
Horizontal coordinate, Y (pixels)
0
200
400
600
800
1000
1200
1400

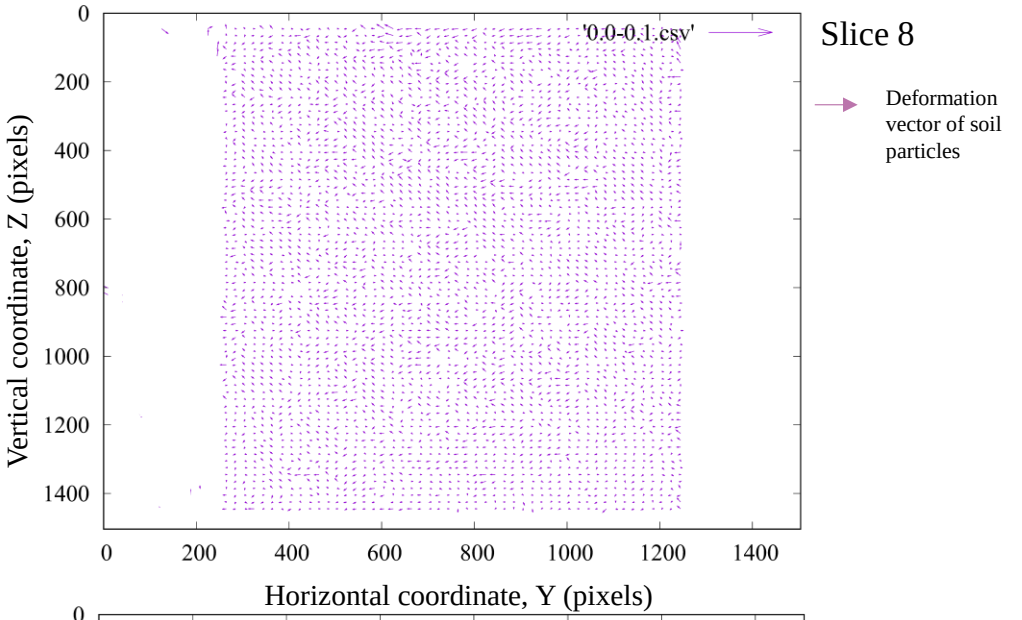
'0.0-0.1.csv'
Slice 8
Deformation vector of soil particles
Vertical coordinate, Z (pixels)
Horizontal coordinate, Y (pixels)
0
200
400
600
800
1000
1200
1400

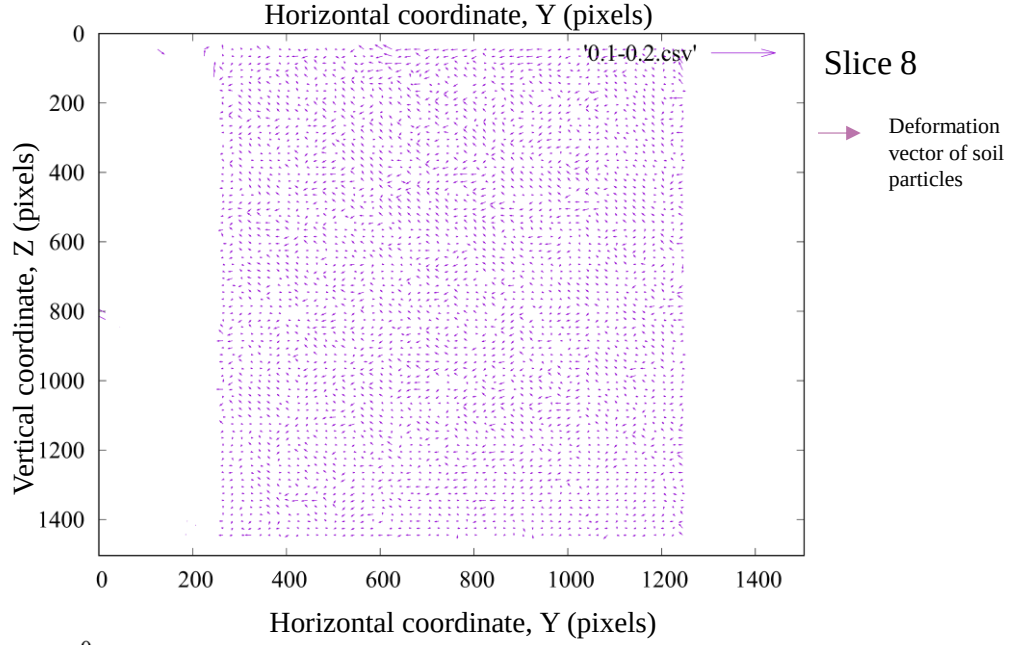
'0.1-0.2.csv'
Slice 8
Deformation vector of soil particles
Vertical coordinate, Z (pixels)
Horizontal coordinate, Y (pixels)
0
200
400
600
800
1000
1200
1400

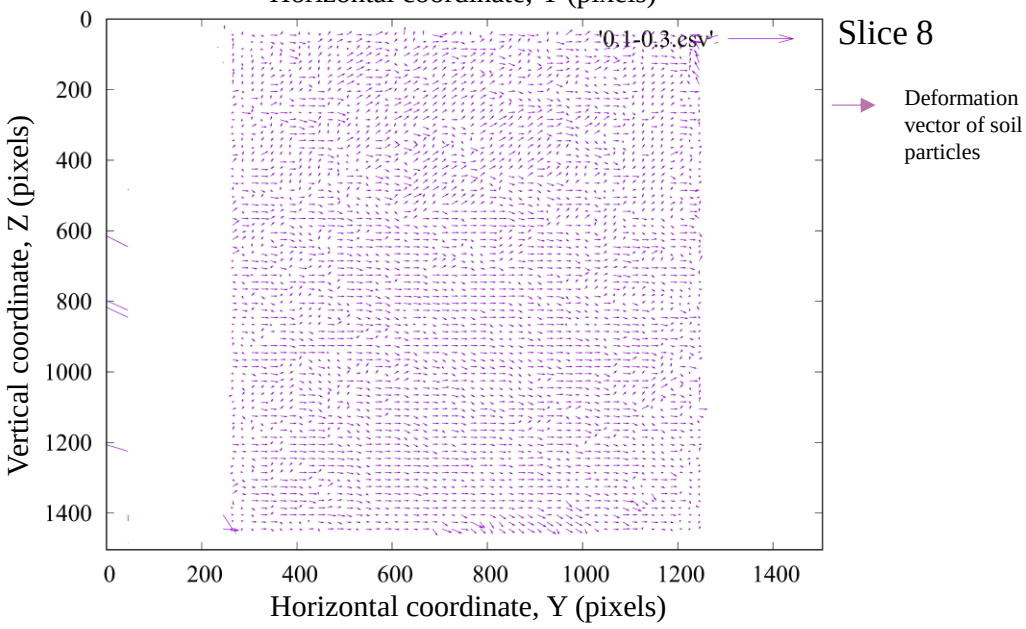
'0.1-0.3.csv'
Slice 8
Deformation vector of soil particles
Vertical coordinate, Z (pixels)
Horizontal coordinate, Y (pixels)
0
200
400
600
800
1000
1200
1400

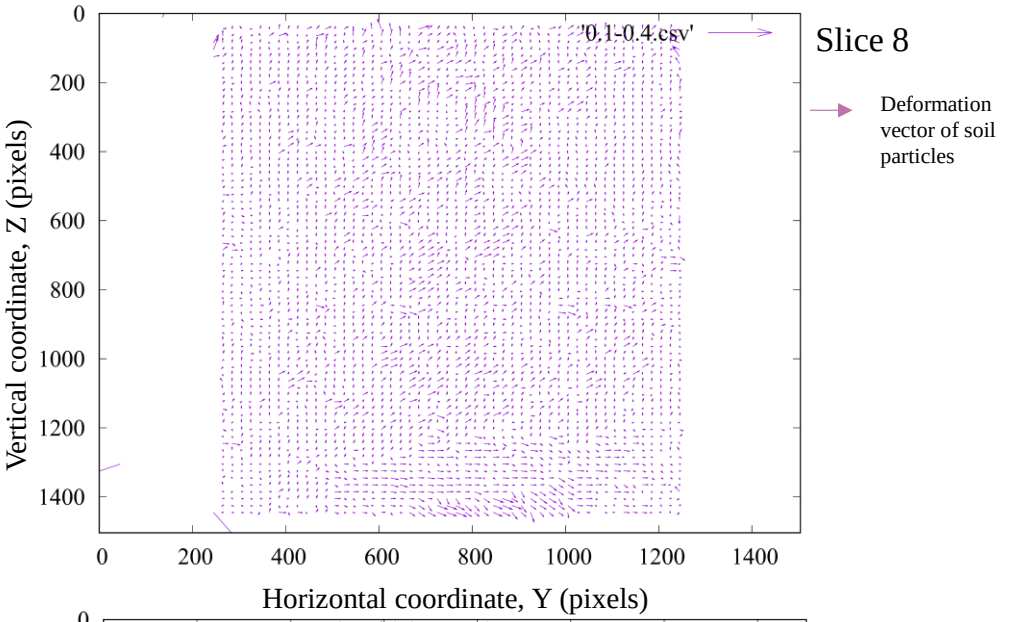
'0.1-0.4.csv'
Slice 8
Deformation vector of soil particles
Vertical coordinate, Z (pixels)
Horizontal coordinate, Y (pixels)
0
200
400
600
800
1000
1200
1400

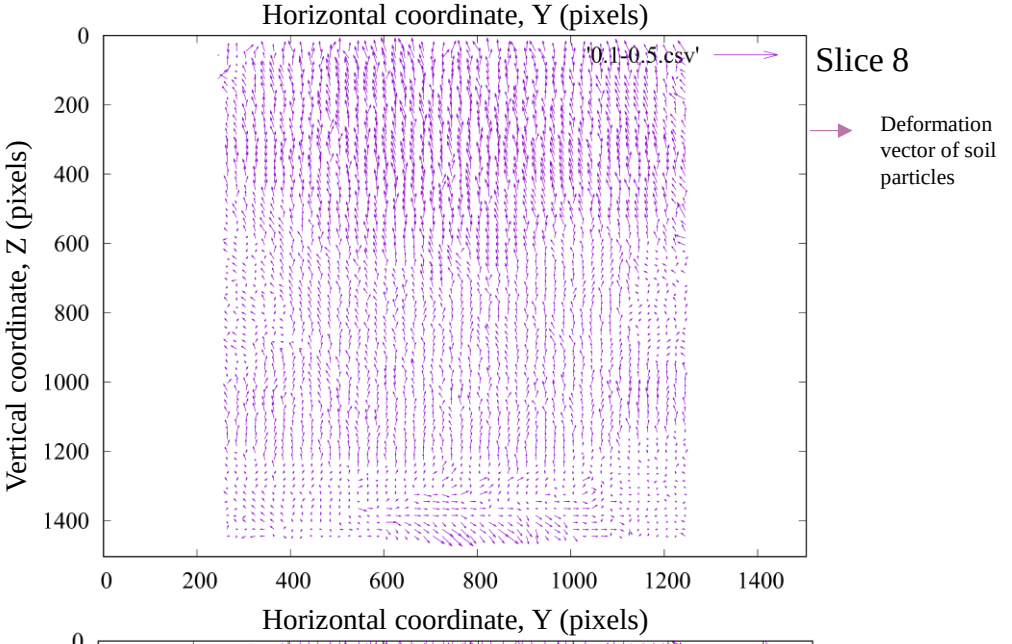
'0.1-0.5.csv'
Slice 8
Deformation vector of soil particles
Vertical coordinate, Z (pixels)
Horizontal coordinate, Y (pixels)
0
200
400
600
800
1000
1200
1400

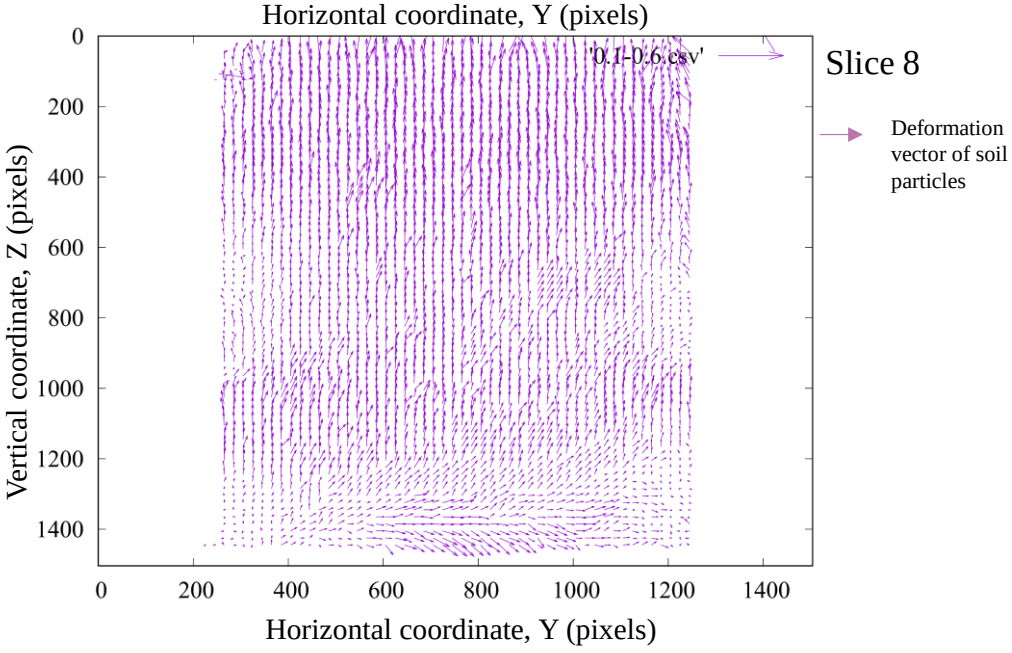
'0.1-0.6.csv'
Slice 8
Deformation vector of soil particles
Vertical coordinate, Z (pixels)
Horizontal coordinate, Y (pixels)
0
200
400
600
800
1000
1200
1400